THE ROLE OF POLYPLOIDY IN THE LIVER AND

ITS IMPLICATIONS FOR CANCER THERAPY

APPROVED BY SUPERVISORY COMMITTEE

_____

Hao Zhu, M.D.

_____

Kathryn O'Donnell, Ph.D.

_____

James Brugarolas, M.D.,Ph.D.

_____

Hongtao Yu, Ph.D.

DEDICATION

Dedicated to my beloved family: Mr. Yunlong Zhang and Mrs. Yurong Liu,

For their unconditional love and support

THE ROLE OF POLYPLOIDY IN THE LIVER AND ITS IMPLICATIONS FOR CANCER THERAPY

by

SHUYUAN ZHANG

DISSERTATION/THESIS

Presented to the Faculty of the Graduate School of Biomedical Sciences

The University of Texas Southwestern Medical Center at Dallas

In Partial Fulfillment of the Requirements

For the Degree of

DOCTOR OF PHILOSOPHY

The University of Texas Southwestern Medical Center
Dallas, Texas

May, 2018

THE ROLE OF POLYPLOIDY IN THE LIVER AND

ITS IMPLICATIONS FOR CANCER THERAPY

SHUYUAN ZHANG

The University of Texas Southwestern Medical Center at Dallas, 2017

HAO ZHU, M.D.

The description of liver polyploidy dates back to the 1940s, but its functional roles are still largely unknown. Numerous observations and studies have suggested that liver polyploidy may participate in multiple biological processes, including regeneration, stress response, and cancer. However, little evidence has established direct causal links between polyploidy and the observed phenotypes, mainly due to the lack of appropriate tools to specifically manipulate ploidy levels without causing other permanent changes. Specifically, whether polyploidy promotes or inhibits cancer is still under debate. Inspired by a phenomenon we observed in somatically mutated mouse livers, where

homozygous *Apc* deletions were more difficult to obtain due to hepatic polyploidy, we aimed to build inducible tools to manipulate liver ploidy levels *in vivo* and systematically study the role of polyploidy in liver cancer. By toggling the weaning time and levels of *Anln* or *E2f8* genes to change liver ploidy levels, we found that liver tumorigenesis was inversely correlated with initial polyploidy levels, suggesting a tumor suppressive role for polyploidy. Moreover, the additional alleles in polyploid cells led to a reduced likelihood of loss of heterozygosity (LOH), which largely contributed to the tumor suppressive effect. These results revealed an important function of polyploidy in mammalian livers and also led us to seek related therapeutic strategies for treating liver cancer. Since hepatocyte polyploidization mainly occurs through cytokinesis failure, we hypothesized that inhibiting cytokinesis could be an effective strategy to suppress liver tumorigenesis while preserving normal liver function. Therefore, we inhibited cytokinesis via *Anln* knockdown in multiple models and found that liver tumor development was significantly suppressed but normal liver function and regeneration capacity were not impaired. These results suggest that cytokinesis inhibition via *Anln* knockdown is potentially a safe and efficacious strategy for suppressing liver cancer. Overall, we uncovered an important role of polyploidy in the liver and explored its potential applications in liver cancer therapy.

ACKNOWLEDGEMENTS

The goals of a Ph.D. are to cultivate good thinking habits, to obtain a sophisticated scientific intuition, and to develop perseverance. Fortunately, with the help from my mentor, colleagues, friends and family, my Ph.D. journey was full of fun and challenges as I traveled towards the fulfillment of these goals.

It was a great fortune for me to have Dr. Hao Zhu as my Ph.D. mentor. Hao is a passionate scientist. His love for science is so obvious and contagious that I also began to appreciate the beauty of science. The most important thing I learned from Hao is a way of thinking: always asking yourself "what are the important questions?", "what is the key experiment?", and "what makes a study robust?". He likes to exchange ideas with us, which drove me to think actively and carefully. Other than a scientific mentor, Hao is also the cheerleader of our group. He is always the most enthusiastic person, making everything that happens in the lab exciting. He not only ensures everyone in the lab works, but also works happily. After each time that I met with him, I would feel so inspired and full of hope for my projects, and even for my life. Therefore, I would like to give great thanks to Dr. Hao Zhu for his valuable guidance and support.

During these five years, I also received so much help from my colleagues on countless occasions. I want to first thank Lin Li for her generous heart. Lin is the first person I worked with after joining the lab. She taught me how to do every single experiment and how to be a nice team member. Except for Hao, she is the most central person in our group. Next, I would like to thank Liem Nguyen, my lab and classmate, who brought laughter to me all the time by arguing with me in a very fun way. I also want to thank other lab members, especially Xuxu Sun, Jen-Chien Chuang, Linwei Wu, Cemre Celen, and Sam Wang, for the time we spent together talking about science,

life, and the future. Additionally, I would like to thank my collaborators, Kejin Zhou, Jason Miller, and Dan Siegwart, for their kind help and constructive suggestions. My sincere thanks also go to my committee members, Dr. Kate O'Donnell, Dr. James Brugarolas, and Dr. Hongtao Yu, for their insightful comments on my projects and for their encouragement for my scientific career. Special thanks to Dr. Daniel Siegwart and Dr. Hongtao Yu, who have been enormously supportive and helpful for my postdoc applications.

Last but not the least, I would like to thank my family and friends, who are always there with me during my ups and downs. I want to express my deep gratitude to my mom and dad for their unconditional understanding and love. They gave me enough freedom and support to let me pursue my dreams. No matter where I am, there is always a place called home, where my parents are, that gives me a sense of security. I also want to give special thanks to my friends, Xiaochuan Tian, Yizhu Lin, Weiwei Chen, and Eryu Xia, who warmed me up during the cold days, cheered me up during the blue days, and helped me out during the tough days. I will never forget the time we spent together, which are not only joyful memories, but also have made me who I am now.

TABLE OF CONTENTS

PRIOR PUBLICATIONS

Zhang S, Zhou K, Luo X, Li L, Tu H, Sehgal A, Nguyen L, Zhang Y, Gopal P, Tarlow B, Siegwart D, and Zhu H. The polyploid state plays a tumor suppressive role in the liver. ***Developmental Cell***. 2018 Feb 26. doi: 10.1016/j.devcel.2018.01.010. PMID: 29429824.

Zhang S, Nguyen LH, Zhou K, Tu HC, Sehgal A, Nassour I, Li L, Gopal P, Goodman J, Singal AG, Yopp A, Zhang Y, Siegwart DJ, and Zhu H. Knockdown of Anillin Actin Binding Protein Blocks Cytokinesis in Hepatocytes and Reduces Liver Tumor Development in Mice without Affecting Regeneration. ***Gastroenterology***. 2017 Dec 20. pii: S0016-5085(17)36717-3. doi: 10.1053/j.gastro.2017.12.013. PMID: 29274368.

Zhang S*, Li L*, Kendrick SL, Gerard RD, and Zhu H. TALEN-Mediated Somatic Mutagenesis in Murine Models of Cancer. *Equal contribution. ***Cancer research***. 2014 Sep 15. 74(18):5311-21. doi:10.1158/0008-5472.CAN-14-0529. PMID: 25070752.

Zhang S**,** Wang S, Zhu H. Cutting short the path to murine liver cancer models. ***Hepatology***. 2015 Jan. 61(1):393-5. doi: 10.1002/hep.27580. PMID: 25345582.

Miller JB*, Zhang S*, Kos P, Xiong H, Zhou K, Perelman SS, Zhu H, Siegwart DJ. *Equal contribution. Non-Viral CRISPR/Cas Gene Editing In Vitro and In Vivo Enabled by Synthetic Nanoparticle Co-Delivery of Cas9 mRNA and sgRNA. ***Angewandte Chemie International Edition***. 2017 Jan 19. 56(4):1059-1063. doi:10.1002/anie.201610209. PMID: 27981708.

Xia P, Zhou J, Song X, Wu B, Liu X, Li D, Zhang S, Wang Z, Yu H, Ward T, Zhang J, Li Y, Wang X, Chen Y, Guo Z, Yao X. Aurora A orchestrates entosis by regulating a dynamic MCAK-TIP150 interaction. ***Journal of molecular cell biology***. 2014 Jun. 6, 240-254, doi:10.1093/jmcb/mju016. PMID: 24847103.

Xia P, Liu X, Wu B, Zhang S, Song X, Yao PY, and Yao X. Superresolution imaging reveals structural features of EB1 in microtubule plus-end tracking. ***Molecular biology of the cell***. 2014 Dec 15. *25*(25), 4166-4173. doi: 10.1091/mbc.E14-06-1133. PMID: 25355949.

Sun X, Chuang JC, Kanchwala M, Wu L, Celen C, Li L, Liang H, Zhang S, Maples T, Nguyen LH, Wang SC, Singner RA, Sorouri M, Nassour I, Liu X, Xu J, Wu M, Zhao Y, Kuo YC, Wang Z, Xing C, Zhu H. Suppression of the SWI/SNF Component Arid1a Promotes Mammalian Regeneration. ***Cell Stem Cell***. 2016 Apr 7. 18(4), 456-466. doi: 10.1016/j.stem.2016.03.001. PMID: 27044474.

Wu L, Nguyen L H, Zhou K, de Soysa, TY, Li L, Miller JB, Tian J, Locker J, Zhang S, Shinoda G, Seligson MT, Zeitels LR, Acharya A, Wang S, Mendell JT, He X, Nishino J, Morrison SJ, Siegwart DJ, Daley GQ, Ng S-Chang, Zhu H. Precise let-7 expression levels balance organ regeneration against tumor suppression. ***Elife***. 2015 Oct 7. 4: e09431. doi: 10.7554/eLife.09431. PMID: 26445246.

Celen C, Chuang JC, Luo X, Nijem N, Walker AK, Chen F, Zhang S, Chung AS, Nguyen LH, Nassour I, Budhipramono A, Sun X, Bok LA, McEntagart M, Gevers EF, Birnbaum SG, Eisch AJ, Powell CM, Ge WP, Santen GW, Chahrour M, Zhu H. Arid1b haploinsufficient mice reveal neuropsychiatric phenotypes and reversible causes of growth impairment. ***ELife***. 2017 Jul 11. pii: e25730. doi: 10.7554/eLife.25730. PMID: 28695822.

Sun X, Wang S, Wei Y, Luo X, Jia Y, Li L, Gopal P, Zhu M, Nassour I, Chuang JC, Maples T, Celen C, Nguyen LH, Wu L, Fu S, Li W, Hui L, Tian F, Ji Y, Zhang S, Sorouri M, Hwang TH, Letzig L, James L, Wang Z, Yopp AC, Singal AG, Zhu H. Arid1a Has Context-Dependent Oncogenic and Tumor Suppressor Functions in Liver Cancer**. *Cancer Cell***. 2017 Nov 13. 32(5): 574-589.e6. doi: 10.1016/j.ccell.2017.10.007. PMID: 29136504.

LIST OF FIGURES

LIST OF ABBREVIATIONS

CIN	Chromosome instability
TSC	Trophoblast stem cell
TGC	Trophoblast giant cell
SAC	Spindle assembly checkpoint
TBA	Tubulin binding agent
CCl_4	Carbon tetrachloride
NAFLD	Nonalcoholic fatty liver disease
NASH	Nonalcoholic steatohepatitis
MMECs	Mouse mammary epithelial cells
LOH	Loss of heterozygosity
ALT	Alanine aminotransferase
AST	Aspartate aminotransferase
DEN	Diethylnitrosamine
DOX	Doxycycline
ESCs	Embryonic stem cells
HDT	Hydrodynamic transfection
Apc	*Adenomatous Polyposis Coli*
HCC	Hepatocellular carcinoma
TSG	Tumor suppressor
ROS	Reactive oxygen species
HFD	High fat diet

FISH	Florescence In Situ Hybridization
GalNAc	N-acetylgalactosamine
ASGPR	Asialoglycoprotein receptor
TRE	Tetracycline responsive promoter element
FAH	Fumarylacetoacetate hydrolase
FRG	$FAH^{-/-}$; *Rag1*$^{-/-}$; *IL-2Rγ*$^{-/-}$
NTBC	2-(2-Nitro-4-trifluoromethylbenzoyl)-1,3-cyclohexanedione
NSCLC	Non-small cell lung cancer
GS	Glutamine synthetase
KO	Knockout
WT	Wild type
min	Minute
PHx	Partial heptatectomy

CHAPTER 1

PROLOGUE

Polyploidy

Polyploidy is a phenomenon whereby cells and organisms contain more than two sets of chromosomes. Polyploids are prevalent in plants and some studies estimate that 30-80% of living plant species are polyploid [1, 2]. Many of these plants are prominent in our daily lives: bananas, potatoes, and peanuts. Moreover, polyploidy is sometimes also tolerated in animals, especially in fish (*Catostomidae, Salmonidae,* etc.)[3] and amphibians (*Syrinidae, Xenopus laevis,* etc.) [4]. In birds and mammals, whole-organism polyploidy is very rare and often results in prenatal death. Nevertheless, high levels of polyploid cells can still be found in mammalian organs such as the bone marrow [5], heart [6], skeletal muscle [7], brain [8], and liver [9]. Moreover, polyploidization is also observed in response to environmental stress. For example, the uterus develops decidual polyploid cells during early pregnancy, which is crucial for successful embryo implantation [10]. In addition, polyploidy is associated with tumorigenesis and tumor progression in many types of cancer [11-13], potentially because polyploidy is associated with chromosomal instability (CIN) [14].

There are several mechanisms that can lead to polyploid cells, as described below [15]. It appears that different reviews use different definitions, e.g., in some reviews, “endoreplication”, “mitotic slippage” and “cytokinesis failure” are all classified as “endoreplication” [16]. The description about each process is separately useful.

1. *Cell fusion*. This is the only mechanism that generates polyploid cells without requiring cell cycle entry. Cell fusion has been observed both in physiological development and pathological events. During embryonic development, myoblasts fuse together to form multi-nucleated fibers called myotubes, representing a terminally differentiated state [17]. Viral infection can cause cell fusion in pathological processes. Many viruses have fusogenic activities which allow them to enter host cells [18]. Although under debate, it is possible that cell fusion occurs at a low rate in hepatocytes. It has been shown that donor bone marrow cells can rescue a genetic liver degenerative defect by fusing with the recipient hepatocytes [19]. Another study that was dedicated to detecting hepatocyte-hepatocyte fusion in mouse liver by using chimeric systems [20]. They identified the hepatocytes that expressed markers from both donors, and reasoned that these hepatocytes were generated by fusion events. However, due to the unavoidable artifacts from extracellular vesicles and a lack of evidence showing the ploidy of “fused” cells, the occurrence of cell fusion in liver is still controversial.

2. *Endoreplication*. Endoreplication, also known as endoreduplication, occurs when a cell goes through G1/S/G2 phases or includes parts of mitosis without initiating cytokinesis. The resulting cellular progenies of endoreplication are mononucleated polyploid cells. This process is extensively studied in *Drosophila* nurse cells, which become polyploid during oogenesis and provide maternal materials to developing oocytes [21]. In mammals, a well characterized example of endoreplication is trophoblast stem cell (TSC) differentiation into trophoblast giant cells (TGC),

which are required for embryo implantation [22]. No mitosis occurs during the polyploidization of TGCs, only S and G phases alternate. This has been proposed as a way to accelerate TGC growth by shortening the duration of cell cycles [23]. Endoreplication also occurs in response to DNA damage. In p53-null cells, prolonged DNA damage signals from persistent telomere dysfunction could induce bypass of mitosis, which results in cell tetraploidization [24].

3. *Mitotic slippage*. During a perturbed mitosis, in the presence of spindle poison, the cell is arrested at metaphase by the spindle assembly checkpoint (SAC), which is activated to ensure that every chromosome is properly attached. Failure to satisfy the SAC causes mitotic arrest, which will lead to cell death during mitosis (mitotic catastrophe) or "mitotic slippage", where the arrested cells "slip" mitosis and enter the next interphase without undergoing chromosome segregation and cytokinesis. Thereby the "mitotic slippage" cells, also referred to as "postmitotic" cells, are polyploid. Tubulin binding agents such as taxanes, epothilones, and vinca alkaloids can activate SAC and therefore induce mitotic slippage [25] [26]. However, which fate will be chosen during mitosis arrest, "mitotic catastrophe" or "mitotic slippage", is still unclear and involves complex mechanisms [27].

4. *Cytokinesis failure*. Cytokinesis is the last step of the cell cycle, during which the mother cell divides into two daughter cells. It requires anaphase spindle reorganization, formation of a cleavage furrow, and abscission. Failed cytokinesis can lead to binucleated polyploid cells, which appears in both physiological and pathological situations. For platelet producing megakaryocytes, the cells can go through anaphase and telophase, but the following cytokinesis fails due to cleavage furrow regression, resulting in up to 128n cells [28]. Polyploidization is essential for megakaryocyte function. Blocking cytokinesis failure of megakaryocyte by ablating *Cdc20* led to significantly decreased ploidy and reduction in platelet production [29]. Interestingly, introducing

alternative polyploidization approaches by deleting *Cdk1* or both *Cdk1* and *Cdk2* could rescue the functional defect [29], suggesting that it is the polyploid state that is required for megakaryocyte function, not necessarily the specific polyploidization mechanism. Injury induced polyploidization via cytokinesis failure also occurs in zebrafish epicardium. During heart regeneration, epicardial tissues form a front of large, multinucleated leader cells, caused primarily by cytokinesis failure [30], and these leader polyploid cells might possess an enhanced potential for surface coverage.

Polyploidy in the liver

Liver is an essential organ that carries out many important functions, such as nutrient synthesis and distribution, storage of amino acids, lipids and carbohydrates, and detoxification of xenobiotics [31]. These functions are conducted primarily by hepatocytes, which account for 70% of cells within the liver. Hepatocytes are relatively quiescent with a turnover rate of 200-300 days, but they are able to rapidly proliferate upon injury [32].

One remarkable feature of hepatocytes is that up to 90% of mouse and 50% of human hepatocytes are polyploid [33, 34], making the liver one of the largest mammalian polyploid organs. During postnatal development, hepatocytes become polyploid mainly through failed cytokinesis [35], leading to binucleation. Mononucleated polyploid cells are subsequently generated from binucleated cell division. In rodents, hepatocyte polyploidization starts upon weaning, and is intimately associated with dietary changes and fluctuations in signaling through the Insulin/Akt pathway [36]. Since liver proliferation slows after 4 weeks of age, polyploidy increases dramatically between weaning and animal maturity, followed by a gradual elevation throughout adulthood.

Ploidy is also dynamically altered upon liver injury and stress. The classic 70% partial hepatectomy protocol induces hepatocyte proliferation accompanied by a reduction in the diploid cells and an increase in the mononucleated polyploid cells [37, 38]. However, the polyploidization route undertaken during regeneration is slightly different than that during development. Miyaoka *et al.* carefully examined the liver regeneration after 70% hepatectomy, and found that most of the hepatocytes entered S phase, revealed by BrdU incorporation, but rarely entered mitosis, demonstrated by phospho-H3 staining, indicating that the cells might also proliferate via endoreplication [37]. Although lacking direct evidence showing specific aberrant cell cycles, this study clearly demonstrated the plasticity of cell cycle regulation in hepatocytes. Except for surgical injury, chemical injury and metabolic stress are also associated with liver ploidy changes. We observed increased liver polypoidy in mouse after repeated administration of carbon tetrachloride (CCl_4), which causes hepatocyte necrosis in the pericentral area. Moreover, in a Wilson's Disease rat model, delayed mitosis and increased polyploidy are associated with excess copper accumulation in the liver [39]. Recently, ploidy levels in nonalcoholic fatty liver disease (NAFLD) was examined [40]. Livers from NAFLD mouse models exhibited elevated levels of polyploidy, and the same was observed in human nonalcoholic steatohepatitis (NASH) patients. Furthermore, oxidative stress was demonstrated to promote liver polyploidization in NAFLD models.

In summary, liver polyploidy is both developmentally regulated and dynamically controlled in the context of cellular stress or disease. However, since the previous studies only characterized associations between liver ploidy and disease states, whether or not polyploidy plays a functional role in liver disease is still unclear.

Liver ploidy, zonation, and "liver stem cells"

The cells residing in liver are heterogeneous, and each hepatocyte is also not identical. The liver lobule is usually classified to three zones traversing the central to portal vein axis: perivenous (around central vein), periportal (around portal triad), and mid-zone (the left over). The gene expression pattern of hepatocytes changes between different zones due to the blood flow, oxygen gradient, and the Wnt signaling gradient emanating from central vein endothelial cells [41, 42]. Interestingly, the hepatocyte ploidy also differs between zones: in general, the periportal zone has the most diploid hepatocytes, followed by perivenous zone; the mid-zone has the highest levels of polyploidy [43].

Polyploidy is frequently considered as a terminally differentiated or functionally mature state, and this is true in some cells such as megakaryocytes [29] and TGCs [44]. Whether this is also true in hepatocytes is still unclear. Many efforts have been made to try to identify the "stem cell" population in liver, but the supporting evidence for the various populations are not yet sufficient and are somewhat contradictory. The first efforts were spent on identifying whether there is a non-hepatic cell population that can give rise to hepatocytes when hepatocyte proliferation is inhibited. Injury-induced proliferation in biliary or biliary-like cells (marked by *Sox9*, *Opn*, *Ck19*, *Lgr5*, *EpCAM*, etc.), long considered as a liver stem or progenitor population, was thought to replenish the hepatocyte pool upon injury [45, 46]. However, many well performed lineage-tracing studies also showed opposing evidence that hepatocytes themselves were the major regenerative cell source during injury [47, 48]. Since different injury models and lineage tracing tools can result in very different cellular behaviors, the variations in study systems can greatly complicate results. Subsequent efforts were made to identify whether there is a specific hepatic subpopulation that can self-renew under physiological conditions or upon injury. Roel Nusse's group lineage labeled *Axin2*+ hepatocytes surrounding the central vein and found that these cells could both self-renew

and give rise to new hepatocytes [41]. Consistent with their zonal location, these cells are more diploid compared to their progeny. Steven Artandi's group labeled a group of hepatocytes expressing higher levels of telomerase reverse transcriptase (*Tert*), and these cells were found to regenerate the liver both in homeostasis and under injury conditions [49]. However, these *Tert*^{high} hepatocytes are distributed in all zones and their ploidy is representative of the overall liver ploidy. The discrepancies between these two studies raises questions about the lineage tracing tools used in these and the similar studies. It has been hypothesized that the knock-in *Sox9-CreERT2* allele introduced alterations in cellular proliferation and fitness, which potentially affected the lineage tracing results [47, 50, 51]. Therefore, the knock-in alleles used in these two studies, *Axin2-ERT2* and *Tert-ERT2*, need more careful characterization to exclude the possibility that knocking in genes to these loci might induce proliferative changes. Moreover, it is also possible that both cell populations, *Axin2+* and *Tert*^{high}, can give rise to hepatocytes, since the 1-year lineage tracing results in both studies showed only around 30% repopulation. This would indicate that hepatocytes have multiple "stem cell" pools, and the lineage hierarchy of hepatocytes is more complex. In conclusion, the existence of "liver stem cells" is still controversial. Moreover, no solid evidence is able to support the idea that polyploid hepatocytes are more differentiated and/or less proliferative than diploid hepatocytes.

Regulators of liver polyploidy

In rodents, liver polyploidization starts during the suckling to weaning transition and is closely related to signaling through the Insulin/PI3K/Akt pathway [36]. Inhibiting Akt activity decreased cytokinesis failure during weaning [36]. Since liver polyploidization involves programmed cell cycle defects (cytokinesis failure and endoreplication), a series of studies have shown that

perturbation of cell cycle regulators can alter the degree of polyploidy. The E2f family represents a group of transcription factors involved in cell cycle transitions. The family contains both activators such as *E2f1*, *E2f2*, *E2f3*, and repressors like *E2f7*, *E2f8*. *E2f8* or *E2f7* deletion leads to upregulation of cytokinesis genes and a completely diploid liver [52], whereas *E2f1* deficiency results in increased polyploidy [53, 54]. Similarly, *Ccne1* and *Ccne2* also play antagonizing roles in liver ploidy regulation. *Ccne1* deletion in mice results in endoreplication defects and decreased polyploidy, while *Ccne2* deletion leads to accelerated DNA synthesis and increased polyploidy [55]. Other cell cycle regulators whose roles in liver ploidy have been studied include *p53* [56], *p21* [57], *Rb* [58], *Cdk1* [59], *Skp2* [60], *Ssu72* [61], and *Survivin* [62], and deficiencies in these genes all cause increased polyploidy. Other than cell cycle genes, microRNAs also have roles in regulating ploidy. The direct targets of miR-122 include a set of cytokinesis genes, and knockout of miR-122 results in the profound and lifelong depletion of polyploid hepatocytes [63]. In spite of the changes in liver ploidy levels, these models were unable to provide convincing information about the functional roles of liver ploidy, mainly because the permanent genetic alterations confound the interpretation of whether or not phenotypes are due to genetic lesions or ploidy changes.

Polyploidy and cancer

Polyploidy and aneuploidy are frequently observed in cancer cells, representing the Chromosome Instability (CIN) state [64, 65]. Since genome duplications in cancer cells often involve the deletion, amplification or translocation of individual chromosomes [66, 67], cancer cells are more often aneuploid rather than conventionally polyploid. David Pellman's group put forth the idea that tetraploidy is an intermediate transition state of cancer cells that are becoming aneuploid [14],

which is a specific iteration of Boveri's hypothesis [68]. This concept is supported by tumor ploidy and cell cycle studies [69-71]. Therefore, polyploidy and aneuploidy are often considered as promoters of cancer development or progression. This idea has been directly tested in p53 null mouse mammary epithelial cells (MMECs), in which the tetraploids generated by cytokinesis failure exhibited a higher frequency of chromosomal mis-segregation and enhanced tumorigenicity [72]. Similarly, Davoli *et al.* showed that persistent telomere dysfunction and genome-wide DNA damage could induce cell tetraploidization also in p53 deficient cells [24], and that tetraploid cells created via the telomere crisis exhibited enhanced transformation [73]. Although these studies establish a link between polyploidy and tumorigenesis, it should not be ignored that all these studies used p53 null cells. Importantly, it has been shown that tetraploidization can activate p53, which in turn blocks cells from entering S phase [74, 75]. Considering the genome maintaining roles of p53, it would be more reasonable to confine these results under p53 null conditions and not generalize to the broad concept of polyploidy. Contrary to the pro-cancer argument about polyploidy, several studies provided evidence supporting a tumor suppressive role for polyploidy. Ganem *et al.* demonstrated that cytokinesis failure could trigger Hippo pathway activation, which led to growth inhibition [76]. Furthermore, when we tried to use genome editing tools to delete the *Apc* tumor suppressor in cells, diploid cells more readily lost heterozygosity of *Apc*, indicating that polyploids may be protected from tumor suppressor loss [77]. Other than for cancer protection, polyploidy is associated with adaptation in other contexts. Tetraploid yeast underwent accelerated environmental adaptation compared to diploid and haploid strains. This was mediated by beneficial chromosome aneuploidy, concerted chromosome loss (random loss of multiple chromosomes so that the cell ploidy returns to nearly diploid level [78]), and point mutations [79]. Some beneficial mutations were even specifically manifested by tetraploid yeasts. Moreover, polyploid

Arabidopsis exhibited higher potassium concentration in leaves, thus enhancing their salinity tolerance and survival after NaCl treatment [80].

The functional role of polyploidy in the mammalian liver has not been fully investigated yet, but several studies previously revealed some unique properties of polyploid hepatocytes. *In vitro* cultured polyploid hepatocytes could divide by forming multipolar spindles, resulting in aneuploid daughter cells with reduced DNA content, a phenomenon called a "reductive division" [81]. Although the prevalence of aneuploidy in normal hepatocytes is debated [82], a pool of aneuploid cells may increase genetic diversity within a tissue to facilitate adaptation to stress [79, 83]. It has also been hypothesized that this diversity may support the development of premalignant cells. However, since the role of aneuploidy in cancer is itself complicated and possibly context-dependent [84], linking polyploidy to aneuploidy does not make its role in cancer more clear.

Although polyploidy has been associated with cancer, its role in tumorigenesis is still unclear. Studies revealing different conclusions have suggested opposing roles for polyploidy, which leads to a more general conclusion that the role of polyploidy in cancer is context-dependent.

Dissertation objectives

The primary focus of this thesis was to define the functional roles of polyploidy in the liver, and to explore the therapeutic potential of polyploidization in liver tumorigenesis. To this end, we engineered mouse models with increased or decreased levels of liver polyploidy while avoiding the introduction of permanent genetic alterations. Moreover, from a therapeutic perspective, we collaborated with Dr. Daniel Siegwart's lab and the Alnylam Pharmaceutical Company to achieve liver specific RNAi targeting of a cytoskeletal gene called Anilin (*Anln*). Our first study explored the possibility of using genome editing tools to introduce somatic mutations in adult livers, and

led us to discover the increased difficulty of deleting tumor suppressor genes in polyploid hepatocytes. Following this lead, we decided to systematically study the role of polyploidy in liver cancer. We used multiple transient genetic manipulation methods to increase and decrease liver ploidy levels in order to faithfully examine the effect of ploidy change on tumorigenesis. Because liver polyploidy is mainly generated by cytokinesis failure, we hypothesized that cytokinesis inhibition might be a strategy to specifically inhibit the growth of transformed cancer cells without impairing normal tissue homeostasis. To this end, we inhibited cytokinesis by knocking down *Anln* in vivo using genetic models or siRNA inhibition, and tested this inhibition in multiple liver cancer and regeneration models. Altogether, with the versatile tools we developed, we hoped we could successfully reveal the functional role of polyploidy in the liver and explore its potential in liver cancer therapy.

CHAPTER 2

METHODOLOGY

Mice

All mice were handled based on the guidelines approved by the Institutional Animal Care and Use Committee at UTSW. *E2F8* KO mice were made by the Children's Research Institute Mouse Genome Engineering Core. CRISPR/Cas9 system was used to target intron 1 and 3, resulting in the deletion of exons 2 and 3. These mice were made and maintained in the C3H/HeJ background. *TG-shAnln* embryonic stem cells were injected into blastocysts by the UTSW Transgenic Core. The designing strategy of this mouse model was according to the paper from Scott Lowe's group [85]. Briefly, the *shAnln* sequence was cloned into the pCol-TGM vector (Addgene #32715) and electroporated into KH2 embryonic stem cells together with a Flpe vector. Validated KH2 clones were then injected into blastocysts to generate knock-in transgenic mice. *TRE-Cas9* mice were generated by Dr. Eric Olson's Laboratory. C57BL/6J-ApcMin/J mice were purchased from the Jackson Laboratory (https://www.jax.org/strain/002020). The inducible *LAP-MYC* mice were carried on a pure FVB strain background. FRG mice and nitisinone (NTBC) were purchased from

Yecuris Corporation (10-0001). All other mice used in experiments were WT C3H/HeJ or FVB mice. All experiments were done in an age and sex controlled fashion unless otherwise noted in the figure legends. The experimental mice were randomized using a simple randomization method.

TALEN Design and Construction

TALENs were designed using the TALE-NT software [86] and assembled using methods described in Cermak *et al.* [87]. To construct TALEN plasmids, intermediary arrays were produced for each TALEN-pair that were compatible for Golden Gate cloning into pC-GoldyTALEN (Addgene, #38143). Adenoviral *Apc* TALENs were subcloned by cutting *Apc* TALENs from pC-GoldyTALEN construct with SpeI and EcoRI to transfer the full gene expression cassette to the adenoviral vector pACCMVpLpA(-)loxP-SSP. The *Apc*-TALEN adenovirus was generated by the Molecular Biology Vector Core, UTSW.

Cell culture and transfection

The H2.35 cell line was obtained from ATCC and has been cultured for less than 6 months. Cells were cultured in DMEM with 4% (vol/vol) FBS, 1x Pen/Strep (Thermo Scientific) and 200nM Dexamethasone (Sigma). For TALEN transfection, cells were transfected with 2 μg of each TALEN arm in 6-well plates by using Lipofectamine 2000 (Life Technologies), and were cultured for 48 or 72 hours before performing assays. For siRNA treatment, cells were transfected with 25pmol siRNA (Life Technologies) in 6-well plates by using Lipofectamine RNAiMAX and OptiMEM (Life Technologies), as described in the manufacturer's instructions. Transfected cells were cultured for 72 hours before performing RNA extraction and fixation for flow cytometry. For the cell synchronization assay, H2.35 cells were synchronized at G2–M phase by a nocodazole

block. Briefly, siRNA transfected cells were treated with 150ng/mL nocodazole (Sigma) at 36 hours after transfection for 8 hours. After releasing, cells were harvested by 4% PFA (Invitrogen) fixation in every 20 minutes, from 0 min until 140 min. Then the cells were subjected to immunofluorescence staining.

Analysis of TALEN Gene Editing

Genomic DNA for transfected cells and mouse liver samples were collected using QuickExtract DNA Extraction Solution (Thermo Fisher Scientific). Genotyping was conducted using PCR, followed by restriction enzyme assay. Mutations were assessed by loss of restriction enzyme digestion. ImageJ was used to quantify the percent TALEN-modified alleles by measuring the intensity of uncut PCR product band vs. total bands post-digestion. To verify mutations, the gel-purified uncut PCR products were cloned into the TOPO TA Cloning Kit (Invitrogen) and sequenced.

Xenograft Experiments

Nude mice were injected s.c. with $1x10^7$ H2.35 parental, H2.35 Apc+/+ (clone #25) or Apc-/- cells (clone #29). Cells were suspended in a 1:1 ratio of Matrigel (BD Bioscience) and serum free media, and 5 tumors for each cell type were inoculated. Tumor volume was calculated according to the formula (length x width2)/2.

Western Blot Assay

Liver tissues were ground in T-PER Tissue Protein Extraction Reagent, cells were lysed in RIPA buffer (Thermo Scientific) and proteins were separated in a 4–20% precast polyacrylamide gel and

transferred to a Nitrocellulose membrane (BioRad). The following antibodies were used: AcV5 (Sigma, A2980), APC (Calbiochem, OP44), anti-β-Actin (Cell Signaling, #4970), Anti-Anln (Abcam 154337), Anti-E2f8 (Abcam 109596), Anti-γH2A.X (Cell Signaling, 2577S), Anti-p-BRCA1 (Cell Signaling, #9009), Anti-p-p53 (Cell Signaling, #9286), Anti-rabbit IgG, HRP-linked Antibody (Cell Signaling, #7074) and Anti-mouse IgG, HRP-linked Antibody (Cell Signaling, #7076).

Hepatocyte Isolation and Transplantation

Primary mouse hepatocytes were isolated by two-step collagenase perfusion. Cell number and viability were determined by Trypan blue exclusion in a hemocytometer. 10^6 viable hepatocytes in 100µl of DMEM without serum were injected intrasplenically into FRG mice. The concentration of NTBC was cycled.

Flow Cytometry

Primary hepatocytes were fixed in 75% ethanol ($2x10^6$/mL) at -20°C. For ploidy analysis, hepatocytes were incubated with 500uL ($2x10^6$ mL) of PI/Rnase Staining Buffer (BD Pharmingen) at 25°C for 15min. Cells were analysed with FACS Aria II SORP machine (BD Biosciences). The transfected H2.35 cells were isolated by trypsinization. Cells ($1×10^6$ mL) were incubated with 10µM Hoechst 33342 (Sigma), 5ug/ml propidium iodide and 5µM reserpine (Invitrogen) for 30min at 37°C. Cells were analysed and sorted using a 100µm nozzle. DNA content was identified using an ultraviolet 355-nm laser.

Histology

Tissue were fixed in 4% paraformaldehyde (PFA) overnight at 4°C, then in 70% ethanol and embedded in paraffin. Sectioning and HE staining were performed by the Molecular Pathology Core at UTSW. To make frozen sections, tissue was fixed in 4% PFA for 2 hours at 25°C, dehydrated overnight in 30% w/v sucrose, embedded in Cryo-Gel (Thermo Fisher) and frozen on dry ice. Sections were 8 μm.

Immunohistochemistry (IHC) and Immunofluorescence (IF)

IF staining of cultured cells. Cells seeded on poly-L-lysine coated glass coverslips (BD Biosciences) were fixed in 4% PFA for 30 minutes and then incubated in 0.5% Triton X-100 (Biorad) in PBS for 15 minutes at 25°C, followed by blocking with 10% FBS-PBS for 1 hour at 25°C. Slides were incubated with primary antibody overnight at 4°C, then fluorophore conjugated secondary antibody for one hour at 25°C, then mounted. The following antibodies were used: AcV5, β-catenin (BD, #610154), anti-glutamine synthetase (GS) rabbit antibody (Abcam, ab49873), anti-Fah antibody (Yecuris, 20-0034), Alexa Fluor® 488 goat anti-rabbit IgG (Invitrogen, A11008), Alexa Fluor® 488 goat anti-mouse IgG1 (Invitrogen, A21121).

IF and IHC on tissue sections. Frozen sections were incubated in blocking buffer (5% BSA and 0.25% Triton X-100 in PBS) for 1 hour at 25°C. Slides were incubated with primary antibody overnight at 4°C, then fluorophore conjugated secondary antibody for one hour at 25°C, then mounted. IHC of paraffin sections was performed in the standard fashion. Detection was performed with the Elite ABC Kit and DAB Substrate (Vector Laboratories). The following primary antibodies were used: Ki67 (Abcam, ab15580), Cyp2e1 (Abcam, ab28146), Pten (Cell Signaling, #9559S), Ctnnb1 (BD Transduction Laboratories #610154), γH2A.X (Cell Signaling, 2577S). Confocal images were taken by Zeiss LSM 780 Upright confocal/multiphoton microscope.

H&E slides were interpreted by a clinical pathologist with expertise in human liver cancer diagnosis.

Early weaning

Male pups from C3H mothers were randomized into two groups at P13 based on their body weight: an early and a normal weaning group. The early weaned mice were placed into a new cage without their mothers and provided with moist food. The normally weaned mice were kept with their mothers and at P21, placed into a new cage without their mothers. Both groups were given a single dose of DEN at P19 (25ug/g) based on their body weights. Tumor burden was examined at 5 months after DEN injection.

In vivo siRNA experiments

For in vivo experiments in C3H, *LAP-MYC, Rosa-rtta; TRE-Cas9,* FVB *and* $P53^{fl/fl}$*;* $Rb1^{fl/fl}$*;* $Rbl2^{fl/fl}$ mice, lipid nanoparticles (LNPs) were used to package either Control (Life Technologies, #4457289), *Anln siRNA* (Life Technologies, #4457308, s87033), *Cdk1* siRNA (Life Technologies, #4457308, s63731) or *E2f8 siRNA* (Life Technologies, #4457308, s99361) at 2 mg/kg, two times a week for a total of 4 times (2 intraperitoneal and 2 retroorbital). LNPs were formulated following previously reported component ratios [88] with the aid of a microfluidic rapid mixing instrument (Precision Nanosystems NanoAssemblr) and purified by dialysis in sterile PBS before injection.

GalNAc conjugated Anln siRNAs

These were obtained from Alnylam Pharmaceuticals. 10mg/ml stock for si*Luc* and si*Anln* was stored at -20°C. The working concentration of the siRNA was 4mg/ml, diluted in PBS. We chose

two *siAnln* (#2 and #4) with good knockdown efficiency for the subsequent experiments. C3H mice were subcutaneously injected with *siLuc, siAnln#2* or *siAnln#4* at 4.0mg/kg since P8-10. Injections were given 4 days apart for a total of 3 times.

Chemical injury experiments

CCl_4 is diluted 1:10 in corn oil (Sigma), and administered IP at a dose of 0.5 ml/kg of mouse as described previously [89]. DEN (Sigma) is diluted in saline and administered IP at different doses, depending on mouse age. For P19 mice, 25μg/g of mouse was injected once; for P24-P27 mice, 75μg/g was injected once; for P34 mice, 100μg/g was injected once.

Partial hepatectomy

Two-thirds of the liver was resected as previously described[90].

Liver function tests

Blood samples (~50μl) were collected retro-orbitally in heparinized tubes. Liver function tests were performed by the UTSW Molecular Genetics Core.

High fat diet experiments

High fat diet (HFD) was purchased from RESEARCH DIETS INC. 60% calories were from fat. Animals were kept on HFD from 1.5 to 8 months of age.

Virus experiments

100µL of Ad-*Cas9-sgPten* (Vectorbiolabs) was retro-orbitally injected at a dose of 10^9 pfu/mouse. 100µL of Adenovirus-GFP (University of Iowa Viral Vector Core) was retro-orbitally injected at a dose of 1.4 X 10^8 pfu/mouse. 100µL of AAV-sgApc (5 X 10^{12} pfu/mouse) was retro-orbitally injected. 100µL of Ad-*Cas9-sgPten* (10^9 pfu/mouse) plus AAV-Cre (University of Pennsylvania Vector Core, 2.5 X 10^{10} pfu/mouse) was retro-orbitally injected. 100µL of Ad-*Cas9-sgPten* (10^9 pfu/mouse) plus AAV-KPL (10^{12} pfu/mouse, Boston Children's Hospital Viral Core) was retro-orbitally injected.

RNA Extraction and RT-qPCR

Total RNA was isolated using Trizol reagent (Invitrogen). For qRT-PCR, cDNA synthesis was performed with 1µg of total RNA using iScript Reverse Transcription Kit (Biorad). See Table S1 for primers used in these experiments. Gene expression levels were measured using the ΔΔCt method as described previously [91].

ROS detection

As described by Sun et al. [92]. For ROS detection in fresh tissues, DHE (Sigma) staining for superoxide was performed. Cryosections (10 µm) were freshly cut and incubated with 10 µM DHE at 37°C for 30 min. Ethidium staining was visualized using laser confocal microscopy (LSM 780, Zeiss) at the UTSW Live Cell Imaging Facility. The red signal corresponded to levels of cellular superoxide anion and the intensities were quantified in 20 cells from five fields for each mouse by ImageJ.

Fluorescence In Situ Hybridization (FISH) assay

Two FISH probes for mChr12 were provided by Dr. Hongtao Yu lab. Bacterial artificial chromosomes were nick translated with the CGH Nick Translation Kit (Abbott Molecular) using Red 580 dUTP and Green 496 dUTP (Enzo Life Sciences). Isolated primary hepatocytes were treated with 0.56% KCL and fixed with cold 3:1 methonal: acetic acid solution. Then the fixed cells were dropped onto slides, and allowed to dry. Then the slides were incubated with probes, covered with coverslips sealed with rubber cement. Slides were incubated at 80°C for 5 min and 37°C overnight. Following incubation, slides were washed in 0.5XSSC+0.1% at 70°C for 5 min, 1XSSC for 3X5 min at room temparature, 4XSSC+0.1% Tween for 5 min at room temperature, and 2XSSC for 5 min, and then mounted with DAPI (Vectorlabs). Samples were analyzed and scored under a Olympus IX83 microscope. For analysis of nuclei ploidy, 2 green and 2 red dots was counted as a 2c nucleus, and 4 green and 4 red dots was counted as a 4c nucleus. 60 nuclei were counted for each sample.

Genomic DNA isolation and sequence processing

50 flash-frozen tumors free of visible normal tissue were used for library preparation. The genomic DNA was extracted using QIAGEN AllPrep DNA/RNA Kit (Cat. 80204). Integrity of genomic DNA was assessed by electrophoresis on 1% agarose gels, and concentration was determined by nanodrop. gDNA was sonicated into 500bp fragments and purified using Genomic DNA Clean & Concentrator Kit (ZYMO RESEARCH). The DNA library was prepared using Ovation Target Enrichment System (NuGEN) following the manufacturer's instructions. Target genes were selected from human HCC and mouse sequencing studies [93-95] and some well-known cancer related genes. The target probes were synthesized by NuGEN. More than 99.5% of the probes

had >90% coverage. The sequencing was performed using a 150 bp single-end protocol on Illumina NextSeq 500 platform.

Sequence processing

BCL files from Illumina Nextseq 500 sequencing were converted to FASTQ files by bcl2fastq (Illumina). After trimming by trim_galore package, BWA-MEM (version 0.7.15) was used to align FASTQ files to reference genome GRCm38 with subsequent processing by Samtools (version 1.3) and Nudup.py (Nugen) to ensure proper file formatting and remove duplicates. Alignments were then recalibrated and realigned by GATK (version 3.5). We acquired 42 million uniquely mapped reads on average for the 53 samples we sequenced with an average on target coverage at 128X and more than 86.6% region has more than 50X coverage.

Identification and annotation of somatic SNVs

To detect somatic variants in tumor samples, we use the somatic variant detection program Mutect (version 1.1.7). 50 tumor samples were called against a panel of 3 normal liver samples from two WT C3H/HeJ mice to the reference genome GRCm38. Variants passed the Mutect high-confidence somatic mutation filters were selected and further filtered against from known SNVs in C3H/HeJ mice provided by http://ftp-mouse.sanger.ac.uk (mgp.v3). SNVs were further annotated using snpEff (version 4.2) and Variant Effect Predictor. SNVs predicted to have High or Moderate impact were compared to a stringent list of 125 driver genes in human cancer by Vogelstein et al [96] to map putative driver genes and mutations. The mutation landscape was graphed by using GenVisR (a package from R Bioconductor) waterfall plot algorithm on putative driver genes for all 50 tumor samples (Figure 6a).

Statistical analysis

The sample size was determined by producing a confidence interval estimate with a specified margin of error to ensure that a test of hypothesis has a high probability of detecting a meaningful difference in the parameter. The data in most figure panels reflect multiple experiments performed on different days using mice derived from different litters. Variation is indicated using standard error presented as mean ± SEM. For each dataset, we first performed the Shapiro-Wilk normality test and the D'Agostino's K-squared test. If the dataset passed the normality test, we then conducted the F-test to see whether the variances of the two groups were equal or not. If variances were unequal, we conducted the hypothesis test using t-test with Welch's correction (assuming unequal variances); if variances were equal, we conducted the hypothesis test using the two tailed student's t-test. If the dataset did not pass the normality test, we then conducted the hypothesis test using non-parametric test Mann-Whitney U test. Statistical significance is displayed as $p < 0.05$ (*) or $p < 0.01$ (**) unless specified otherwise. The investigators were blinded during the processes of mice treatments and data analysis. Image analysis for the quantification of cell proliferation, *Pten* deletion, GFP+ cells, liver surface tumor and malignant nodule numbers were performed in a blinded fashion.

CHAPTER 3

TALEN MEDIATED SOMATIC MUTAGENESIS IN MURINE MODELS OF CANCER

Introduction

Genome-sequencing has identified many uncharacterized genetic lesions in hepatocellular carcinoma (HCC), the third most common cause of cancer related death in the world [97-101]. These efforts have introduced an overwhelming amount of information that remains correlative until functionally validated. Since there are few effective therapies for HCC, and virtually no prognostic or predictive markers based on molecular understanding of the disease, it would be important to increase our understanding of HCC genetics. RNAi has traditionally been used to assess gene function in cell lines, but this technology fails to generate genetic nulls and is also plagued by off-target effects [102]. The most powerful studies of in vivo gene function involve genetically engineered mice, but these approaches are time consuming. Conditional knockouts and transgenics often result in organ-wide or whole-body mutants that do not accurately model disease states. Thus, faster and better methods for modeling somatic mutations in mouse models are needed.

Recently, powerful tools for genome engineering have been developed, including Transcription Activator-Like Effector Nucleases (TALENs) [87, 103, 104] and Clustered Regularly Interspaced Short Palindromic Repeats (CRISPRs) [105-107]. Genome-editing techniques are usually employed in cell culture, but they are also being introduced in vivo to make knockout zebrafish [108-110], xenopus [111, 112], rats [113] and even floxed mice [114-117]. However, these animals are generally made from embryonic stem cells or mutated zygotes and result in germline mutants. These methods increase experimental efficiency, but do not offer a fundamentally new way to model alterations in cancer genes in vivo.

In this study, we used liver cancer as a platform to determine if TALENs can accurately and efficiently target genes in vitro and in vivo. To demonstrate this, we chose to focus on driver genes with well-understood functions in tumor initiation and maintenance. The WNT signaling pathway is frequently altered in HCC, with 32.8% and 1.6% of HCCs harboring *β-catenin* and *Adenomatous Polyposis Coli* (*Apc*) mutations, respectively [98]. We designed TALENs directed against *β-catenin* and *Apc* and employed them to generate isogenic HCC cell lines. Next we asked if TALENs were able to generate somatic mutations after delivery into mouse liver using hydrodynamic transfection (HDT) [118]. Surprisingly, HDT of *β-catenin* TALENs consistently generated *β-catenin* induced murine tumors. The same method was not able to efficiently induce homozygous *Apc* loss in vivo, a finding that was due in part to the high number of polyploid hepatocytes in the liver. To increase the efficiency of tumor suppressor editing, we packaged TALENs in adenoviral vectors. After delivery of these Ad-TALENs, we found that approximately 5% of cells in the liver had completely lost *Apc* function. These results show that efficient and physiologic liver cancer mouse models can be generated with in vivo TALEN delivery.

Generating targeted mutations in isogenic liver cell lines

Isogenic cell lines can be used to precisely understand the contribution of a genetic alteration toward cellular phenotypes. We first designed a pair of TALENs that target *β-catenin*, a commonly mutated gene in HCC [119]. Mutations in *β-catenin* are frequently found in codons 32, 33 and 45 because these codons are within a negative regulatory motif containing an E3 ubiquitin ligase recognition region [120]. When this motif is abrogated, *β-catenin* stability increases due to the lack of ubiquitinylation and degradation. Thus, we engineered TALENs to target the region around codons 32 and 33 in exon 2 (Figure 1A). To first test TALEN efficiency in vitro, we transfected these *β-catenin* targeted TALENs into H2.35 cells, an immortalized hepatocyte cell line. Using an antibody against AcV5, an epitope tag fused to each TALEN, we detected high protein levels of the TALEN pair (Figure 1B). Because the TALEN target region in *β-catenin* includes an XmnI enzyme site, TALEN mutated PCR products cannot be digested by XmnI. Using endonuclease digestion, we found that the TALEN editing efficiency was 27.4% (Figure 1C). After TALEN cutting, double-strand DNA breaks are repaired by Non-Homologous End Joining (NHEJ), thus the resulting mutations are variable in distinct cell clones. As expected, subcloning and sequencing of the uncut band revealed deletion and insertion mutations, or indels, in the TALEN targeting region (Figure S1). Normally, *β-catenin* is localized on the cell membrane and cytoplasmic *β-catenin* degradation is facilitated by the *Apc/Axin* complex and subsequent ubiquitinylation. Among H2.35 cells treated with the TALEN pair (but not with individual TALENs), 5-10% had cytoplasmic *β-catenin* staining as measured by IF (Figure 1D), indicating that the *β-catenin* mutations result in increased cytoplasmic protein stability.

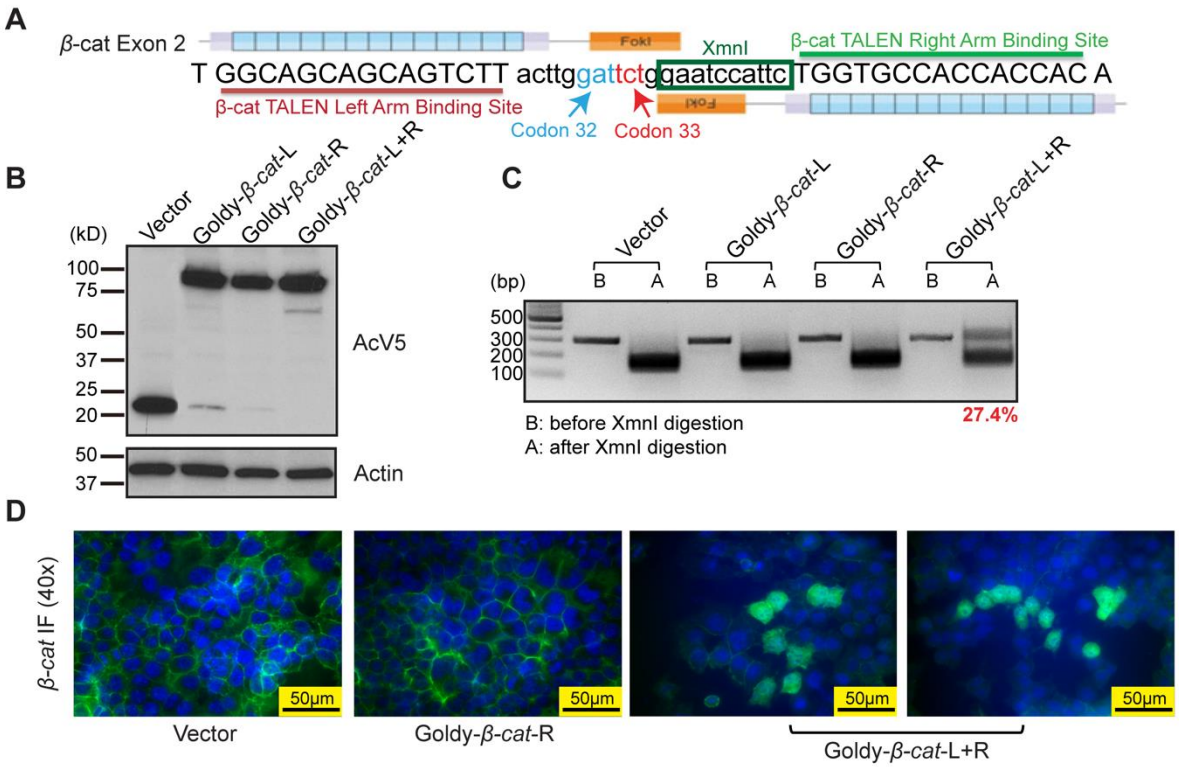

Figure 1. *β-catenin* TALENs are effective and efficient in vitro.

(A) Design of *β-catenin* (*β-cat*) GoldyTALEN. The target region contains *β-catenin* codon 32 and 33 and an XmnI cut site between the two TALENs. (B) Protein expression of *β-catenin* TALENs in H2.35 cells. H2.35 cells were transfected with GoldyTALEN control vector, single TALENs, or TALEN pairs. Cells were harvested and subjected to western blot 48 hours after transfection. AcV5 is an epitope tag fused to the TALENs. (C) *β-catenin* TALEN efficiency in H2.35 cells. Genomic DNA was PCR amplified for the region targeted by TALENs and digested by XmnI. The uncut band in A lane is mutated DNA. TALEN efficiency is determined by the ratio of uncut band vs. total bands. (D) IF staining in H2.35 cells for *β-catenin*. Cells were fixed 72 hours after

transfection and stained for *β-catenin* (Green). Cytoplasmic localization of *β-catenin* (arrow) is seen in cells treated with the TALEN pair.

In addition to oncogenes like *β-catenin*, we also wanted to target tumor suppressors. *Apc*, a tumor suppressor in the Wnt signaling pathway, is commonly mutated in hepatic adenomas [121], hepatoblastomas [122] and HCCs [123]. Our *Apc* TALENs were designed to target exon 9 (Figure 2A). Transfection of the *Apc* TALEN pair into H2.35 cells resulted in high TALEN expression (Figure 2B) and a 71% mutation efficiency (Figure 2C). Because *Apc* is required for *β-catenin* degradation, we found that approximately 2-5% of *Apc* TALEN transfected cells had *β-catenin* localization in the cytoplasm (Figure 2D). We then performed single cell clonal analysis, and found that 13.9% of the clones were homozygous (5/36) and 50% were heterozygous (18/36) for *Apc* mutations in exon 9 (Figure S2A). Subcloning and sequencing of the TALEN targeted gene region showed the expected indels (Figure S2B). Next, we expanded wild-type *Apc* clone (#25) and homozygous *Apc* mutant clone (#29) and confirmed the expected *Apc* protein levels (Figure 2E). The mutation in clone #29 caused a pre-stop codon (TAA) at codon 342 (Figure 2E). This would theoretically result in a 41kD truncated protein, but this was not seen on western blot likely because the truncated protein is degraded soon after translation (Figure 2E). Next, we subcutaneously transplanted these clones into nude mice and measured the growth of these xenografts (Figure 2F). The homozygous *Apc* mutant tumors grew faster than both the WT and parental H2.35 tumors (Figure 2F). These results confirm the efficiency and specificity of the *β-catenin* and *Apc* TALENs in vitro and in xenograft models of HCC.

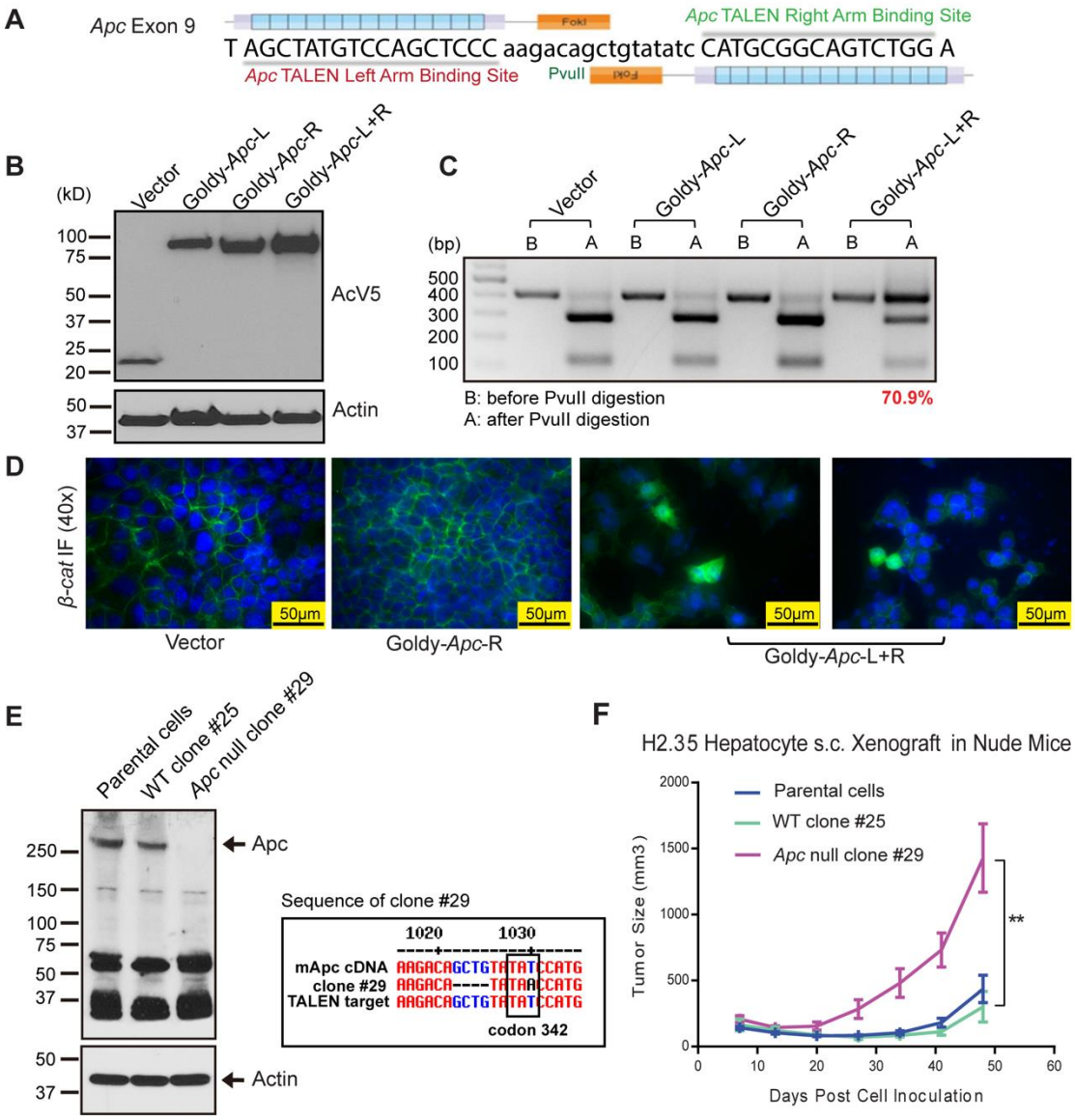

Figure 2. *Apc* TALENs are effective and efficient in vitro and in xenografts.

(A) Design of *Apc* GoldyTALEN. The target region in exon 9 contains a PvuII cut site. (B) Protein expression of *Apc* TALENs in H2.35 cells. H2.35 cells were transfected with GoldyTALEN vector, single TALENs, or the TALEN pair. Cells were harvested and subjected to western blot 48 hours after transfection. (C) *Apc* TALEN efficiency in H2.35 cells. Genomic DNA was PCR amplified

for the region targeted by TALENs and digested by PvuII. TALEN efficiency is determined by the ratio of uncut band vs. total bands. (D) IF staining in H2.35 cells for *β-catenin*. Cells were fixed after 72 hours of transfection and then stained for *β-catenin* (Green). Cytoplasmic localization of *β-catenin* (arrow) is seen in cells treated with the TALEN pair. (E) Western blot for *Apc* in H2.35 cell clones and the sequencing data of *Apc* mutant clone #29. The H2.35 parental cells and WT clone #25 express full length *Apc,* and mutant clone #29 has no full length *Apc,* as well as the predicted truncated *Apc*. (F) Growth curve of the H2.35 xenografts subcutaneously transplanted into nude mice.

TALEN mediated mutagenesis in murine livers can drive tumor development

In order to directly perform mutagenesis in vivo, we delivered TALENs into the liver via hydrodynamic transfection (HDT). The liver has the highest levels of gene expression after HDT [124]. Consistent with this, western blot and IHC showed high TALEN protein expression 8 hours after HDT (Figure 3A, B). To ensure that tumors would form within one year, we introduced the liver carcinogen *Diethylnitrosamine* (DEN) at 2 weeks of age. We also used mice on the C3H strain background, which has a high predisposition for liver cancer [125]. Starting at 7 weeks of age, we performed weekly HDT for five weeks to introduce *β-catenin* targeted TALENs (schema shown in Figure 3C). At 34 weeks of age, there was extensive tumorigenesis in both control and TALEN HDT groups (Figure 3D**;** Figure S3A). TALEN injected mice did not harbor more frequently or larger tumors than saline injected mice. However, 3 out of 4 mice in the *β-catenin* TALEN treated group harbored tumors with a red, fleshy appearance (Figure 3D and Figure S3A), while tumors with this gross morphology were not seen in the control group (Figure 3D and Figure S3A). Histologic examination revealed that these red fleshy tumors were more poorly

differentiated HCCs with reduced fatty droplets (Figure 3F), which likely explained the distinct tumor color. In each of these tumors, genotyping and sequencing identified in-frame mutations that the *β-catenin* TALENs were designed to induce, while tumors without this appearance did not harbor *β-catenin* mutations (Figure 3E; Figure S3B and C).

To determine if TALENs could generate tumors without an accelerating carcinogen, we next performed the same HDT procedure in C3H mice without giving DEN. At 34 weeks, we found that in the GoldyTALEN vector alone treated group, 3 of 5 mice had small single liver tumors, most of which were less than 5mm in diameter (Figure 3G and Figure S4A). None of these tumors contained *β-catenin* mutations in the TALEN targeted region (Figure 3H and Figure S4B). However, all of the *β-catenin* TALEN treated mice developed liver tumors, and 2 of 5 mice had large tumors (Figure 3G and Figure S4A). 4 of 5 mice had tumors with *β-catenin* mutations (Figure 3H and Figure S4B), and no mutations were found in adjacent normal tissue (Figure S4B). These sequencing results again confirmed that the mutations were caused by TALEN genome editing, and all were in-frame (Figure S4C).

Next, *β-catenin* and *Glutamine Synthetase* (GS) immunostains were used to analyze the tumors for Wnt pathway dysregulation. GS is a transcriptional target of Wnt signaling and its expression is normally restricted to peri-central vein hepatocytes. GS positivity in non-peri-central hepatocytes indicates aberrant Wnt activation, which could be caused by events such as constitutive *β-catenin* activation or *Apc* loss [126]. In tumors from mice that were not treated with TALENs, no GS or cytoplasmic *β-catenin* could be seen. In contrast, all tumors harboring TALEN mediated *β-catenin* mutations had both GS overexpression and *β-catenin* mis-localization (Figure 3F and I). These results show that HDT of TALENs is sufficient to create targeted somatic

mutations in the liver and also induce HCCs in the presence or absence of other tumor promoting agents.

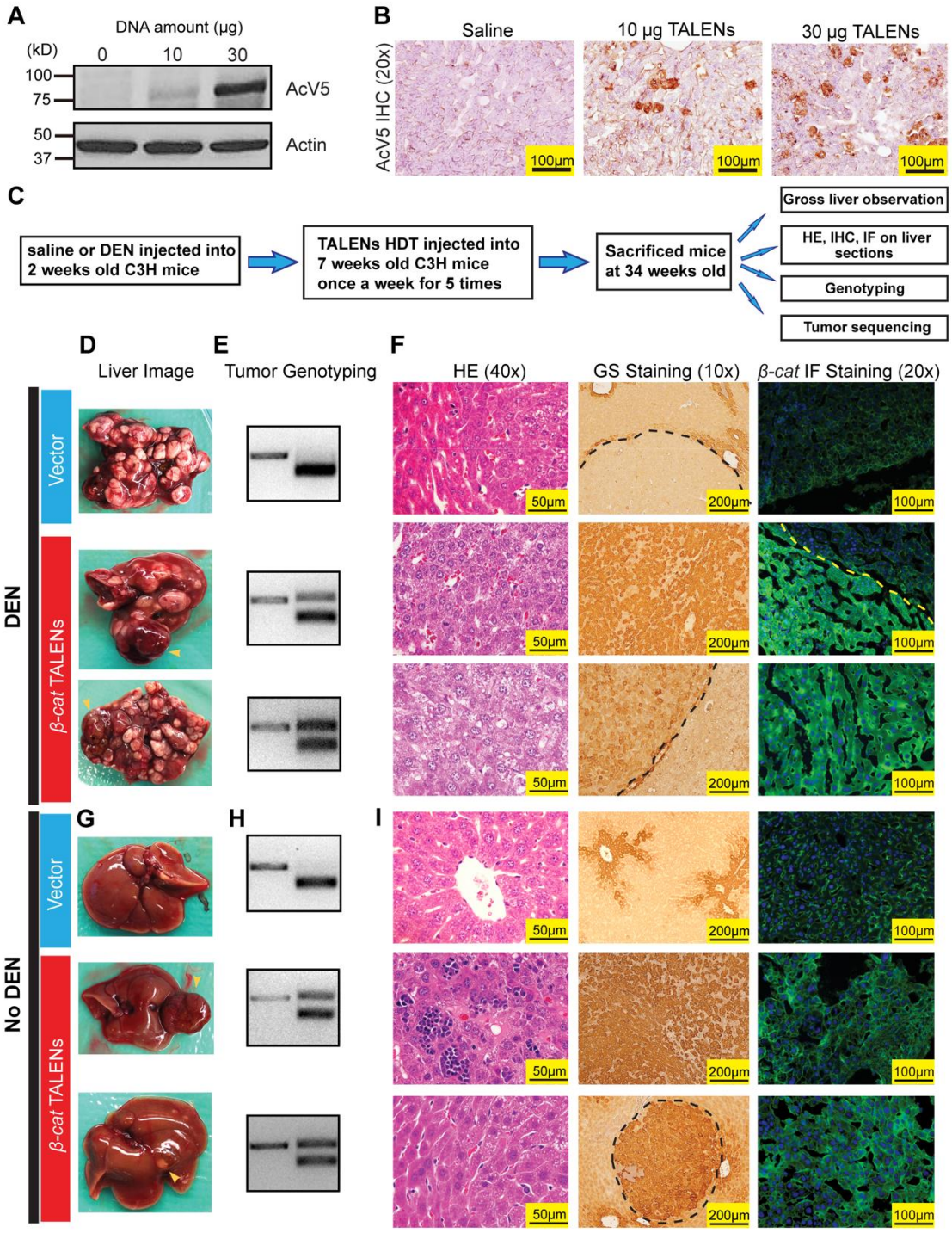

Figure 3. TALEN mediated somatic mutagenesis in murine livers can drive tumor development.

(A) Protein expression of *β-catenin* TALENs in liver 8 hours after HDT. C3H mice were HDT administrated with saline, 10μg or 30μg of each TALEN. (B) IHC for AcV5 showing liver *β-catenin* TALEN expression after HDT injection. (C) Schema for using *β-catenin* TALENs to induce mutations in C3H mice. (D) Gross liver images of the C3H mice treated with GoldyTALEN vector (20ug) or *β-catenin* TALENs (10ug of each) plus DEN according to the schema in (C). Yellow arrows point to red, fleshy tumors, which were only found in *β-catenin* TALEN treated mice. (E) Tumor genotyping of the above mice. For *β-catenin* TALEN injected mice, the red, fleshy tumors were genotyped (if these tumors were identified). (F) H&E staining (40X), GS IHC staining (10X) and *β-catenin* IF staining (20X) of the tumors and livers from the above mice. For *β-catenin* TALEN injected mice, the red, fleshy tumors were genotyped (if these tumors were identified). (G) Gross liver images of the C3H mice treated with GoldyTALEN vector (20ug) or *β-catenin* TALEN (10ug of each) without DEN. The red, fleshy tumor is indicated by the yellow arrow. (H) Tumor genotyping of the above mice. (I) H&E staining (40X), GS IHC staining (10X) and *β-catenin* IF staining (20X) of the tumors and livers from the above mice.

Polyploidy protects the liver from TALEN mediated tumor suppressor loss

While oncogene activation is a common mechanism of liver tumorigenesis, it would also be important to develop models for homozygous tumor suppressor loss. HDT using our previously validated pair of *Apc* TALENs resulted in a 7-19% mutation rate in vivo (Figure 4A). Despite this

high rate, we did not observe frequent ectopic GS expressing cells representing *Apc* homozygous clones or any tumors with exon 9 *Apc* mutations, with or without DEN (Figure S5).

Up to 90% of mouse hepatocytes and 50% of human hepatocytes are polyploid [33, 81, 127, 128]. Because of this unique feature of the liver (Figure 4B), we hypothesized that polyploidy might protect the liver from homozygous loss of tumor suppressors. To examine this hypothesis, we analyzed the ploidy distribution of H2.35 cells using flow cytometry and identified distinct 2c and 4c populations (Figure 4C). Because 4c populations could represent either tetraploid cells in G0/G1 phase (4n, 4c) or diploid cells in G2/M phase (2n, 4c), we counted chromosome numbers in these populations after karyotyping, revealing that the 2c and 4c populations contained high frequencies of diploid (2n) and tetraploid (4n) cells, respectively (Figure 4C and D). To test if tetraploid hepatocytes are less likely to mutagenize all copies of *Apc* than diploid hepatocytes, we co-transfected H2.35 cells with *Apc* TALENs and a GFP plasmid. To select successfully transfected cells, we isolated GFP+ diploid or tetraploid hepatocytes by flow cytometry and grew them as single cell clones (Figure 4E and F). Genotyping of these clones showed that there was a higher frequency of homozygous *Apc* mutant clones in the diploid than in the tetraploid population ($n = 4$ experiments; $p = 0.013$, Figure 4G). These results indicate that polyploidy is one potential mechanism of protecting against LOH, and show that improved TALEN delivery methods are required to efficiently delete tumor suppressors in the liver.

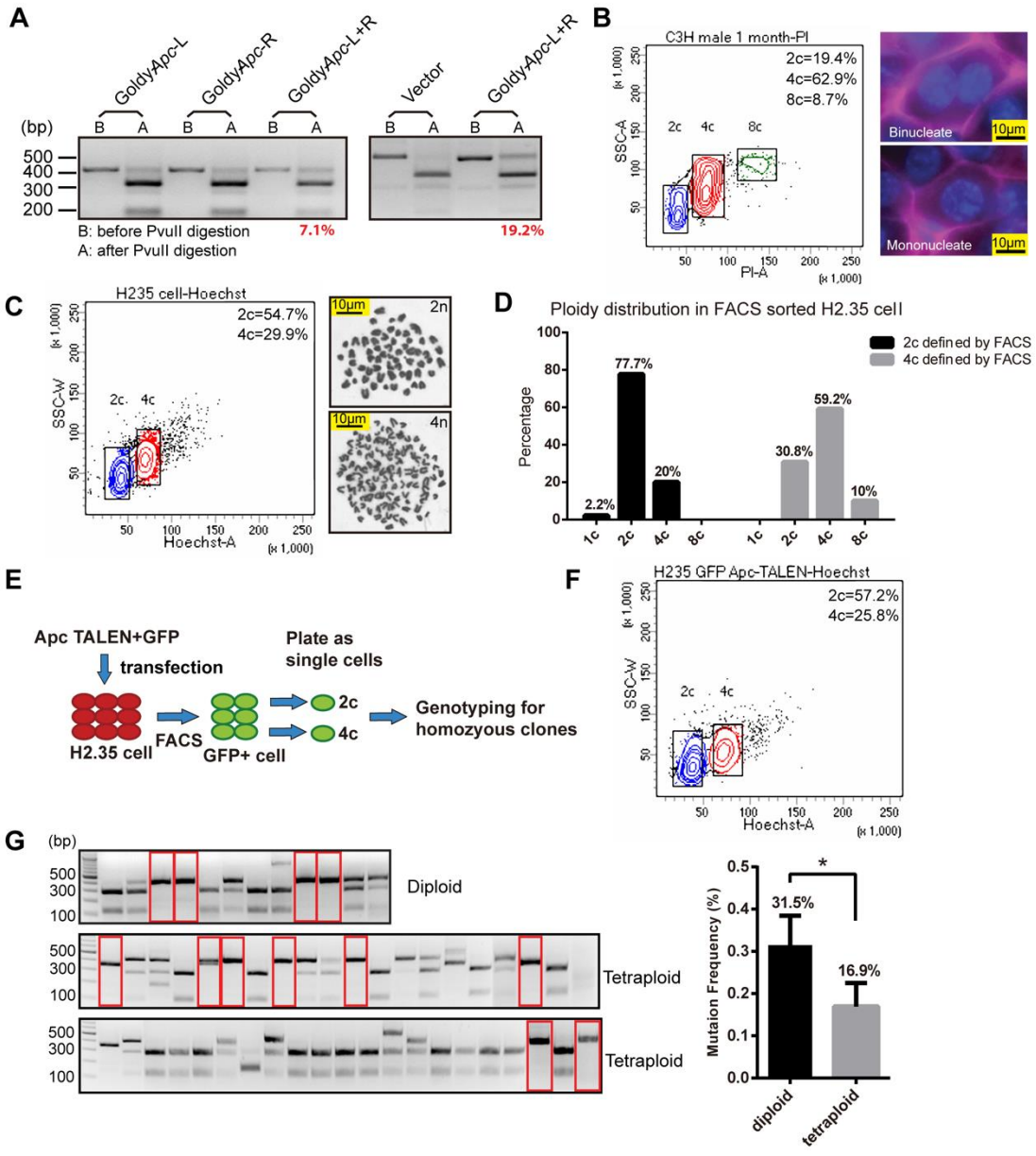

Figure 4. Hepatocyte polyploidy protects the liver from TALEN mediated tumor suppressor loss.

(A) Genotyping of mouse liver treated with *Apc* TALENs by HDT. Mice underwent HDT with GoldyTALEN vector (20ug), *Apc* single TALENs (20ug), or TALEN pair (10ug of each TALEN)

at 6 weeks of age, then weekly x 4 (left panel) or x 2 (right panel). (B) FACS showing DNA content distribution, as stained by PI/RNAse, of primary hepatocytes in a 1 month old C3H mouse. The right two panels are liver IF images showing a mononucleated and a binucleated hepatocyte. *β-catenin* (purple) stains the membrane. (C) The left panel shows the DNA content distribution for H2.35 cells, which were stained by Hoechst 33342 and sorted into 2c and 4c populations. Representative karyotypes of the sorted cells are shown. (D) Ploidy distribution within the sorted populations. 50 cells were counted for each population. (E) Experiment assessing the efficiency of TALEN induced *Apc* LOH in diploid vs. tetroploid cells. H2.35 cells were transfected with TALENs and a GFP plasmid. GFP+ cells were sorted and separated by ploidy and plated as single cell clones. Genotyping was performed on individual clones. (F) DNA content distribution (Hoechst 33342) of the H2.35 cells transfected with *Apc* TALENs. (G) Genotyping of the H2.35 cell single clones described in (E) and (F). The red rectangles highlight homozygous clones. The experiment was performed four times and the overall percentage of homozygous clones is shown on the right.

Adenovirus TALEN delivery increases mutagenesis efficiency in vivo

Besides polyploidy, a major barrier to obtaining high mutagenesis rates is the low efficiency of HDT (Figure 3B). To overcome this issue, we packaged our TALENs into adenovirus (Ad-TALENs). We cloned *Apc* targeting TALENs into the adenovirus shuttle pACCMVpLpA(-)loxP (Figure 5A) and made high-titer adenovirus expressing *Apc* TALENs (designated Ad-*Apc*-TAL-R/L). Each TALEN (Ad-*Apc*-TAL-R and L) was packaged separately because TALENs were too large to be included in a single adenoviral shuttle. We first confirmed that proteins of the correct

size are produced (Figure 5B), and that *Apc* is efficiently mutated after transfection of the adenoviral plasmids into H2.35 cells (Figure 5C). After packaging into adenovirus, all the viral plaques carrying the left TALEN resulted in slightly truncated protein (Figure 5D and Figure S6). Nevertheless, the right TALEN protein was intact, so we injected the TALEN adenoviruses into the tail veins of mice.

Besides attempting to improve the efficiency of TALEN delivery, we also tried to increase the probability of generating cells with *Apc* LOH by using the Apc^{Min} mouse strain. This mouse contains a heterozygous mutation in codon 850 of *Apc*, which results in a truncated, non-functional protein [129]. Since the Apc^{Min} mutation site is in exon 16, our TALEN target genotyping assay was still specific for quantifying TALEN induced mutagenesis rates in exon 9. As expected, Ad-*Apc*-TAL-R/L exhibited much higher in vivo expression as assessed by western and IF (Figure 5D and E). This led to a 33% mutagenesis rate in exon 9, which is an improvement over the 7-19% rate seen after HDT (Figure 4A compared to Figure 5F). Based on this mutation rate, we calculated that employing Apc^{Min} would approximately double the frequency of LOH to 5%. Consistent with this, many cells expressed GS three weeks after infection. Compared to Ad-*Apc*-TAL-R alone, injecting the TALEN pair resulted in ectopic GS staining outside the central vein (n = 3, Figure 5G). The percentage of the ectopic GS+ cells was approximately 2-4%.

To enable further expansion of these GS+ cells, we dissociated and isolated primary hepatocytes from Ad-*Apc*-TALEN injected Apc^{Min} mice and transplanted them into $Fah^{-/-}$;$Rag2^{-/-}$;$Il2rg^{-/-}$ (FRG) mice via splenic injection. The FRG mouse is an immunodeficient model of Tyrosinemia that is a hepatocyte transplant recipient model [130]. These mice are susceptible to liver failure unless they are treated with 2-(2-Nitro-4-trifluoromethylbenzoyl)-1,3-cyclohexanedione (NTBC). After transplantation, we gradually withdrew NTBC until body weight

stabilized, indicating engraftment of donor cells. Three months post-transplantation, we sacrificed the FRG mice transplanted with Ad-*Apc*-TALEN treated *Apc*^{Min} hepatocytes and found large GS+ clones (n = 4 mice, Figure 5H). Mice transplanted with untreated control *Apc*^{Min} hepatocytes had no GS+ clones (n = 2 mice, Figure 5H). This showed that adenovirus packaged TALENs could achieve higher mutagenesis efficiency than HDT, and resulted in detectable tumor suppressor LOH in vivo. We did not observe tumors in these *Apc*^{Min} or FRG mice, likely because the tumor latency of *Apc* deficient livers is 7-12 months [131].

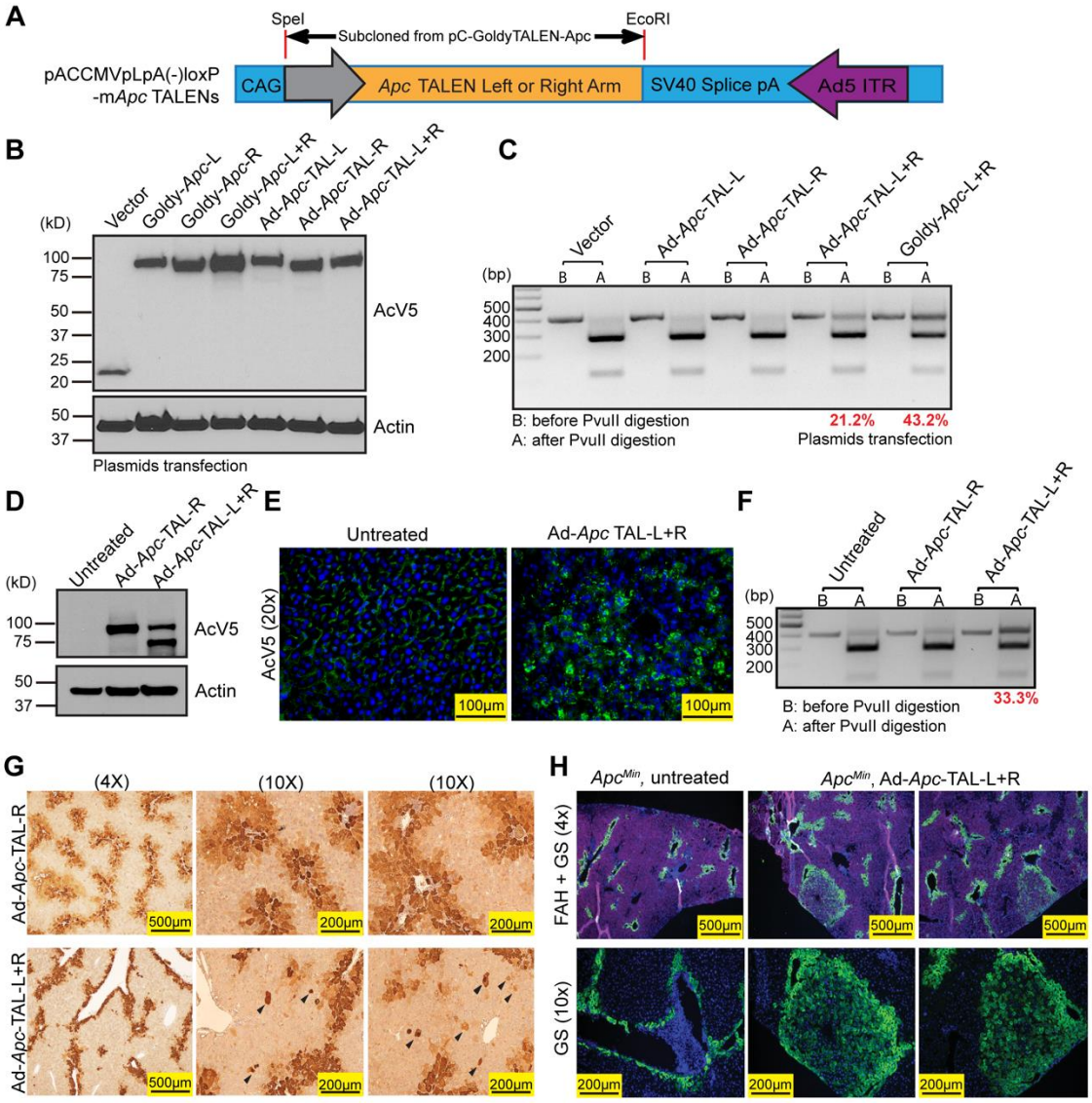

Figure 5. Adenovirus TALEN delivery increases mutagenesis efficiency in vivo.

(A) The construct map of the Adenovirus plasmid containing *Apc* TALENs. (B) Protein expression in H2.35 cells transfected with pC-Goldy-m*Apc* TALEN and pACCMVpLpA(-)loxp-m*Apc* TALEN plasmids. (C) Genotyping of the transfected H2.35 cells. (D) Protein expression level from the Apc^{Min} liver 24 hours after injection with Adenovirus *Apc* TALENs. (E) AcV5 IF staining (green) of the Apc^{Min} mice. (*F*) Genotyping of treated mice showing and efficiency of about 33.3%. (G) IHC staining for GS three weeks after adenovirus injection. n = 3, and two independent livers shown here. Ectopic GS+ cells found outside of the central vein region (arrowheads). (H) IF staining for GS (green) and *Fah* (red) from the FRG mice. Mice (n = 4) were euthanized 3 months after transplantation with TALEN treated or untreated Apc^{Min} hepatocytes.

Discussion

In cancer, somatic alterations in oncogenes and tumor suppressors are much more common than germline mutations. Carcinogens have been used to introduce random somatic mutations, but targeted mutations are important to study and more difficult to generate. Although shRNAs and transposons have been used with success in vivo [85, 132], these technologies come with major drawbacks. First, it is very difficult for shRNAs to completely eliminate the expression of proteins. For the shRNAs that are effective, the microRNA biogenesis machinery could be overwhelmed, thus altering the normal production of endogenous microRNAs. In addition, shRNAs have many off-target effects that can contribute to tumorigenesis [133, 134]. There are also disadvantages for transposons delivered in vivo using the Sleeping Beauty transposase. Transposons carrying an

overexpression construct can be used to generate overexpression models, but transgenes are randomly integrated and not under the control of endogenous regulatory elements.

TALENs represent a technology that allows efficient generation of targeted mutations, but their range and accuracy, especially in vivo, are just beginning to be explored. Theoretically, these highly-specific nucleases can obviate many of the problems and weaknesses of shRNAs and transposons, but extensive analysis will be required to confirm this. Using TALENs, we aimed to generate and study somatic mutations found in cancer without first having to generate conditional knockout mice, a major roadblock in cancer genetics. We focused our efforts on the liver, the site of a devastating tumor type with few treatment options, and where gene delivery has been optimized for a variety of applications [135-138].

By directly delivering TALENs against *β-catenin* and *Apc* into mice, we successfully introduced targeted mutations against these two genes, and generated *β-catenin* induced liver neoplasms. This is a remarkable result since TALENs have not yet been used to develop in vivo mouse tumor models. This method could save time and resources because experiments can be done in wild-type mice and within one generation. Another important advantage is that cells are mutated in a mosaic fashion, which is more physiologically relevant and models the evolutionary realities of cancer development. Therefore, this method introduces a way to faithfully study genetic events in HCC progression. These tools can also be used to test combinations of mutations that might synergize to promote cancer.

Although our method works well to mutate *β-catenin*, we had difficulty generating homozygous mutations in *Apc*, a two-hit tumor suppressor gene. Our studies suggest that polyploidy might be one way in which liver cells suppress tumor suppressor loss and tumorigenesis. Since approximately 70% of hepatocytes in adult livers are polyploid, this could be a powerful

form of tumor suppression. However, polyploidy could also potentially make a cell more vulnerable to oncogenic mutations, so further studies need to directly test this hypothesis in vivo. Given this issue, we increased the efficiency of *Apc* TALENs by employing adenoviral vectors. Adenoviral TALEN resulted in a higher mutagenesis rate and even observable *Apc* null cells. The presence of highly repetitive modules in TALENs leads to adenoviral recombination events that might preclude the ability to generate intact TALENs for all targeted loci. In fact, one of our TALENs was frequently truncated when packaged into adenovirus, though this did not impair its nuclease activity in vivo (Figure 5D and G). Shorter TALENs with fewer DNA binding modules could alleviate this situation. Directly delivering CRISPRs, which do not have repetitive modules, should also be exploited to induce mutations in vivo. In fact, delivering CRISPRs with HDT was recently used to effectively "cure" FAH mice [139]. Regardless of the technology, achieving a substantially higher mutagenesis rate will require major improvements in the delivery of these tools, either by viral or non-viral methods. Nevertheless, we found that the ease of using TALENs to generate permanent somatic genetic change will allow faster and better ways of understanding the fate of mutant cells in vivo. This work provides the first example of using genome editing to generate targeted cancer mutations and tumors directly in an adult organ. This work could serve as a starting point for understanding novel genetic alterations in cancers of many tissues.

Acknowledgements

This chapter was published as Zhang, Li, et al. 2014 [77].

Lin Li also made major contributions to this work.

CHAPTER 4

THE POLYPLOID STATE PLAYS A TUMOR SUPPRESSIVE ROLE IN THE LIVER

Introduction

Polyploid cells and organisms contain more than two homologous sets of chromosomes. Polyploidy is prevalent in plants, fish, and salamanders [140], but rare in mammals except in the cells of the heart, marrow, and liver. Surprisingly, up to 90% of rodent and 50% of human hepatocytes are polyploid, making the liver one of the largest polyploid organs in mammals [33, 34]. In rodents, liver ploidy dramatically increases around weaning (P14-P21) and continues to increase with age [141, 142]. The dominant mechanism for polyploidization is cytokinesis failure that leads to binucleated hepatocytes [142]. To a lesser extent, hepatocyte endoreduplication also contributes to polyploidy via replication of the nuclear genome in the absence of cell division [15]. Thus, polyploid hepatocytes (tetraploids, octoploids, etc.) can be bi- or mononuclear. Postnatal liver polyploidization is developmentally regulated, but ploidy is dynamic and can increase with surgery [143], fatty liver disease, and oxidative stress [40]. Given the prevalence and extreme

extent to which polyploidy occurs in the liver, it is remarkable that there is little known about the impact of polyploidy on tissue function or cancer risk.

The diverse functions for polyploidy in other cellular contexts can inform our expectations for polyploidy in hepatocytes. In yeast and plants, polyploidy promotes adaptation to environmental stresses, in some cases through the production of genetically diverse aneuploid daughter cells [79, 144]. Recently, it was shown that a subset of polyploid hepatocytes undergo reductive cell divisions prone to missegregation, leading to the accumulation of aneuploid cells [81]. Though the prevalence of aneuploidy in the liver is debated [82], aneuploidy may represent a means by which adaptive genetic diversity or premalignancy could evolve. Whether or not polyploidy in the normal liver is a risk for or protective against cancer is unknown. In support of the premalignancy concept, many cancers show evidence for genome doubling events [64, 145]. In seminal work, Fujiwara *et al.* showed that tetraploidy in *p53* null mouse mammary epithelial cells is a chromosomally unstable state that predisposes to transformation [72]. Since normal polyploid cells in the liver have intact *p53*, probably do not proliferate as much, and likely have a much lower risk for genome instability, the relevance to wild-type tetraploid cells in vivo is uncertain.

As an argument against increased cancer risk, the polyploid state in hepatocytes has been associated with terminal differentiation and limited proliferation [41]. Furthermore, Ganem *et al.* demonstrated that tetraploid hepatocyte proliferation/transformation is suppressed by the Hippo pathway [76]. In other studies, 4c and 8c hepatocytes divide efficiently and contribute as much to proliferation, growth, and regeneration as 2c hepatocytes during liver growth and in transplant assays (Figure S7A)[81]. Overall, it is unclear if there are substantial differences in the proliferative rates of diploid and polyploid hepatocytes. In theory, polyploids could also be

protected from cancer due to increased tumor suppressor dosage [146]. Although illuminating, these data from diverse organisms and contexts make it difficult to predict how polyploidy might influence the function of normal liver cells and their risk for transformation.

The influence of polyploidy is likely to be context dependent, mirroring the situation for aneuploidy, which can be tumor suppressive in untransformed cells and oncogenic in cancer cells [147-149]. Although the relationship between polyploidy and cancer has been interrogated in cell culture [73, 150], it has never been rigorously interrogated in the context of a major organ in vivo. We believe that it is fundamentally important to investigate the role of physiologically programed polyploidy in one of the largest organs in the body. Here, we specifically focus on the influence of polyploidy on regenerative capacity and transformation risk in the normal liver.

Direct causal connections between polyploidy and tissue function in vivo have not been established because polyploidy is usually not treated as an independent variable. Defects in genes required for cell cycle or cytokinesis (*Trp53, Rb,* or *Cdk1)* can dramatically alter ploidy [56, 58, 59], but interrogation of mice with these germline mutations cannot distinguish the effects of ploidy from the persistent pleiotropic effects of these mutations. For example, *Cdk1* knockout (KO) hepatocytes cannot complete mitosis and are dramatically polyploid (up to 32N or greater). As a consequence, liver-specific *Cdk1* KO mice are unable to undergo malignant transformation, but whether this is specifically due to polyploidy or permanent *Cdk1* deficiency is unclear [59]. In contrast, *E2f7*/*E2f8* double KO livers are almost entirely comprised of diploid hepatocytes, but these mice have no physiological or regenerative phenotypes [52, 151]. Recently, *E2f8* KO livers were shown to accelerate tumorigenesis, but it is unknown if this is due to transcriptional effects of *E2f8* deficiency or to the diploid state of *E2f8* KO hepatocytes [152]. Likewise, Zhang et al. showed that *Yap* activation promotes polyploidy and cancer, but it is unclear if the ploidy itself

directly impacts tumor biology independent of *Yap* [153]. Due to the lack of appropriate tools and the inability to assess the chronic impact of ploidy change, the role polyploidy plays in diseases involving long-term cell division cycles remains unclear. Here, we developed multiple methods and in vivo reagents to transiently, reversibly alter ploidy and found that the polyploid state suppressed liver tumorigenesis by buffering against tumor suppressor loss.

Premature weaning promoted polyploidy and protected against liver tumor development

To answer these questions, we reasoned that the transient, reversible control of ploidy state would represent a fundamental advance to enable the elucidation of ploidy functions. Since the predominant mechanism of widespread hepatocyte polyploidization is cytokinesis failure, a phenomenon temporally associated with weaning in rats [154], we asked if differential weaning times could transiently influence ploidy in mice. By weaning wild-type (WT) mice at P13 (premature weaning) or P21 (normal weaning) (Figure 6A), we found that prematurely weaned mice had significantly more binucleated hepatocytes (Figure 6B) and increased cellular ploidy (Figure 6C) at 19 days of age. To induce liver tumors, we gave a single intraperitoneal (IP) dose (25μg/g) of the agent diethylnitrosamine (DEN) to both cohorts at P19, a time point when ploidy states were divergent. Notably, the expression of Cytochrome P450 and other differentiation genes were not significantly different between premature and normal weaning mice (Figure S7C, D). Five months later, pre-weaned mice with greater ploidy at P19 exhibited significantly reduced gross and microscopic tumor burden (Figure 6D, E), suggesting that polyploidy could exert tumor suppressive effects. Since weaning is confounded by factors other than ploidy, we also used additional methods to control ploidy state.

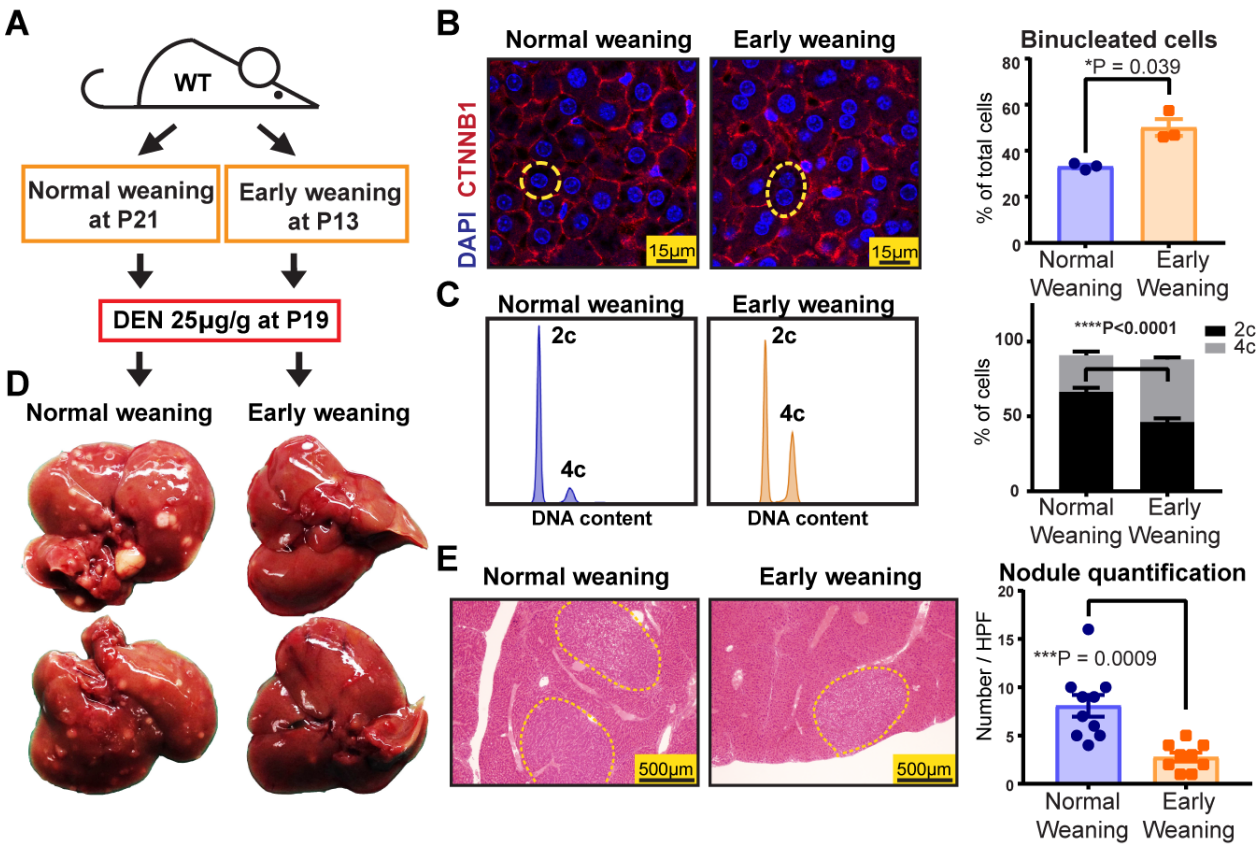

Figure 6. Premature weaning promoted polyploidy and was protective against HCC development.

(A) WT mice were weaned at P13 and P21 to induce differences in polyploidization. Diethylnitrosamine (DEN) was injected to both cohorts at P19 to induce hepatocellular carcinoma (HCC) formation. (B) DAPI and CTNNB1 immunofluorescence staining identified nuclei and cell membranes (left panel). Representative mononucleated and binucleated hepatocytes are circled by the yellow dashed lines. The percentages of binucleated hepatocytes are quantified on the right (4 images were analyzed and averaged per mouse, n = 3 mice per group). (C) Ploidy distribution was analyzed by flow cytometry. Representative histograms show DNA content as stained by PI. Compiled data from the two groups are shown on the right (n = 8 mice in each group). (D) Gross

tumor burden was examined five months after DEN. (E) Microscopic tumor nodules are circled by yellow dashed lines. The right panel shows nodule quantification (Tumors from one section of an entire lobe was quantified per mouse, n = 10 and n = 9 for normal and early weaning groups).

In vivo siRNAs revealed that the polyploid state protected against tumorigenesis

To inducibly toggle polyploidy without introducing permanent genetic lesions, we used siRNA to transiently knockdown genes that affect ploidy. We targeted *Anillin (Anln)*, an actin binding protein required for cytokinesis [155](Figure S7F, G) and *E2f8*, a transcription factor required for polyploidization [52]. In vivo, *Anln* and *E2f8* siRNA vs. *scramble* siRNA (siCtrl) delivery in lipid nanoparticles from P10-P20 [156] resulted in significant knockdown of *Anln* and *E2f8* mRNA and protein (Figure 7A, B and Figure S7H). As expected, cellular ploidy was significantly increased after *Anln* knockdown and decreased after *E2f8* knockdown (Figure 7C). Confocal imaging based ploidy characterization revealed that siAnln treated livers had significantly larger cell and nuclear size, while the siE2f8 treated livers showed the opposite (Figure 7D, E). Since cell and nuclear size correlate with DNA content, this suggested significant ploidy changes. To quantitatively distinguish mono- vs. binucleated tetraploids, we integrated flow and confocal imaging data (Figure 7F). This revealed that siAnln hepatocytes were 32% mononuclear diploid, 32% mononuclear tetraploid, and 32% binuclear tetraploid. siE2f8 hepatocytes were 64% mononuclear diploid, 17% mononuclear tetraploid, and 16% binuclear tetraploid. Furthermore, a Florescence In Situ Hybridization (FISH) assay confirmed the existence of mono- and binuclear tetraploids (Figure 7G, H). Overall, this indicated that both mononuclear and binuclear tetraploids were increased in siAnln vs. control livers and in control vs. siE2f8 livers.

Altered ploidy did not impact overall health, liver mass, body mass, hepatocyte differentiation, *CYP450* expression, or proliferation (Figure S8A-E). Moreover, we challenged these mice to acute regeneration assays such as partial hepatectomy and hepatotoxin treatments. Hepatectomy was performed at 5-6 weeks of age, when changes in ploidy was still observed (Figure S8F). Liver/body weight ratios after 2/3^{rds} partial hepatectomy were not significantly different between different ploidy groups (Figure S8G). No differences in necrosis and proliferation arose after one dose of DEN or carbon tetrachloride (CCl4) (Figure S8H, I). These results showed that polyploid and diploid hepatocytes were equivalently able to survive, recover, and proliferate after injuries. These findings are consistent with previous studies in mice with ploidy alterations [52, 151], again demonstrating that ploidy state has minimal influences on post-natal liver growth and regeneration, likely because only 2-4 cell division cycles are required for recovery after these profound, acute injuries.

Having established that inducible inhibition of *Anln* and *E2f8* allowed us to alter ploidy without introducing irreversible genetic mutations, we next evaluated the impact of ploidy on tumor development. We injected DEN (75μg/g x 1 dose) into mice four days after the last dose of siCtrl, siAnln, or siE2f8 (siRNA delivery schema in Figure 7A). Six months later, siE2f8 treated livers with more diploid cells had significantly increased gross tumor burden, microscopic tumor nodules, and liver/body weight ratio than siCtrl livers (Figure 7I, J and Figure S9A-C). In contrast, siAnln treated livers with more polyploid cells showed the opposite. To further exclude the possibility of residual siRNA effects, we also introduced DEN at 14 days, rather than 4 days, after the last siE2f8 injection. Polyploidy again demonstrated a potent tumor suppressive effect (Figure 7K and Figure S9D). To generate higher levels of polyploidy, we developed two additional and distinct N-acetylgalactosamine (GalNAc) conjugated siRNAs against *Anln*. The exposed GalNAc

moiety mediates siRNA uptake via Asialogycoprotein receptors (ASGPR), which are specifically expressed by hepatocytes. Subcutaneous injections of these siRNAs (3 x 4mg/kg doses between P8-P20) resulted in high levels of polyploidy when compared to mice treated with Luciferase siRNA (siLuc) (Figure S9E). After DEN (75μg/g at P26), the siAnln mice also exhibited less tumors (Figure S9F). To avoid the possibility of *Anln* specific effects, we also induced liver polyploidy by knocking down *Cdk1* with an in vivo siRNA (Figure S9G). At P24-26, or 4 days after the last dose of siRNA, mice were injected with DEN (75μg/g). 6 months after DEN, si*Cdk1* treated mice exhibited reduced tumor burden (Figure S9H), again supporting the tumor protective role of polyploidy. Altogether, these findings suggested that the degree of liver polyploidy is anti-correlated with the efficiency of carcinogenesis.

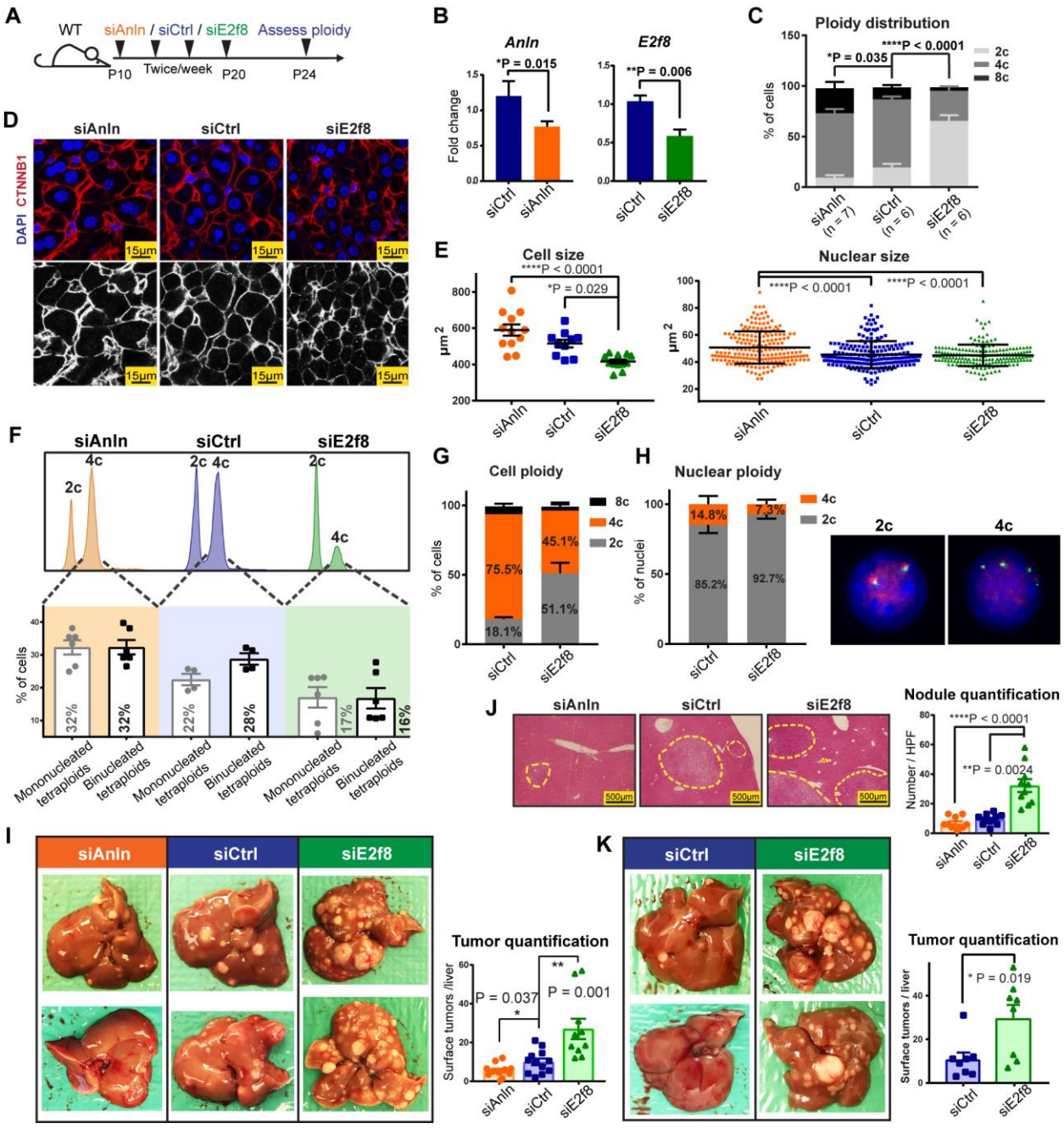

Figure 7. In vivo siRNAs that toggled ploidy revealed that the polyploid state protected against tumorigenesis.

(A) Schema for the siRNA experiment: *Anln*, *E2f8*, and scramble siRNAs (siCtrl) were encapsulated into lipid nanoparticles and injected into WT C3H strain mice starting at P10. Four

total injections (two intraperitoneal and two retro-orbital) were performed twice per week. Between P24-26, hepatocytes were dissociated for ploidy analysis or mice were injected with DEN (75μg/g). Tumor burden was examined six months later. (B) mRNA knockdown after *Anln* and *E2f8* siRNA treatments. RT-qPCR was performed on the liver 4 days after the last siRNA dose. (C) Average cellular ploidy distribution within livers, as determined by PI staining and flow cytometry (n = 6 mice in each group were analyzed). (D) Confocal images of DAPI and CTNNB1 stained siRNA treated livers. The bottom images highlight CTNNB1 staining alone, marking membranes and cellular outlines. (E) Cross-sectional cell and nucleus size measurements. Each group includes 12 total analyzed image fields from 4 individual mice. For nucleus size quantification, each data point is one nucleus; for cell size quantification, each data point is an average of the cell sizes from one image and 3 images were taken from each mouse. (F) Representative cellular ploidy distribution of siRNA treated livers (upper panel). The lower panel shows the distribution of mono- and binucleated tetraploid hepatocytes. Calculations were performed as follows: % of mononucleated tetraploid cells = % tetraploid cells by FACS - % binucleated cells by confocal (images from Figure 7D, n = 3 images were counted for each mouse, 2 mice for each group). (G) Cellular ploidy distribution of siRNA treated livers, as determined by Flow Cytometry (n = 2 mice/group). (H) On the left is the nuclear ploidy of the above siRNA treated livers, as determined by FISH. 60 nuclei were analyzed for each mouse. On the right are representative images showing a 2c and a 4c nucleus. 2 green and 2 red signals identify a 2c nucleus. 4 green and 4 red signals identify a 4c nucleus. (I) Gross tumor burden of siRNA treated livers harvested 6 months after DEN injection. Quantification of liver surface tumor numbers (right panel). (J) H&E liver histology showing tumor nodules circled by dashed lines (left panel). Quantification of microscopic nodules (right panel). (K) Tumor burden in mice treated with DEN

at later time points after siRNA delivery. Mice were treated with four doses of siRNAs. 14 days after the last siRNA injection, one dose of DEN (100μg/g) was given, and 7.5 months later, tumor burden was assessed (n = 8 in each group). The liver surface tumors were quantified in the right panel.

E2f8 knockout and Anln shRNA mice confirmed the protective effects of polyploidy

Given the formal possibility that siRNAs or lipid nanoparticles could have off-target or non-specific effects, we also used Cas9 to generate whole-body *E2f8* KO mice (Figure S10A), which have predominantly diploid hepatocytes in adulthood (Figure 8A). Interestingly, we observed that *E2f8* WT, Het and KO livers had equivalent levels of ploidy at P15, and only diverged in ploidy state by P27 (Figure 8A and Figure S10B). We hypothesized that if ploidy is a specific and essential factor causing tumor suppression in *E2f8* KO livers, then mutagenizing and inducing cancer at P15 would not result in differences in liver tumor development, while inducing at P27 would result in large differences. Indeed, DEN given at P15 (25μg/g) resulted in no cancer differences between the three groups, while DEN at P27 (75μg/g) caused more liver tumors in *E2f8* Het and *E2f8* KO mice when compared to *E2f8* WT mice (Figure 8B-E, Figure S10C). These results further demonstrated that the *E2f8* gene itself contributed little to cancer development independent of the differences in ploidy seen at P27.

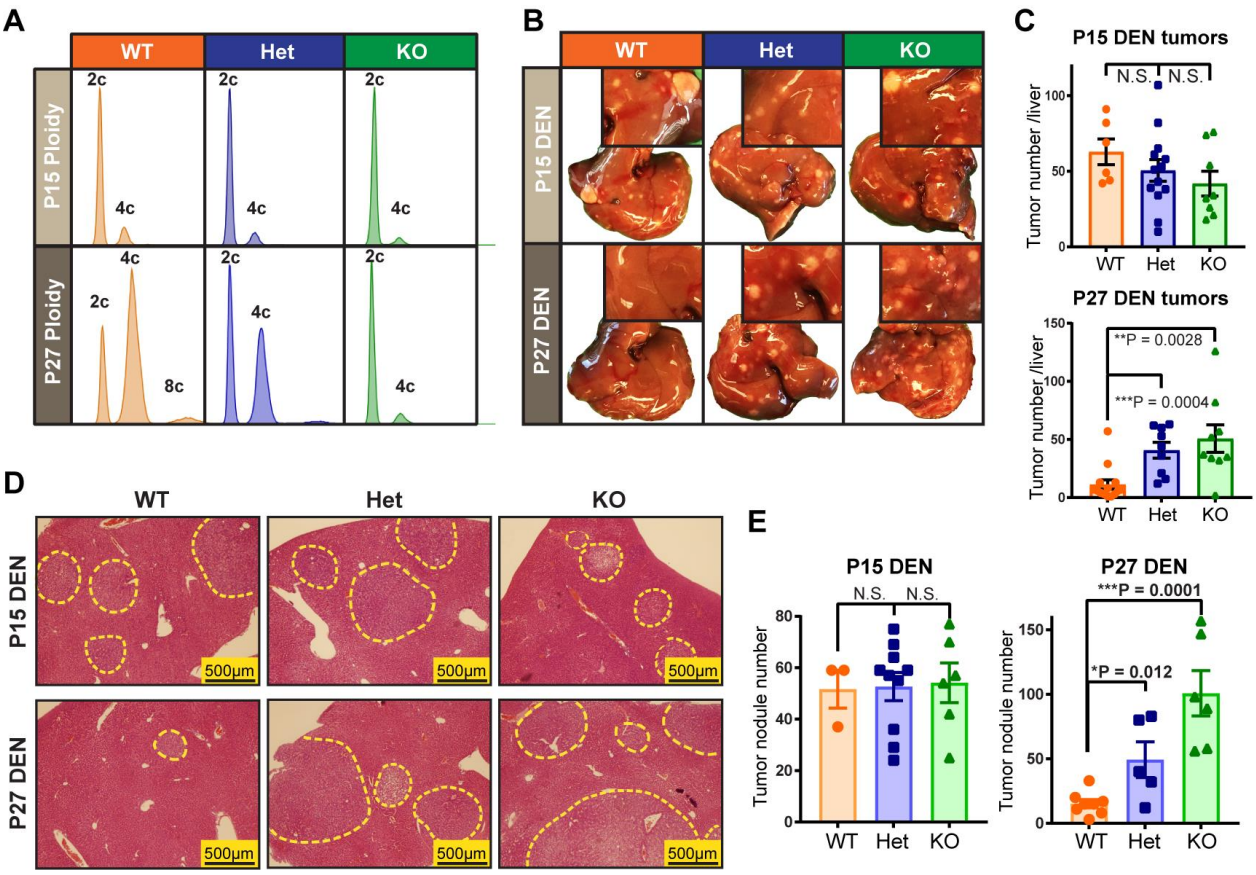

Figure 8. Reduced ploidy accounted for the increased tumorigenesis associated with *E2f8* deficiency.

(A) Representative cellular ploidy of *E2f8* WT, *E2f8* Het, and *E2f8* KO livers at P15 and P27, as analyzed by flow cytometry. (B) DEN was introduced by IP injection in one cohort at P15 (25μg/g) and in another cohort at P27 (75μg/g). Gross tumor burden was evaluated 4.5-5 months later. The inset images show higher magnification images that more clearly exhibit tumor burden. (C) Liver surface tumor quantification of *E2f8* WT, Het, and KO mice given DEN at P15 or P27. (D) Histology of *E2f8* WT, Het, and KO livers show microscopic tumor nodules (circled by dashed yellow outlines). (E) Quantification of tumor nodules per unit of cross sectional area.

Next, we wanted to generate a more potent and versatile mouse model to increase polyploidy. In addition, our goals were to drive greater levels of polyploidy and to employ a small inhibitory shRNA distinct from the siAnln used above in order to corroborate on target effects on *Anln*. Thus, we created a doxycycline (dox)-inducible transgenic mouse expressing an shRNA against *Anln*. Transgenic mice were derived from embryonic stem cells containing *Rosa-rtTA* and a GFP + sh*Anln* cassette under the control of a tetracycline responsive promoter element (TRE) (Figure S10D, E; transgenic design based on Scott Lowe's group [157]). Dox could be used to induce *Anln* suppression in a temporally specific fashion (Figure 9A). *Rosa-rtTa* alone or *Rosa-rtTa*; *TRE-shAnln* (hereafter called *Rosa* and *TG-shAnln*) transgenic mice exposed to dox water from P0-P20 showed normal growth, development, and liver function (Figure S10F-H). *Anln* mRNA levels were suppressed by 50% (Figure 9B), which resulted in more polyploid livers at multiple time points after dox withdrawal (Figure 9C-E). These livers were similar to what was seen with *Anln* siRNA treatment, but had more profound levels of polyploidization. In addition, GFP protein (and likely *Anln* shRNA) completely disappeared by 15 days after dox withdrawal (Figure 9F), demonstrating the reversibility of *Anln* suppression.

Polyploid livers resulting from transient suppression of *Anln* were almost completely protected from DEN induced tumorigenesis, confirming the siRNA results (Figure 9G, H). We then wanted to exploit this model to analyze the function of polyploidy in a carcinogenesis model caused by another clinically important mechanism. Steatohepatitis represents an increasingly relevant risk factor for HCC and has been associated with an increase in polyploidy [40]. To induce long term fatty liver disease and HCC, we fed mice with high fat diet (HFD) after transiently inducing ploidy changes (Figure 9I). After eight months, *Rosa* and *TG-shAnln* mice had similarly high levels of steatosis and liver function abnormalities (Figure 9J-L and Figure S10I), but 50%

of control livers while no polyploid livers developed HCC (Figure 9M, N). In summary, multiple murine models increasing and decreasing ploidy corroborated the fact that higher levels of polyploidy suppressed liver tumors in diverse cancer models.

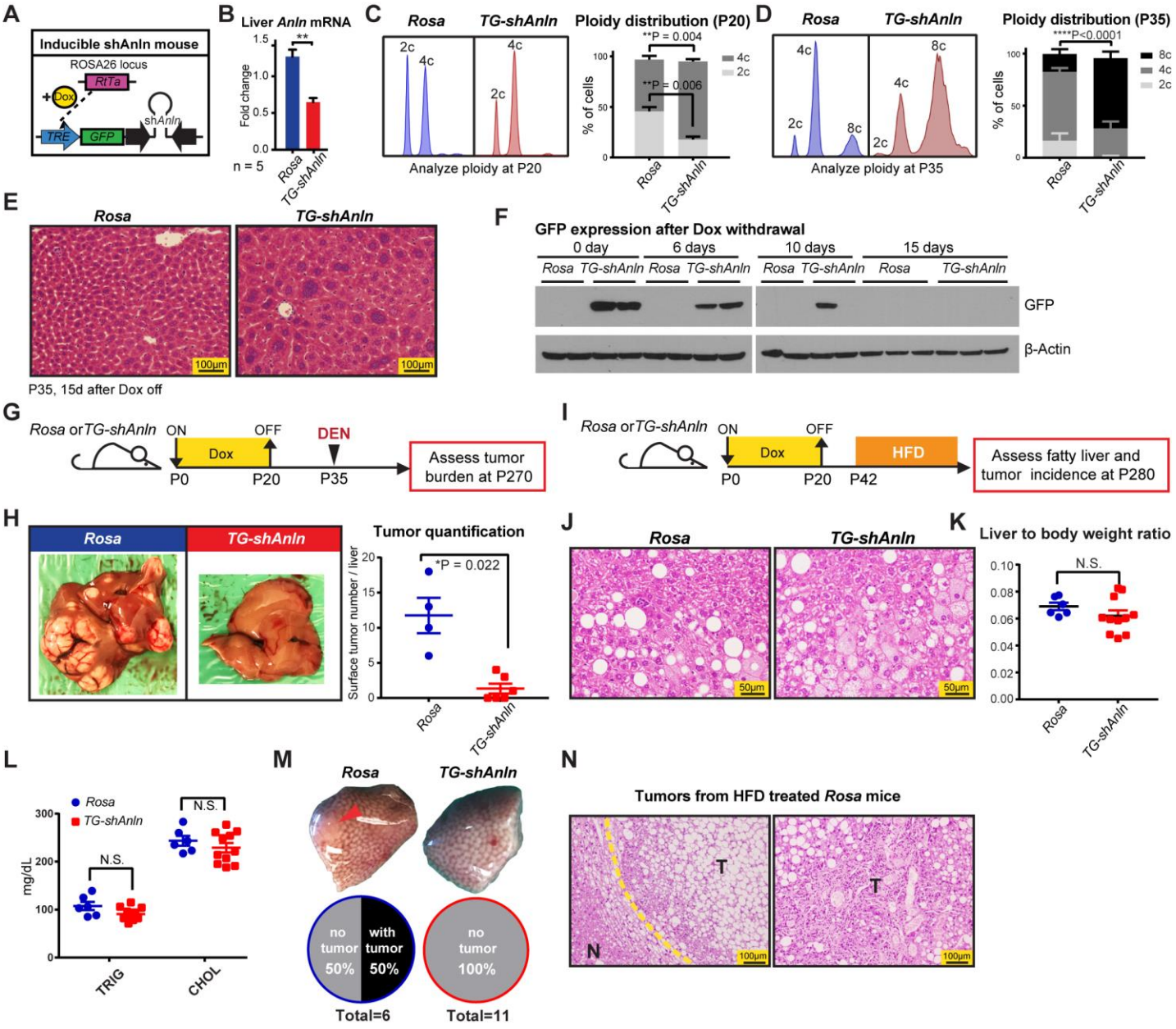

Figure 9. An inducible transgenic mouse model to temporally control polyploidization shows protection against DEN and high fat induced HCCs.

(A) An inducible double-transgenic mouse model carrying sh*Anln* cassette under the control of a tetracycline responsive promoter element (TRE). These mice carry a *Rosa-rtTA* knockin construct, allowing induction of *Anln* suppression with Doxycycline (Dox) water. (B) Transient Dox induction from P0 to P20 suppressed *Anln* mRNA levels in the liver. (C) Representative cellular ploidy distribution of *TG-shAnln* livers treated with dox from P0-P20 was determined by PI staining and flow cytometry at the age of P20 (left panel). On the right is the average ploidy distribution (n = 3 mice in each group). (D) Representative cellular ploidy distribution of *TG-shAnln* livers treated with dox from P0-P20 was determined by PI staining and flow cytometry at the age of P35 (left panel). On the right is the average ploidy distribution (n = 6 mice in each group). (E) H&E staining showing large, multinucleate hepatocytes in the induced group. (F) Western blots showing stability of GFP protein expression after dox induction and withdrawal. (G) Schema for the DEN induced HCC experiment in inducible shRNA mice: Transient dox treatment from P0-P20 in *Rosa-rtTa* or *TG-shAnln* mice established ploidy differences. At P35, mice were injected with DEN (100μg/g). Tumor burden was examined 8 months later. (H) Representative gross tumor burden from the DEN experiment. Quantitation on the right. (I) Schema for the high fat diet (HFD) induced HCC experiment in inducible *TG-shAnln* mice: Transient dox treatment mice established ploidy differences. Starting at P42, mice were given ad libitum HFD (60% calories from fat). Tumor burden was examined after 8 months. (J) H&E of *Rosa* and *TG-shAnln* HFD treated livers. (K) Liver to body weight ratios of HFD treated *Rosa* and *TG-shAnln* mice. (L) Triglyceride and cholesterol levels of *Rosa* and *TG-shAnln* mice after 8

months of HFD. (M) Representative gross tumor burden from the HFD experiment. 50% (3 of 6) of Rosa mice had tumors, while no (0 of 11) TG-*shAnln* mice carried tumor. (N) H&E of tumors from *Rosa* control mice given HFD. Yellow dotted line is the boundary between non-tumor tissue (labeled "N") and tumor ("T").

Polyploids were protected from tumor suppressor LOH but not oncogene activation

To probe underlying mechanisms in the DEN model, we first asked if ploidy significantly regulated metabolic properties that would influence tumorigenesis. DEN is first bioactivated by CYP450 family enzymes to become α-hydroxylnitrosamine [158]. Expression of CYP450 enzymes in general and zonation of Cyp2e1 in particular were unchanged in livers with distinct ploidy (Figure S8C and Figure S11A). Elevated levels of reactive oxygen species (ROS) secondary to hepatotoxins are known to accelerate tumor initiation [159], but ROS levels were unchanged between siRNA treated mice and between *E2f8* WT/Het/KO mice (Figure S11B-D). It is also known that following the DEN bioactivation, an ethyldiazonium ion is formed, binds DNA, and causes genotoxic damage [158]. Though DNA damage markers such as p-Brca1, p-p53, and p-γH2A.X increased after DEN, the magnitude of induction was similar between groups (Figure S11E, F). Altogether, livers with altered ploidy did not exhibit differential xenobiotic metabolism, oxidative stress, or DNA damage responses.

Since the mutagenic activities of DEN were quantitatively similar, it was possible that ploidy differentially influenced tumor suppressor (TSG) loss and proto-oncogene activation. We first performed a theoretical calculation to estimate the risk of TSG loss and oncogene activation in tissues with 10,000 diploid cells vs. 5,000 tetraploid cells (which are ~2x larger). Both tissues contain 20,000 sets of chromosomes (Figure 10A). Assuming 10% of TSGs are mutated in one

massive DNA damaging event, then the rate of loss of heterozygosity (LOH) in a diploid cell is $0.1^2 = 0.01$, while for a tetraploid cell it is $0.1^4 = 0.0001$. Thus, 100 cells vs. 0.5 cells (on average) achieve LOH in diploid vs. tetraploid tissues of the same mass. For simplicity, we can also assume that the oncogene activating mutation rate is also 0.1. The probability this mutation occurs in a diploid cell is $1\text{-}0.9^2 \approx 0.19$, while in a tetraploid cell it is $1\text{-}0.9^4 \approx 0.34$. Although the probability is higher for tetraploid cells, diploid vs. tetraploid tissues have 1900 and 1700 cells at risk once total cell numbers are accounted for. This calculation suggests that polyploid tissues are dramatically protected against TSG LOH but are at similar risk for oncogene activation. This model is oversimplified since tumorigenesis involves much more subtle and complex genome alterations [160, 161], but it is still likely to be informative because TSG LOH is an important part of carcinogenesis.

To challenge this hypothesis, we first examined the impact of oncogene activation in mice with different levels of polyploidy, we overexpressed *MYC* using a liver specific driver (*LAP-tTa*) and a dox-inducible promoter (*TRE-MYC*) (Figure S12A) [162]. Prior to inducing *MYC* overexpression, we gave *LAP-tTA; TRE-MYC* mice four doses of siRNA to transiently alter ploidy (Figure 10B, Figure S12A). At P30, significant differences in ploidy, but not *MYC* expression levels, were observed (Figure S12B, C). Dox withdrawal at P25 leads to transformation of less than 1% of *MYC* expressing cells, a dynamic range that allowed us to sensitively quantitate the influence of ploidy on tumor initiation. Nine weeks post-induction, tumor development and liver to body weight ratios were indistinguishable between siRNA treated ploidy groups (Figure 10C), showing that ploidy had little impact on *MYC* oncogene induced tumorigenesis.

Next, we tested whether TSG LOH is more difficult to achieve in hepatocytes with wholesale genome duplications. To quantitate the dynamics of TSG loss, we engineered an

adenovirus carrying Cas9 and a guide strand RNA targeting *Pten* (Ad-*Cas9-sgPten*) (sgRNA was validated in reference [163]), a commonly inactivated TSG in HCC. 14 days after IV Ad-*Cas9-sgPten* delivery into mice with different levels of ploidy, *Pten* LOH was assessed with immunohistochemistry (Figure 10D). The frequency of hepatocytes with complete *Pten* deletion was inversely proportional to the extent of polyploidy (Figure 10E). To confirm that the degree of ploidy did not change susceptibility to adenoviral infection, we verified that equal numbers of cells expressed GFP after Adenovirus-GFP delivery (Figure S12E). To rule out the possibility of a *Pten* specific-phenomenon, we also assessed *Apc*, a TSG in the WNT pathway. We injected an Adeno-associated virus carrying a guide strand against exon 8 of *Apc* (AAV-*sgApc*) into dox-inducible *Cas9* mice (*Rosa-rtTa; TRE-Cas9*) subjected to siRNA induced ploidy changes (Figure 10F). In vitro, this particular *sgApc* effectively mutagenized *Apc* (Figure S12F) and had previously been used to generate *Apc* null hepatocytes [77]. To quantitate the number of *Apc* null clones in vivo, we probed for ectopic Glutamine Synthetase (GS), a specific and sensitive marker of aberrant WNT activation in the liver [131]. Strikingly, more diploid livers were much more susceptible to *Apc* LOH than control livers, and more polyploid livers harbored the fewest GS+ cells (Figure 10G). These data support the concept that polyploid livers are protected from TSG loss and are not more sensitive to oncogene activation.

To show that polyploidy also protects from cancers that arise from TSG loss, we used a mouse strain with conditional alleles in important tumor suppressor genes: $P53^{fl/fl}$; $Rb1^{fl/fl}$; $Rbl2^{fl/fl}$ [164]. First, we changed the ploidy of these mice using control and *E2f8* siRNAs (Figure 10H), then mice were injected with Ad-*Cas9-sgPten* as well as AAV-Cre to delete TSG alleles in a mosaic fashion. 2.5 months after viral injection, siCtrl treated mice exhibited lower tumor burden compared to siE2f8 mice (Figure 10I). In addition, we used another HCC model that is caused by

TSG loss. We targeted *Pten*, *P53*, and *Lkb1* in wild-type mice. We used Ad-Cas9-gPten and an AAV containing guide strands against *P53* and *Lkb1* (AAV-KPL) [165]. This AAV also contains a guide against Kras as well as a $Kras^{G12D}$ HDR template, so this model is not entirely driven by TSG loss. After ploidy was changed with siRNAs (Figure S12G), mice were injected with the Ad-*Cas9-sgPten* and AAV-KPL. Two months later, siAnln treated mice exhibited the fewest tumors, followed by siCtrl and siE2f8 treated mice (Figure S12H). These cancer models both support the hypothesis that polyploidy protects from tumorigenesis caused by TSG loss.

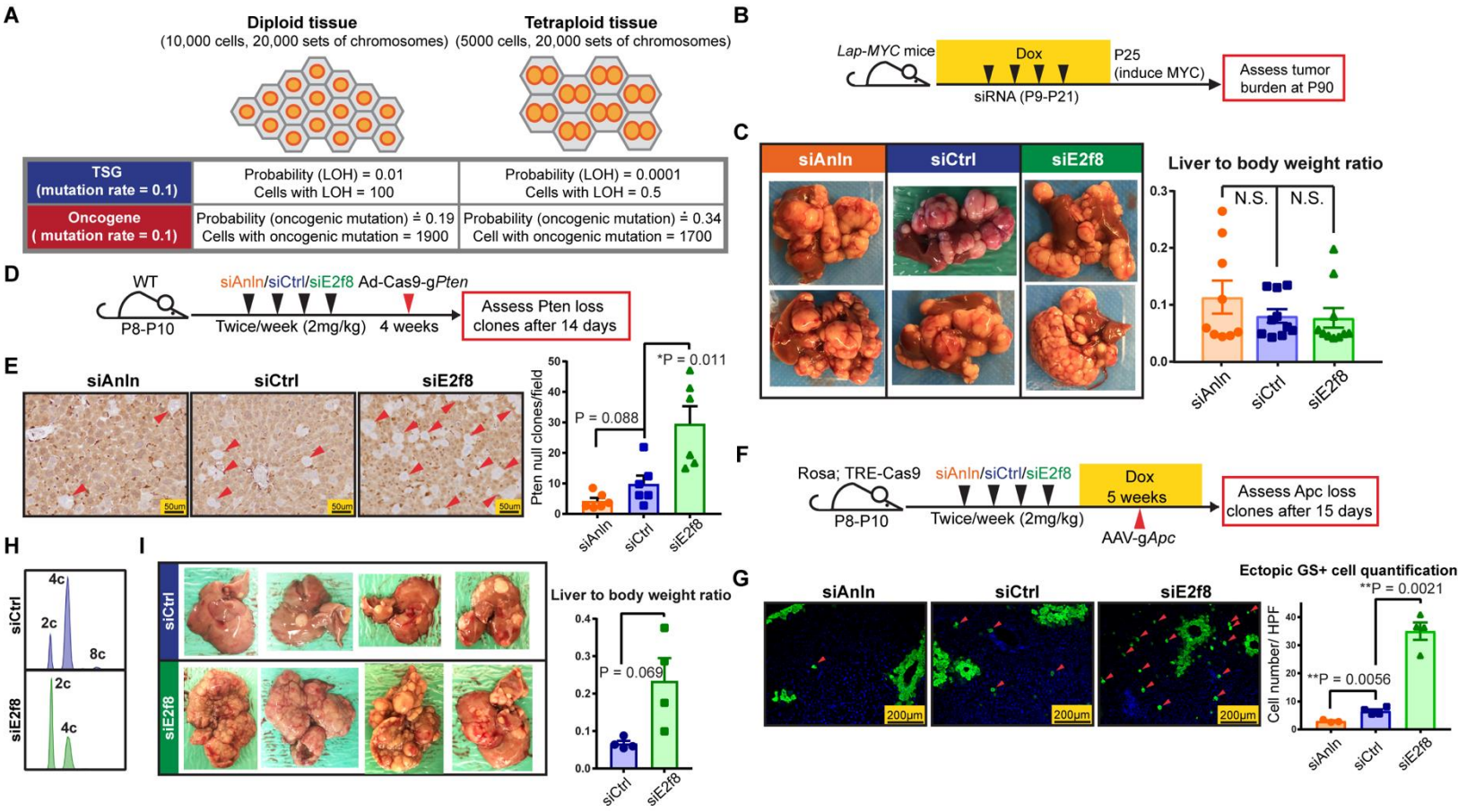

Figure 10. Polyploids were protected from tumor suppressor LOH but not oncogene activation.

(A) Theoretical calculation of the risk of TSG loss and oncogene activation in tissues with diploid vs. tetraploid cells. (B) Schema of the *LAP-MYC* experiment: prior to inducing *MYC* overexpression by dox withdrawal at P25, *LAP-tTA; TRE-MYC* mice were given four doses of siRNA to transiently alter ploidy, as described in previously. At P30, ploidy distribution and *MYC* expression levels were measured; At P90, tumor burden was assessed. (C) Tumor burden at P90 (left panel). Liver to body weight ratios, another metric of tumor burden, are shown in the right panel. (D) Schema of the Ad-*Cas9-sgPten* experiment: WT mice were given four doses of siRNA to alter ploidy; one week later, adenovirus carrying Cas9 and a *Pten* sgRNA (Ad-*Cas9-sgPten*) was injected into these mice (10^9 pfu/mouse); 14 days later, LOH was assessed by PTEN IHC. (E) PTEN staining (left panel) on siAnln, siCtrl, and siE2f8 treated livers 14 days after virus injection. Red arrowheads point to the cells without PTEN, quantification on the right. (F) Schema of the AAV-sg*Apc* experiment: Dox inducible *Rosa-rtta; TRE-Cas9* mice were given four doses of siRNA to alter ploidy. Five days later, dox (1g/L) was given to induce Cas9 expression. Two weeks after the last dose of siRNA, AAV-*sgApc* (5×10^{12} pfu/mouse) was retro-orbitally delivered; 15 days later, the *Apc* LOH was estimated by Glutamine Synthetase (GS) IF. (G) GS staining (left panel) 15 days after AAV-sg*Apc* injection. Red arrowheads point to ectopic GS positive cells that result from homozygous *Apc* deletion. Note that the normal, non-ectopic GS staining that surrounds central veins (CV) was not quantified. Ectopic GS positive cells per imaging area were quantified in the right panel. (H) Representative cellular ploidy distribution of $P53^{fl/fl}$; $Rb1^{fl/fl}$; $Rbl2^{fl/fl}$ hepatocytes treated with 4 doses of siRNAs (siCtrl or siE2f8) from P10-P21, as determined

by PI staining and flow cytometry at P24. (I) One week after ploidy was altered with siRNAs, the mice were injected with Ad-*Cas9-sgPten* (10^9 pfu/mouse) and AAV-Cre (2.5×10^{10} pfu/mouse). Tumor burden was examined 2.5 months later. Liver to body weight ratios (right).

Reduced susceptibility to tumor suppressor LOH paired with reduced tumorigenesis in more polyploid livers suggested that DEN-induced tumors were dependent on tumor suppressor loss. Previously, DEN was shown to preferentially select for oncogenic mutations (*Hras* and *Ctnnb1*) in studies focused on identifying mutations in these pathways [166, 167]. We aimed to more broadly and thoroughly map the mutational landscape of these tumors, so we sequenced 242 of the most commonly mutated genes in human and murine HCCs in 50 individual DEN induced tumors (Figure 11A). We did identify a core group of recurrent, mutually exclusive mutations in oncogenes such as *Egfr* (Phe254Ile), *Hras* (Gln61Arg), and *Braf* (Val637Glu), but a majority of the most commonly mutated genes were bona fide TSGs such as *Mll2* (*Kmt2d*), *Brca2*, *Arid1a*, *Atm*, *Apc*, and *Tsc2*. Overall, these data suggest that DEN tumor transformation depends on TSG loss in addition to EGFR-RAS-MAPK pathway activation, further supporting the idea that tumor protection in polyploids is in part mediated through retention of WT tumor suppressor alleles.

Given that the mammalian liver is comprised of a mixture of polyploid and diploid cells, our work would predict that HCCs more likely originate from diploid cells. If this was true, it would follow that liver tumors are also more frequently diploid rather than polyploid. We found that even tumors arising from siCtrl mice with polyploid cells were predominantly diploid (Figure 11B, C). In human HCCs examined by flow cytometry, HCCs were more often comprised of diploid as opposed to polyploid cells [168-171]. Altogether, this suggests that human HCCs more likely arise from diploid cells, consistent with the idea that the polyploid state is less compatible

with cancer development.

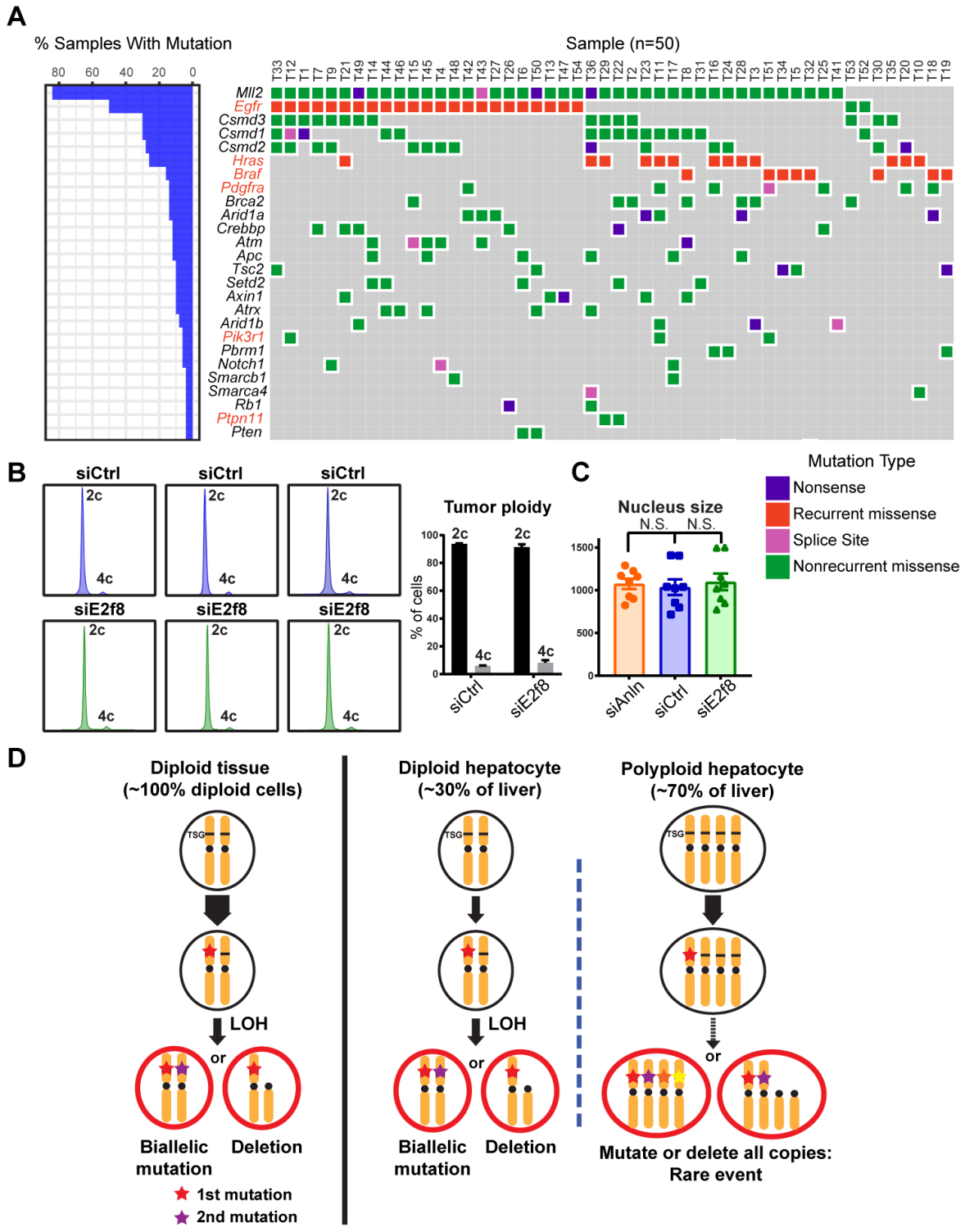

Figure 11. Tumor suppressor mutations are prevalent in liver tumors from diploid and polyploid mice.

(A) Targeted sequencing on 50 DEN induced liver tumors. 242 of the most commonly mutated genes in human and murine HCC were sequenced. Genes highlighted in red are oncogenes and those in black are TSGs. (B) Cellular ploidy distribution of DEN induced tumors from siRNA treated mice. Data is averaged on the right (tumor n = 10). (C) Nucleus sizes of tumors from siRNA treated mice. The nucleus size was quantified using Photoshop based on H&E staining images. 4 mice in each group were quantified, 2 tumors per mouse. (D) This model depicts how TSGs could be lost in diploid and polyploid cells. Note that the liver contains both diploid and polyploid cells.

Discussion

The fact that some animals and organs are polyploid, with cells containing whole genome duplications, has perplexed scientists for decades. It is known that 50-80% mammalian hepatocytes are polyploid, and conditions such as chronic hepatitis, steatohepatitis, and oxidative stress have all been associated with increased polyploidy [40, 172], but it is unknown if ploidy changes represent compensation, cause, or bystander effect of such disease states. Analyses of genetically engineered knockout mice with mostly polyploid or diploid hepatocytes have not been able to unequivocally link ploidy with cellular fitness, regeneration, or cancer [52, 59]. In part, this is because the reagents used to assess the response of ploidy states to injuries usually confound the effects of ploidy with the effects of the prominent cancer related genes used to change ploidy.

Here, we devised multiple in vivo methods to alter liver ploidy in a reversible fashion, such that long-term consequences of such changes could be assessed and compared. In agreement with

previous studies [52, 81], we found that polyploidy had little impact on acute injury or liver regeneration, but chronically, the polyploid state demonstrated tumor suppressive functions in multiple cancer models. In general, the extent of ploidy increase or decrease in different siRNA, GEMM, and inducible transgenic models appeared to correlate with tumor number and burden. Moreover, we believe that this protection is due in large part to buffering against TSG loss rather than limiting proliferation after oncogenic insults, at least for the DEN model. As shown in Figure 11D, cells within predominantly diploid tissues lose their tumor suppressors through classical LOH mechanisms. In contrast, polyploid hepatocytes harbor up to 16 alleles for each TSG, thereby buffering against a second or even third hit. Consistent with this, DEN tumors were most often diploid, suggesting a diploid origin. This is consistent with human data showing that HCCs are predominantly diploid [168-170]. We also showed that *MYC* induced oncogenesis in the liver was agnostic to ploidy states. It is possible the strong oncogenic effect of *MYC* overcame tumor protective effects of ploidy, but the effects of other oncogenes may be more influenced by polyploidy.

It is also important to note that we have only altered ploidy in the benign liver and not within established tumors, thus it is possible that increasing ploidy within cancer cells would cause genome destabilizing effects documented by others [72, 73, 153]. This would be in line with aneuploidy studies, which have shown that aneuploidy is either tumor suppressive or oncogenic depending on context [148, 149, 173]. Polyploidy will probably also demonstrate context dependency, but it is important to underscore that the extensive polyploidy found in the normal liver is an extremely important context to fully understand. Our findings suggest that in the setting of normal hepatocytes, TSG buffering could be an important tumor suppressive function of polyploidy.

We believed that it was essential to use mouse models to interrogate the role of ploidy in cancer because it is the most rigorous way to examine tumor initiation. For example, in vivo and in vitro human HCCs, which are already transformed, cannot be used to study ploidy's role in the transition state between normal and malignant cells. We also used cancer models that were the most reflective of human disease states. The DEN model generates cancers that are not dependent on singular, artificially strong genetic drivers such as *Yap* or *Akt*. Using expression profiling, Snorri Thorgeirsson showed that DEN induced mouse HCCs were more similar to poor survival human HCCs than other mouse cancer models [174]. Also, Allan Balmain's group recently argued for the use of chemically induced mouse cancer models because they more accurately reflect the diverse genomics of human cancers [175]. Indeed, the tumors in our study harbored a wide diversity of oncogenic and tumor suppressor mutations that reflect the biology of human HCCs.

The DEN model may resemble the types of liver cancers caused by acute exposure to mutagens such as aflatoxin. Although HCC in the US is commonly caused by chronic etiologies (HBV, HCV, alcohol, NASH), acute liver injury and mutagenesis by aflatoxin is a common problem in tropical and sub-tropical climates in Africa, Asia and South America [176]. It is conceivable that polyploidy in part evolved to mitigate the cancer risk associated with these types of acutely acting liver mutagens, which frequently induce lethal cancers during the reproductive years. We believe that polyploidy in the context of acute injury events are essential to understand because these may be the types of massive toxic events that mammalian livers have evolved to buffer against.

Despite the importance of acute liver injuries, it is possible that polyploidy might have different implications for chronic injury. The high fat diet model (Figure 9) involves chronic nutritional stress that can contribute to cirrhosis and HCC in patients. Our data suggests that in this

chronic context, polyploidy is protective against HCC development. Work on this and other liver cancer models will help to determine if polyploidy in the liver is generally tumor suppressive or is dependent on factors such as the nature of the genetic driver lesion or environmental injury.

In future studies, it would be also interesting to determine if there are specific diploid populations in the liver that have greater cancer risk and if this risk can be modulated with ploidy manipulations. Previously, Wang et al. identified a "stem-like" hepatocyte population around the central vein [41]. This population of cells repopulated the liver in the absence of injury and were 60% enriched for diploid cells, but it is unknown if the diploid or polyploid cells within this Axin2 compartment have greater self-renewing capacity or tumorigenic potential. It is possible that increasing ploidy in this population might change regenerative capacity or cancer risk. Given that most hepatocytes are capable of extensive proliferation [48, 81], it is also possible that other diploid populations, whether or not they are stem cells, could respond to distinct liver injuries and contribute to cancer formation. In this study, we aimed to answer a fundamental question about polyploidy in liver biology, but it is possible that transient or persistent polyploidzation not only serves physiologic functions but could be exploited therapeutically.

Acknowledgements

This chapter was published as Zhang et al. 2015 [177].

CHAPTER 5

KNOCKDOWN OF ANLN BLOCKS CYTOKINESIS IN HEPATOCYTES AND REDUCES LIVER TUMOR DEVELOPMENT IN MICE WITHOUT AFFECTING REGENERATION

Introduction

Cytokinesis is essential for complete cell division and is a process shared by most mitotic cells[178]. Thus, inhibiting cytokinesis to treat cancer could lead to detrimental outcomes for normal tissues containing cells that undergo repeated cell division[72, 179-181]. In contrast, the liver uniquely undergoes cytokinesis failure to generate polyploid cells as part of its normal postnatal development process[33, 182, 183]. More than 50% of adult rodent hepatocytes are polyploid, harboring four or more copies of chromosomes in their nuclei, as opposed to 2c diploid cells[154, 184, 185]. It is likely that human hepatocytes also undergo cytokinesis failure during liver maturation[33, 34, 186]. Given this tolerance for cytokinesis failure, we hypothesized that the liver would be amenable to cytokinesis inhibition as an anti-cancer strategy.

Previously, it was shown that livers without *Cdk1*, a critical cyclin dependent kinase and mediator of cytokinesis, developed normally and was able to regenerate after partial

hepatectomy[187]. These livers had enlarged hepatocytes that were massively polyploid due to cell cycle abnormalities and incomplete cytokinesis. Moreover, these liver-deficient *Cdk1* mice developed less cancer after diethylnitrosamine (DEN) mutagen treatment[187]. However, that study did not address whether cytokinesis failure could be tolerated in the context of chronic injuries that demand long-term regeneration and tissue restoration. This is an essential point as hepatocellular carcinoma (HCC), the most common form of primary liver malignancy, occurs most commonly in the setting of long-term chronic damage, such as alcohol use or viral hepatitis. In addition, it is not clear if cytokinesis inhibition would prevent cancer proliferation in a cell autonomous fashion or promote cancer development by worsening a damaged tissue microenvironment in a non-cell autonomous fashion.

To interrogate the effects of cytokinesis in cancer formation, we targeted a protein that is specifically important for cytokinesis rather than one like CDK1, which influences all stages of mitosis. ANLN is an evolutionarily conserved actin binding protein that serves as a key mediator of cytokinesis[188, 189]. ANLN contains conserved N-terminal actin and myosin binding domains, a C terminus Anillin homology domain and a PH domain which binds to RhoA, Ect2, and Septins[189, 190]. ANLN binds to all three types of actin filaments[189, 191, 192] as well as other important cytoskeletal components, serving as a scaffolding protein to coordinate cytokinesis in space and time. The exact mechanisms by which ANLN functions in cytokinesis remains incomplete, but its presence is important during multiple stages of cytokinesis[193-195].

Previous studies suggested that *ANLN* overexpression contributes to human cancer growth and implicated ANLN as a potential therapeutic target. *ANLN* siRNA knockdown in breast cancer and non-small cell lung cancer (NSCLC) cell lines inhibits proliferation[196, 197]. Moreover, *ANLN* expression was shown to serve as an independent prognostic marker for breast cancer

patients[198]. However, it is unknown if ANLN is required by normal or malignant hepatocytes for cytokinesis and cell division, and no study has investigated the role of ANLN in liver cancer development.

Here, we generated multiple methods and models for *Anln* inhibition that successfully induced cytokinesis failure. We then tested the effects of blocking *Anln* in multiple cancer models and found that *Anln* inhibition impaired tumor initiation and growth and could extend overall survival. Importantly, we found that *Anln* suppression did not contribute significantly to liver tissue damage, nor did it impair normal liver functions and the capacity to regenerate after both acute and chronic injuries. Collectively, these preclinical results in multiple endogenous liver cancer models suggest that inhibiting cytokinesis is a tolerable and effective HCC prevention strategy in the setting of liver damage.

Anln is required for cytokinesis

To find a specific target involved in cytokinesis, we first examined the results of a previously performed RNAi screen that identified essential cell cycle regulators[155]. We assessed four candidate genes associated with cytokinesis defects (*Incenp, Cdk1, Ect2,* and *Anln*). To determine which ones were required for cytokinesis in liver cells, we performed siRNA knockdowns in a SV40 transformed hepatocyte cell line called H2.35 (Figure S13A). 72 hours after siRNA transfection, we performed flow cytometry to examine changes in cellular ploidy. *siAnln* transfected cells underwent much more dramatic increases in polyploidization (Figure S13A, Figure 12A-B), thus we chose to focus exclusively on *Anln*. Further analysis with live imaging showed that *siAnln* cells failed to complete cytokinesis (Figure 12C), and became large and multinucleated (Figure 12D).

To further examine the precise stage at which *Anln* is essential, we used immunofluorescence to examine mitosis and cell division (Figure 12E). Aurora B kinase, used to identify distinct stages of mitosis, is co-localized at the invaginating cleavage furrow during cytokinesis. siRNA treated cells were synchronized at the G2/M stage by nocodazole. After nocodazole was removed, Aurora B is localized to DNA in both siRNA groups at time 0 min. Both groups showed Aurora B localization at centromeres, marking relatively normal metaphase (40 min). At 80 min, *siScr* treated cells continued with normal anaphase and telophase, marked by localization of Aurora B at the cleavage furrow, while *siAnln* treated cells did not form a normal cleavage furrow, indicating a failure to enter anaphase/telophase. *siScr* cells completed cytokinesis at around 120 min, but *siAnln* treated cells still appeared to be frozen in anaphase and could not generate a cleavage furrow or contractile ring. 92% of *siScr* cells completed mitosis including cytokinesis, compared to 24% of *siAnln* cells (Figure 12F, n = 25-36 cells analyzed per group). These data demonstrated that dividing cells require normal levels of ANLN to complete cytokinesis.

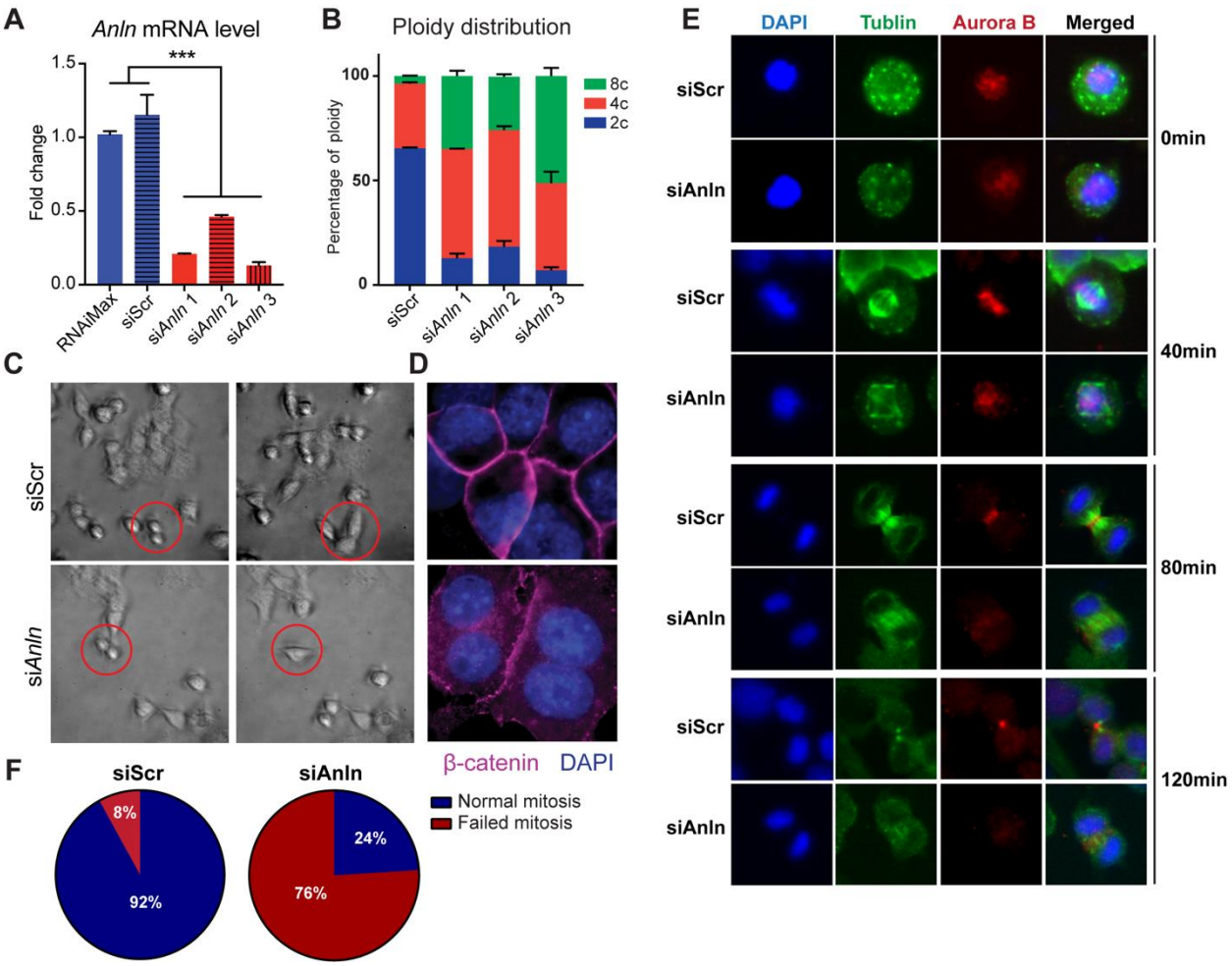

Figure 12. *Anln* is a cytokinesis regulator and is required for cytokinesis.

(A) *Anln* mRNA levels in H2.35 cells after siRNA knockdown, as measured by RT-qPCR. si*Anln* #1 was selected for subsequent animal experiments. (B) Ploidy distribution in H2.35 cells treated with either *siScr* or 3 different *Anln* siRNAs. (C) Live imaging of H2.35 cells treated with either siScr or si*Anln* #1. Red circles are around cells undergoing or attempting division. Live imaging initiated 36 hours after transfection. Images were taken every 3 min. Videos are included in the Supplemental materials. (D) DAPI and Ctnnb1 immunofluorescence staining of *siScr* and *siAnln* treated H2.35 cells. DAPI marks nuclei and Ctnnb1 marks cell membranes. (E) Immunofluorescence staining for DAPI (blue), tubulin (green) and Aurora B (red) in H2.35 cells

during mitosis. H2.35 cells were transfected with siScr or siAnln. 36 hours after transfection, cells were blocked with 150ng/mL nocodazole for 8 hours, washed, then given fresh media. Immediately after changing to fresh media, the time lapse started, and the cells were fixed with PFA in every 20 min for 140 min. The cells were then subjected to immunofluorescence staining. (F) Quantification of normal mitotic events. 25-36 cells were counted for each group. Only cells in anaphase and telophase/cytokinesis (80 min and later) were included.

ANLN is overexpressed in liver cancers and is associated with poor prognosis

To determine whether *ANLN* has important roles in human cancer, we examined *ANLN* expression in multiple malignancies. RNA-seq data from The Cancer Genome Atlas showed that *ANLN* mRNA expression is upregulated in most tumor types when compared to normal tissues (Figure 13A). In support of putative oncogenic activities, higher *ANLN* expression is known to correlate with higher metastatic frequency[199] and poorer prognosis[200] (Figure 13B, from www.proteinatlas.org and Figure 13C from www.prognoscan.org). We then focused on the liver specifically and analyzed data from Oncomine showing that *ANLN* was expressed 2-fold higher in 35 HCCs as compared to 10 normal adjacent liver tissues (Figure 13D). We confirmed this upregulation of *ANLN* mRNA in our own collected matching pairs of HCC and normal tissues (Figure 13E). Furthermore, an HCC tissue microarray showed that *ANLN* protein levels were significantly higher in tumors compared to normal liver tissues (Figure 13F).

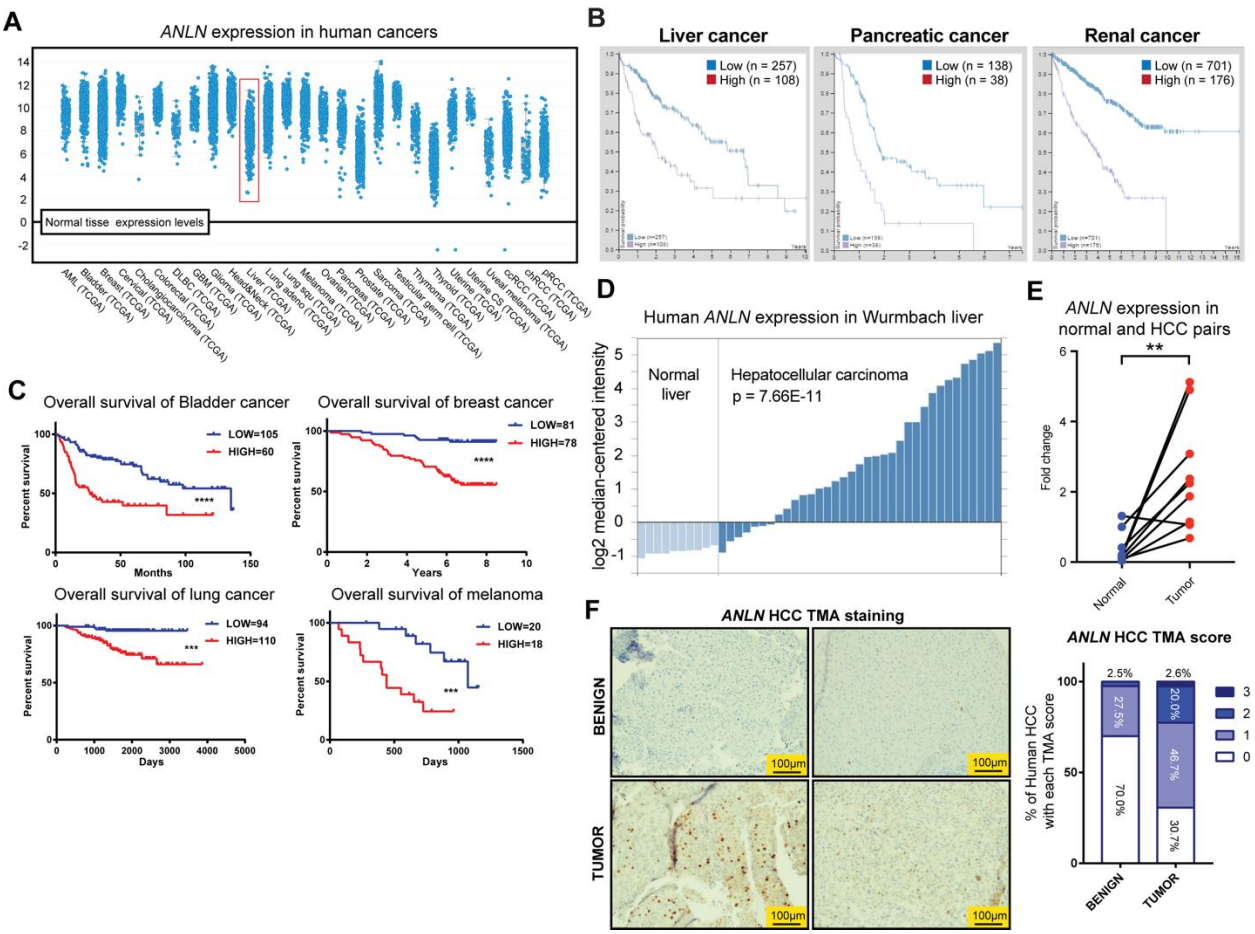

Figure 13. *ANLN* is overexpressed in liver cancers and is associated with poor prognosis.

(A) Human *ANLN* expression in different tumor types from the TCGA database. Adapted from cBioPortal: http://www.cbioportal.org/index.do. (B) Overall survival for patients with high and low *ANLN* expression in liver, pancreatic and renal cancers (https://www.proteinatlas.org). (C) Overall survival curves for patients with high and low *ANLN* expression in bladder, breast, lung, and skin cancers. Adapted from http://www.abren.net/PrognoScan/. (D) Human ANLN mRNA expression levels in normal liver and HCC tissues (Oncomine). (E) RT-qPCR data showing human *ANLN* expression in matched normal and HCC pairs. (F) ANLN HCC tissue microarray with 48

tumors and matching benign tissues. The *ANLN* expression level was scored based on the staining: 0: not detected; 1: low; 2: medium; 3: high. The percentage of human HCC with each TMA score is shown on the right.

In vivo Anln knockdown impaired MYC-induced liver tumorigenesis

To determine if *Anln* and cytokinesis are required for liver tumor development in an endogenous cancer model, we delivered *Anln* siRNA into the well-established *MYC* driven hepatoblastoma model[162]. This is an aggressive cancer model in which human *c-MYC* is overexpressed in the liver by withdrawing doxycycline (dox) water at the time of birth (Figure S13B). This model has 100% penetrance and a median survival of approximately 50 days. To suppress *Anln* expression, we packaged *siAnln* or *siScr* in lipid nanoparticles[201] and injected the LNPs intravenously into *LAP-MYC* mice from p10 to p25 (Figure 14A). The 5A2-SC8 dendrimer LNP was selected due to its ability to deliver siRNAs to hepatocytes and tumor cells with minimal carrier-induced hepatotoxicity.[201] *Anln* mRNA levels were significantly reduced in normal liver tissues after the dosing regimen (Figure 14B). There was no difference in the liver to body weight ratios between *siScr* and si*Anln* groups at P34, which is when macroscopic liver tumors first appear in this model (Figure 14C). At P34, si*Anln* treated mice exhibited significantly fewer tumor nodules on gross and histologic examination (Figure 14D-F). Moreover, *siAnln* treated mice survived significantly longer (Figure 14G; $p < 0.05$). These results suggested that elevated *Anln* expression and cytokinesis are required for efficient transformation and tumor initiation in the *MYC*-induced hepatoblastoma model.

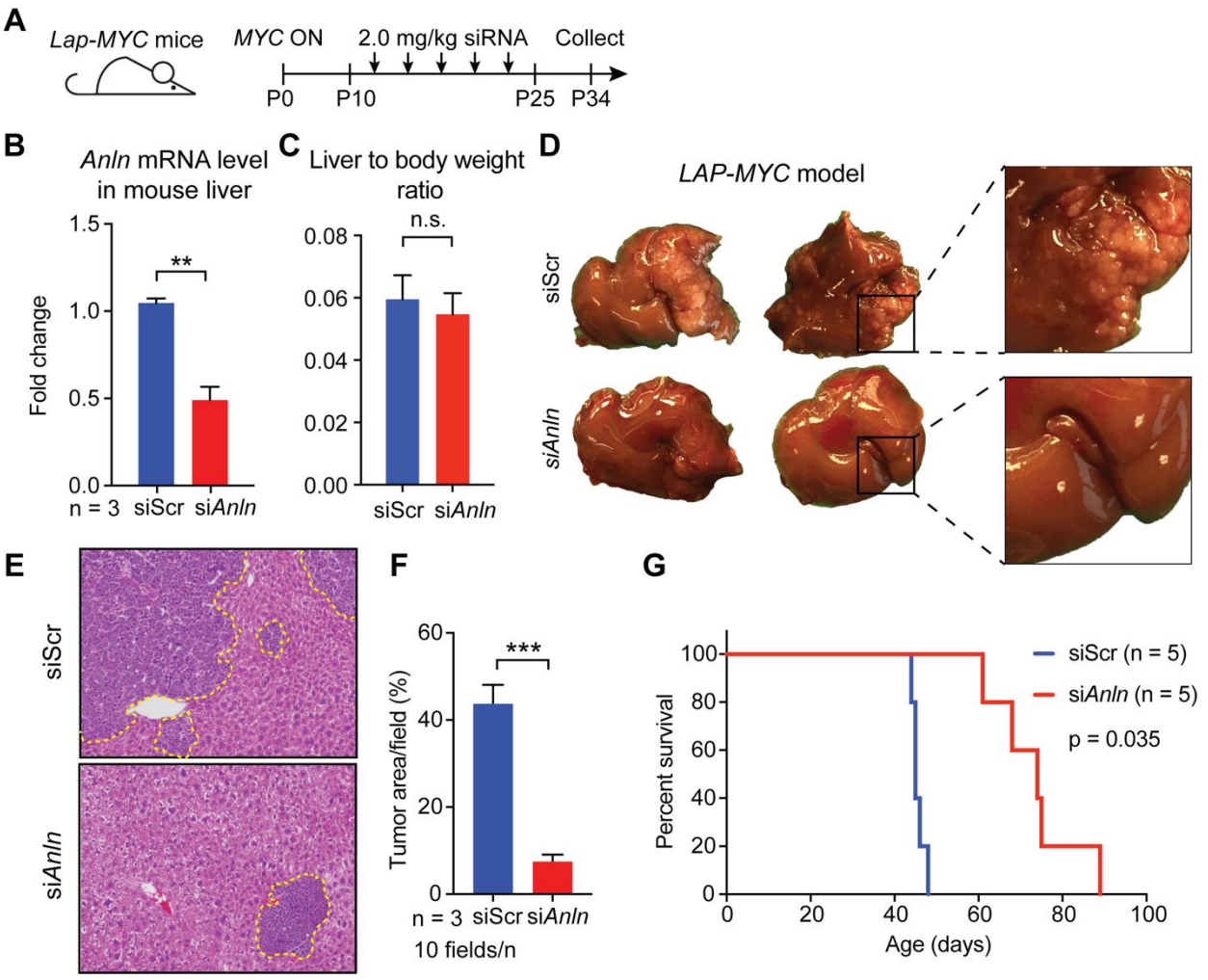

Figure 14. In vivo *Anln* knockdown impaired *MYC*-induced liver tumorigenesis.

(A) A schematic of the induction and treatment regimen. Dox was withdrawn at P0 to induce human c-*MYC* expression. IV delivery (two intraperitoneal and three retro-orbital) of in vivo siRNAs packaged in LNPs started at P10 and lasted until P25. Dosing was twice per week at 2 mg/kg. (B) *Anln* mRNA levels as determined by RT-qPCR in *MYC*-induced livers treated with either in vivo *siScr* or *siAnln*. (C) Liver-to-body weight ratios of *MYC*-induced mice treated with either in vivo *siScr* or *siAnln* at P34. (D) Gross liver images of *MYC*-induced mice treated with either in vivo *siScr* or *siAnln* at P34. Macroscopic tumors were observed in *siScr* but not in *siAnln*

treated livers. (E) H&E staining showing microscopic cancer lesions (circled by yellow dotted lines). (F) Quantification of tumor area/field in the H&E staining in both siScr and si*Anln* treated mice. 10 random fields per mouse (n = 3 mice) were analyzed. (G) Kaplan-Meier survival of *MYC*-induced mice treated with either in vivo *siScr* or *siAnln.*

Anln suppression impaired tumor engraftment in a chronic liver damage model

To inhibit *Anln* expression in a temporally-specific and prolonged fashion, we developed a retroviral doxycycline (dox)-inducible Tet-on system to drive the expression of either scrambled (*shScr*) or *Anln* shRNA (*shAnln*) (Figure 15A, vector obtained from Scott Lowe's lab[202]). After testing 10 distinct *Anln* shRNAs, *shAnln* #2 and #3 were selected based on their knockdown efficiency (Figure 15B). Similar to siRNA experiments, H2.35 cells stably infected with *shAnln* #2 or #3 underwent polyploidization after three days of dox induction, indicating ongoing mitosis with cytokinesis failure (Figure 15C). To determine whether this retroviral system was truly inducible, we measured proliferation of cells stably infected with either *shScr* or *shAnln*. While there were no differences in proliferation in the absence of dox, *shAnln* 2 and 3 containing cells showed significant growth inhibition after dox exposure (Figure 15D).

We next tested the effects of *Anln* inhibition in a chronic liver damage model based on hereditary tyrosinemia[203]. Without treatment, the livers of fumarylacetoacetate hydrolase $(FAH)^{-/-}$; $Rag1^{-/-}$; $IL\text{-}2R\gamma^{-/-}$ (*FRG*) mice accumulate a toxic metabolite called fumarylacetoacetate, develop liver failure, and subsequently die. The injured liver microenvironment contributes to the development of cirrhosis and HCC[204]. To effectively treat this liver disease, mice and human patients are normally given NTBC (2-(2-nitro-4-trifluoromethylbenzoyl)-1,3-cyclohexanedione), a drug that clears fumarylacetoacetate and effectively maintains a healthy liver. Because *FRG*

livers experience extensive hepatocyte destruction, these mice can be used as efficient transplant recipients for normal hepatocytes or HCC cells[203, 205, 206].

We transplanted the stably shRNA infected H2.35 cell lines into immunosuppressed *FRG* mice via splenic injection, which led to the homogenous delivery of cancer cells throughout the liver. This models widespread intrahepatic metastasis in the setting of chronic liver damage. After splenic transplantation, we withdrew NTBC to induce liver damage in host tissues, and kept half of the *shScr* and *shAnln* H2.35 transplanted mice on regular water and the other half on dox water to drive shRNA expression (Figure 15E). After 49 days, we found that the mice without dox induction had similar levels of tumorigenesis (Figure 15F). In contrast, the *shAnln* mice exposed to dox water had significantly fewer tumor nodules than the *shScr* mice (Figure 15F). GFP expression allowed us to detect greater clonal expansion of *shScr* donor cells (Figure 15G). These data collectively indicated that suppressing *Anln* could impair the engraftment and expansion of HCCs within a chronically injured liver disease model.

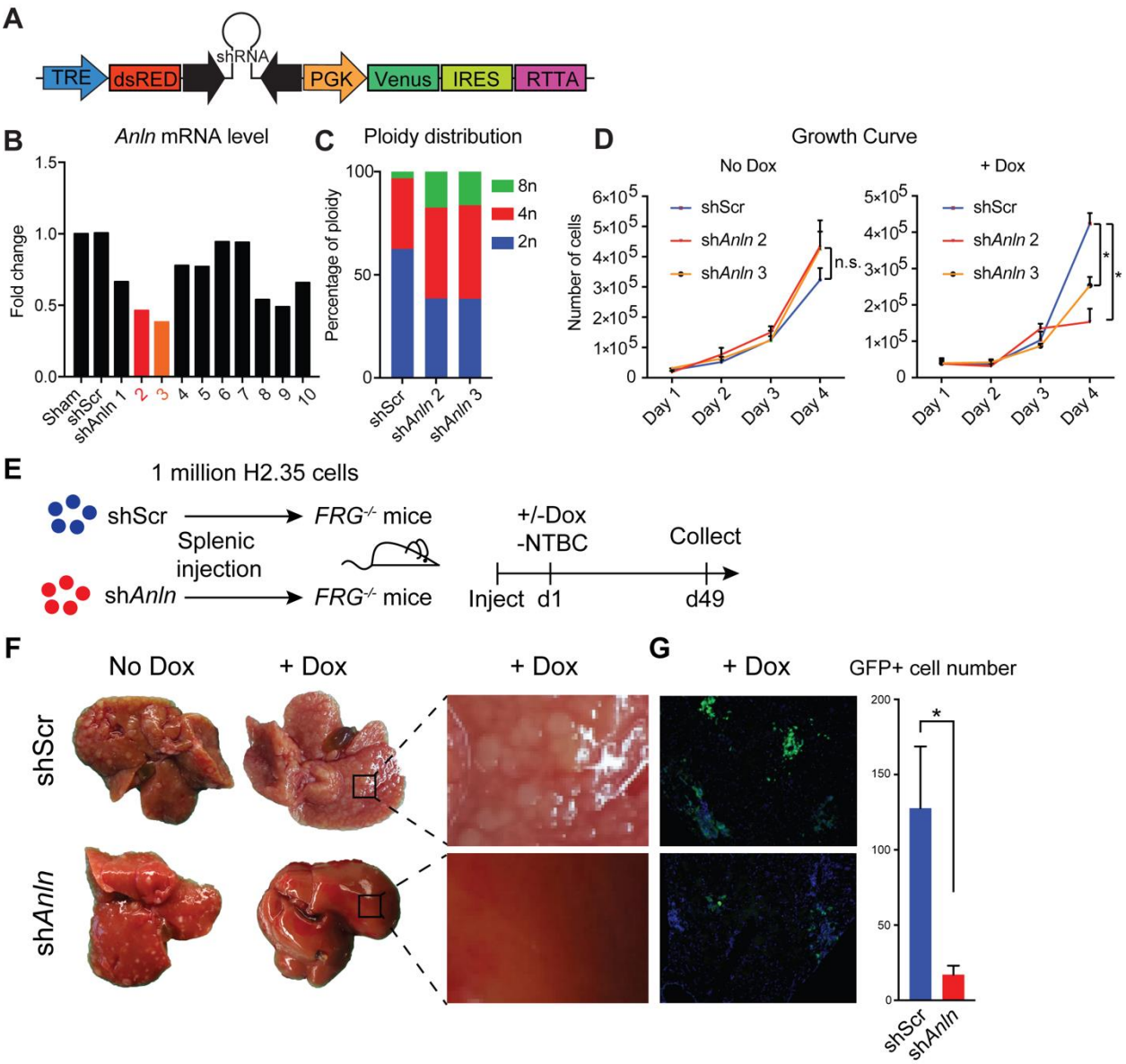

Figure 15. *Anln* suppression impaired tumor engraftment in a chronic liver damage model.

(A) Retroviral TRMPVIR construct. (B) To screen for knockdown efficiency of 10 distinct *shAnln's*, *Anln* mRNA levels in H2.35 cells were measured by RT-qPCR. (C) Ploidy distribution in H2.35 cells treated with either *shScr*, *shAnln* #2, or *shAnln* #3. (D) Proliferation assays in uninduced and dox-induced H2.35 cells containing either *shScr*, *shAnln* #2, or *shAnln* #3. (E) A

schematic of the *FRG* transplantation experiment. (F) Gross images of *FRG* livers transplanted with either *shScr* or *shAnln* with or without dox induction. (G) On the left are fluorescent images showing GFP+ H2.35 donor clones stably infected with either *shScr* or *shAnln*. On the right is the quantification of GFP+ H2.35 cells per field, 5 fields for each liver.

Anln suppression in transgenic mice prevented HCC formation in a DEN + CCl_4 model

The *MYC* experiment showed that *Anln* suppression was effective against hepatoblastoma development in a non-injured environment and the *FRG* experiment showed that *Anln* suppression was effective in a cell-autonomous fashion within a chronic liver injury model. Ultimately, the most critical question is whether or not potent *Anln* suppression in all cells of the liver would be safe and/or effective in a clinically relevant, chronic liver injury model. Towards these ends, we engineered a dox-inducible transgenic mouse expressing *shAnln* #2. Transgenic mice were derived from embryonic stem cells containing *Rosa-rtTA* and a GFP expressing sh*Anln* cassette under the control of a tetracycline responsive promoter element (*TRE*) (Figure S13C; transgenic design based on[85]). Dox could be used to induce shRNA and *Anln* suppression in a temporally specific fashion. *Rosa-rtTa* alone or *Rosa-rtTa; TRE-shAnln* (hereafter called *Rosa* and *TG-shAnln*) transgenic mice exposed to dox water from P0-P20 showed normal growth, development, and liver function. We had previously found that *Anln* mRNA levels were suppressed by 50% in this model resulting in hyperpolyploid livers after dox withdrawal[207]. This mouse model demonstrated that transient *Anln* suppression in vivo was sufficient to increase polyploidy.

We first tested the tumorigenesis in this model with DEN alone, and the *TG-shAnln* mice exhibited strong inhibition of tumor development (Figure S13D). HCC in the western world most often arises in microenvironments characterized by chronic inflammation, fibrosis, and hepatocyte

proliferation. In mice, this scenario can be mimicked by introducing DEN followed by biweekly carbon tetrachloride (CCl_4) to induce chronic injury[208]. We gave *Rosa* and *TG-shAnln* mice DEN at P15, exposed both cohorts to dox to induce *shAnln* in the experimental group starting at P32, then started biweekly CCl_4 injections at P39 (Figure 16A). After 8 weeks of CCl_4 injury, liver function tests revealed lower AST and ALT levels in *TG-shAnln* group (Figure S13E). After 12 weeks of CCl_4, *TG-shAnln* mice exhibited almost no frank HCC development especially when compared to the multifocal disease seen in control mice (Figure 16B, C). Moreover, liver to body weight ratios were much higher in the *Rosa* group, likely due to the higher tumor burden (Figure 16C). Examination of liver histology showed similar levels of liver pathology as compared to control mice (Figure 16D). qPCR for fibrosis genes from the non-tumor compartment showed that *Col1a1* and *Col1a3* were modestly higher in *TG-shAnln* mice, suggesting a trend toward greater collagen deposition and fibrosis (Figure 16E). However, trichrome quantification revealed similar level of fibrosis in control and *TG-shAnln* livers (Figure 16F). Also, we did not identify a reduction in proliferation within *TG-shAnln* livers (Figure S13F, G). Moreover, there was no significant difference in genotoxicity (Figure S13H). These results showed that inhibiting cytokinesis almost completely blocked tumorigenesis in a chronic injury liver model without major effects on liver damage and repair.

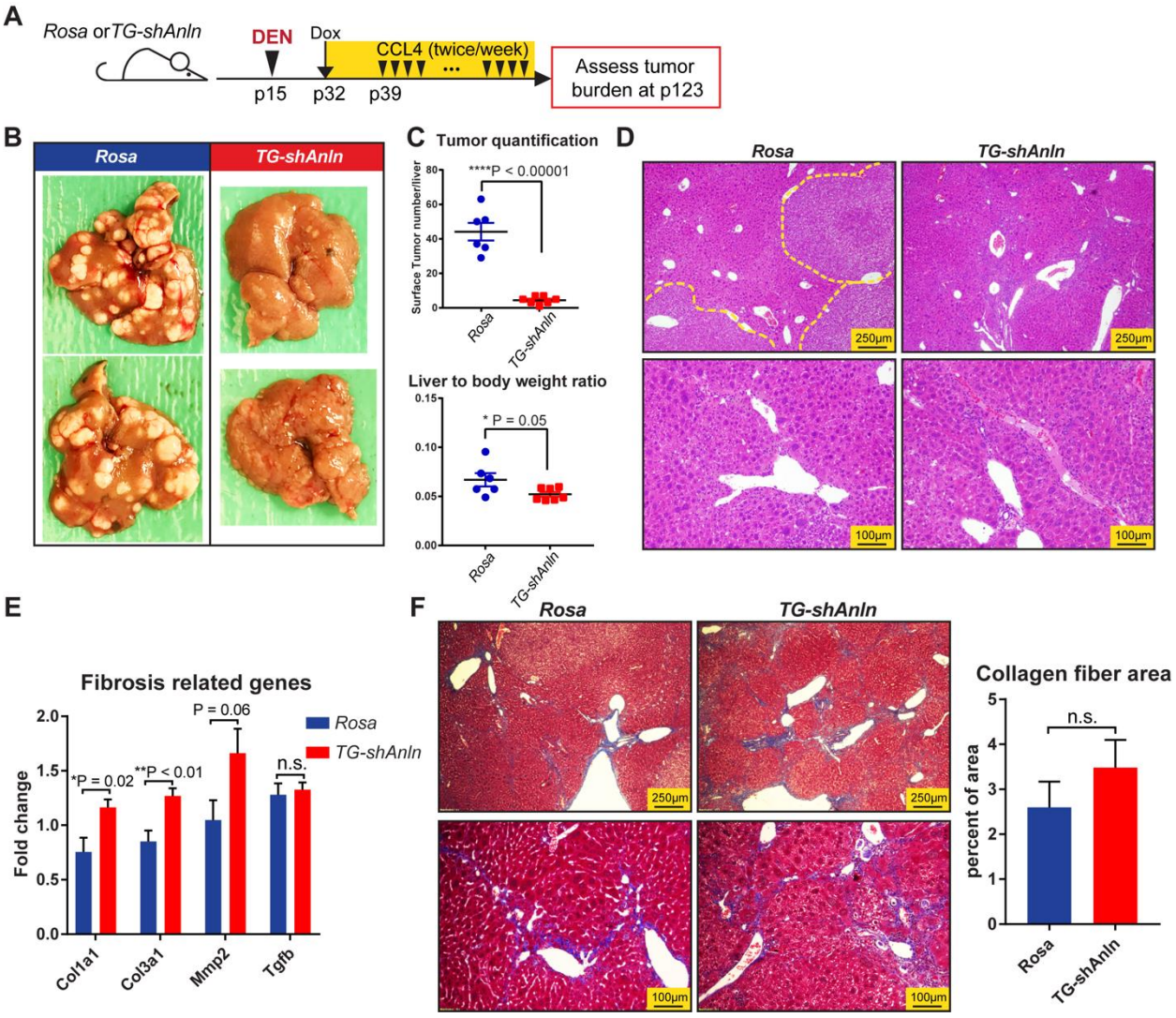

Figure 16. *Anln* suppression in transgenic mice prevented HCC formation in a DEN + CCl_4 model

(A) Schema for the DEN + chronic CCl_4 mediated HCC experiment in inducible shRNA mice. At P15, mice were injected with DEN (25μg/g). At P32, dox was started and one week later (P39), twice per week IP CCl_4 injections were started. Tumor burden was examined after 12 weeks of chronic CCl_4 injury (24 total doses). (B) Representative gross tumor burden from *Rosa* and *TG-shAnln* mice. (C) Liver surface tumor quantification and liver to body weight ratios. (D) H&E

histology of *Rosa* and *TG-shAnln* livers show tumor nodules (circled by dashed yellow outlines). (E) qPCR for fibrosis related genes in *Rosa* and *TG-shAnln* livers as described in (A) (n = 6 mice per group). (F) Trichrome staining showing collagen deposition in *Rosa* and *TG-shAnln* livers. On the right, quantification of trichrome+ areas (n = 4 mice in each group, 3 liver fragments were taken from each mouse, and 3 images were taken from each liver fragment, a total of 36 images examined per treatment group).

Anln suppression in transgenic mice did not impair liver function or regeneration

Although *Anln* suppression could effectively inhibit liver cancer development in multiple settings, it was possible that it could also harm normal cells through the blockade of cytokinesis. To examine the effect of suppressing *Anln* on normal liver, we first assessed liver gene expression after *Anln* suppression and cytokinesis inhibition. There was no significant impact on liver differentiation gene expression after *shAnln* induction from P0-P20 (Figure 17A and B). This is also corroborated by Glutamine synthetase and Cyp2e1 immunostaining on control and *Anln* suppressed liver tissues (Figure 17C). Although suppression of *Anln* did not cause liver damage or changes in cellular differentiation, we hypothesized that there might be negative effects on cell growth and regeneration after injury, since induction of *shAnln* led to downregulation of cell cycle genes in the *TG-shAnln* livers (Figure S13I). After partial hepatectomy in adult *Rosa* and *TG-shAnln* mice that had been induced with dox for one week, we saw no differences in liver to body weight ratios after 40 hours, 3 days and 7 days of regeneration (Figure 17D). There were similar numbers of mitotic cells as detected by phospho-H3 (Figure 17E-G). Likewise, expression of cell cycle genes was unchanged (Figure S14A). *TG-shAnln* livers did exhibit significantly larger hepatocytes 7 days after surgery (Figure S14B-E). After we challenged mice with two doses of

CCl_4, *TG-shAnln* mice did not exhibit higher AST or ALT levels compared to control mice (Figure 17H). Together, these data demonstrated that suppression of *Anln* and cytokinesis did not have a detrimental impact on liver regeneration after acute injuries.

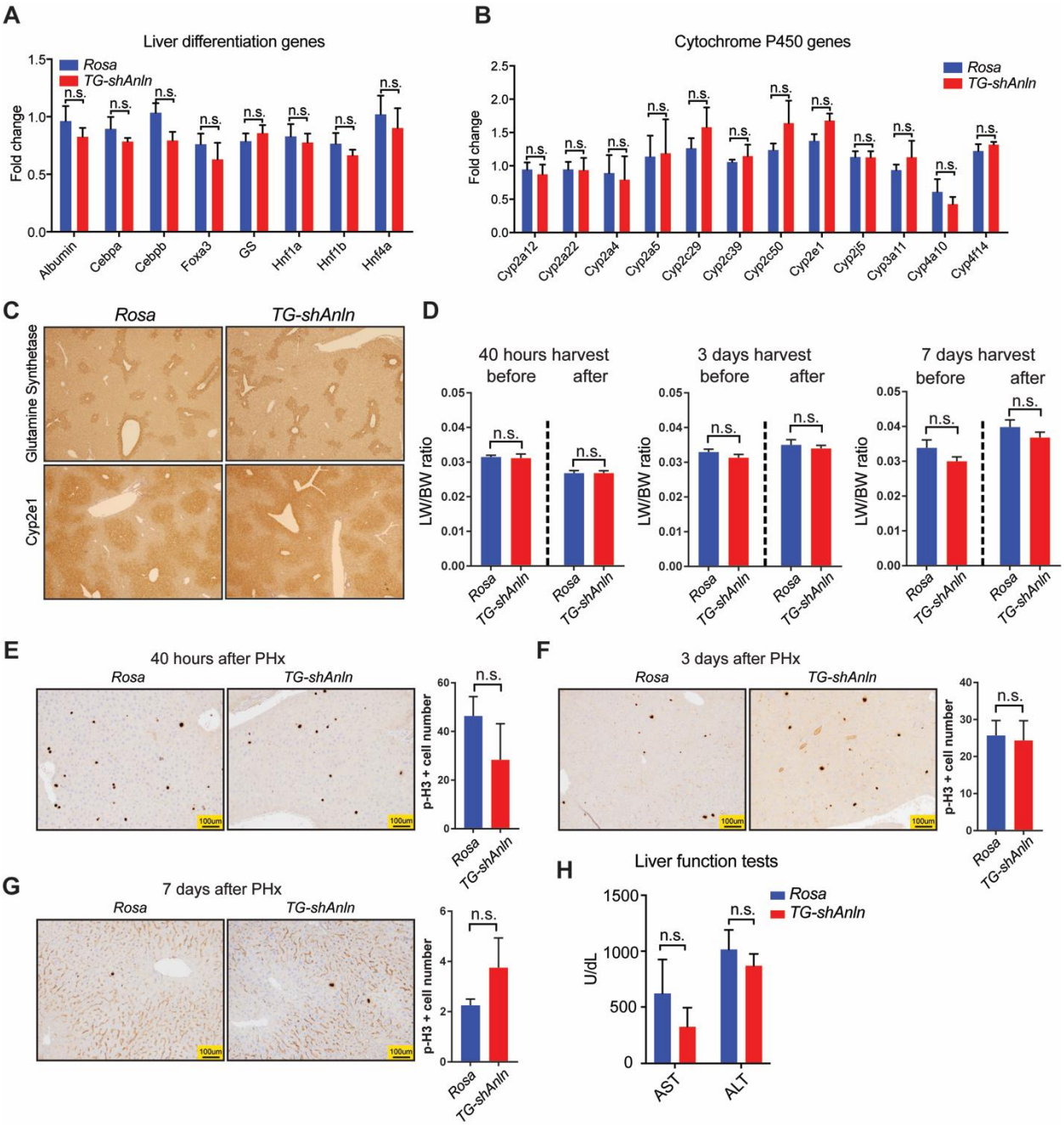

Figure 17. *Anln* suppression in transgenic mice did not impair liver function or regeneration. (A) qPCR for liver specific differentiation genes and transcription factors in *Rosa* and *TG-shAnln* livers (n = 5 per group). *Rosa* and *TG-shAnln* mice were given dox water (1g/L) after birth at P0 until P21, when livers were harvested. (B) qPCR for Cytochrome P450 genes in *Rosa* and *TG-shAnln* livers (n = 5 per group). (C) Glutamine synthetase (upper) and Cyp2e1 staining (lower panels) in *Rosa* and *TG-shAnln* livers. (D) Liver to body weight ratios of regenerating livers at 40 hours, 3 days and 7 days after partial hepatectomy. Six week old *Rosa* and *TG-shAnln* mice were given dox for 7 days before surgery, then underwent 70% partial hepatectomy and remnant livers were harvested and analyzed at 40 hours, 3 days and 7 days after surgery (n = 3 mice per group for the 40-hour and 3-day time points, n = 4 for 7 day time point). (E) Phospho-H3 staining in *Rosa* and *TG-shAnln* livers at 40 hours, (F) 3 days, and (G) 7 days after hepatectomy. Quantifications are shown on the right. (H) Liver function tests of *Rosa* and *TG-shAnln* mice after two doses of CCl_4 given 3 days apart. The mice were induced with dox water (1g/L) one week before the first CCl_4 injection (n = 7 and 7).

GalNAc mediated siAnln delivery inhibited cancer but did not impair liver regeneration

Even after performing toxicity experiments in *Rosa-rtta* induced shRNA transgenic mice, we still had questions regarding long-term safety. First, it was unclear if the whole-body shRNA expression in the *TG-shAnln* might have potentially masked liver damage via the knockdown of *Anln* in other cell types (lymphocytes, for example). In addition, it is well known that shRNAs can cause liver toxicity in part due to high-dose mediated saturation of endogenous microRNA processing machinery. Moreover, LNPs that are used to package siRNAs can cause toxicity

independent of the target, an issue that we previously studied in the context of improved LNP development.[201] To circumvent some of these concerns, we asked if we could safely and effectively block liver cancer using an alternative small RNA delivery strategy, which involves attaching N-acetylgalactosamine (GalNAc) to nucleic acid molecules. Hepatocytes express the Asialoglycoprotein receptor (ASGPR), which mediate the uptake and clearance of circulating glycoproteins with exposed GalNAc. These siRNA reagents would allow us to test potential effects of hepatocyte-specific knockdown at clinically achievable doses.

23 different siRNAs against *Anln* were screened using a luciferase based platform. Six of the best siRNAs against *Anln* and a control siRNA against firefly luciferase (si*Luc*) were then GalNAc-conjugated. After in vivo testing, siRNA #1 (hereafter referred to as si*Anln* or GalNAc-*siAnln*) was selected for subsequent in vivo experiments (Figure S15A). Consistent with the *TG-shAnln* model, the GalNAc-*siAnln* treated livers did not show altered expression of differentiation markers (Figure S15B).

We then tested liver regeneration after GalNAc-si*Anln* using a panel of liver injury models. We first challenged the mice with partial hepatectomy and harvested livers at 40h, 3 days, and 7 days after surgery. No differences in liver to body weight ratios between si*Luc* and si*Anln* treated mice were detected at any time points (Figure 18A and B). Mitosis rates were also similar, as assessed by phospho-H3 (Figure S15C-E). Next, we used CCl_4 to test regeneration under both acute and chronic injuries. Again, we started the weekly siRNA (4 mg/kg) 1 week prior to CCl_4, which was given twice per week chronically. si*Anln* treated mice failed to show higher AST, ALT and TBIL after acute (1 week) or chronic (6 weeks) CCl_4 injury (Figure 18C and Figure S16B). Albumin and glucose in si*Anln* treated mice were slightly lower than controls after 8 weeks of CCl_4 (Figure 15A, C), but these parameters were still within normal limits. Moreover, cell cycle

genes were similarly expressed between the two groups (Figure S16D), suggesting unimpaired liver regeneration. As an indication of cytokinesis inhibition and siRNA efficacy, *GalNAc-siAnln* treated livers possessed larger hepatocytes as compared to controls (Figure S16E, F).

We then used the *FRG* hepatocyte transplantation system to more stringently test hepatocyte proliferation in the setting of *Anln* suppression. Because the transplanted hepatocytes are required to proliferate multiple rounds in order to repopulate the *FRG* liver, this model exerts a greater demand on proliferation. *FRG* recipients of wild-type primary hepatocytes were treated with weekly GalNAc-si*Luc* or GalNAc-si*Anln* (4 mg/kg). The GalNAc-si*Anln* treated mice exhibited similar body weights compared to controls (Figure 18D). 45 days after transplantation, the body, liver, and liver/body weight ratios were unchanged (Figure 18F). Hepatocyte repopulation efficiency as measured by FAH IHC was similar between groups (Figure 18E). Furthermore, *Anln* knockdown was confirmed and cell cycle gene expression was unchanged (Figure S16G, H). Finally, we confirmed the efficacy of GalNAc-si*Anln* on DEN-mediated and *LAP-MYC* tumorigenesis (Figure 18G, H), suggesting that GalNAc-*siAnln* delivery is able to inhibit tumors in multiple settings. Taken together, these results demonstrated that suppression of *Anln* was able to effectively inhibit HCC but did not significantly impair liver regeneration after acute and chronic injuries.

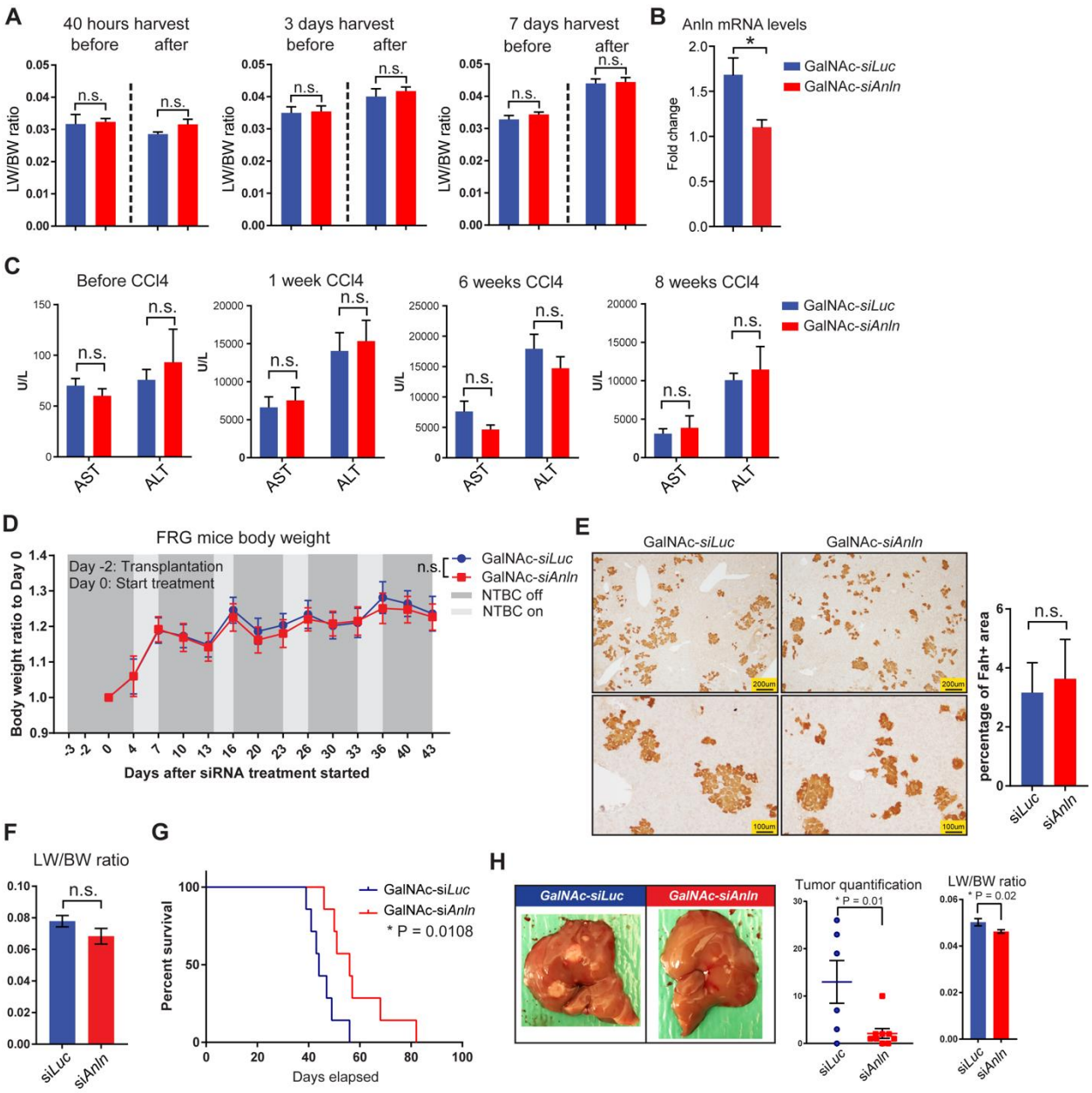

Figure 18. ***GalNAc mediated siAnln delivery inhibited cancer but did not impair liver regeneration.***

(A) Liver to body weight ratios of resected and regenerated livers after partial hepatectomy. Six-week old CD1 mice were given GalNAc-si*Luc* or GalNAc-si*Anln* (4mg/kg) 1 week before surgery, then underwent 70% partial hepatectomy. Remnant livers were harvested and analyzed at 40 hours,

3 days and 7 days after surgery (n = 3-5 per group). (B) *Anln* mRNA levels of the above mice, as measured by qPCR. (C) Liver function tests of mice before and after 1, 6, and 8 weeks of twice weekly CCl_4 injections. Mice were treated with weekly GalNAc-si*Luc* or GalNAc-si*Anln* (4mg/kg) (n = 7) starting 1 week before injury. (D) Body weights of *FRG* mice over 45 days of siRNA treatments. *FRG* mice received $1x10^6$ primary hepatocytes from wild-type B6 mice. Two days after transplantation, mice were randomly divided into weekly GalNAc-si*Luc* (4mg/kg, n = 6) and GalNAc-si*Anln* (4mg/kg, n = 7) treated groups. The mice were put on a NTBC water cycle (7 days without NTBC followed by 3 days with NTBC), starting one day before transplantation. The Y-axis shows the ratio of the current body weight relative to the initial body weight. (E) FAH immunostaining. The percentages of the FAH positive areas are quantified on the right (n = 4). (F) Liver to body weight ratios of *FRG* mice after 45 days of siRNA treatment. (G) Kaplan-Meier survival of *MYC*-induced mice treated with either GalNAc-s*iLuc* or GalNAc-s*iAnln. Lap-MYC* mice were taken off dox (*MYC* on) at birth. 4 mg/kg weekly siRNA treatments started at P8-P10 (n = 7). (H) Representative tumor burden from C3h mice (left). C3h mice were given one dose of DEN (75ug/g) at P26. At P57, they were randomized to GalNAc-si*Luc* (4 mg/kg, n = 6) or GalNAc-si*Anln* (4 mg/kg, n = 9) groups, and started to receive siRNA treatment every two weeks. Mice were sacrificed at P230. On the right is the surface tumor quantification and liver to body weight ratios.

Discussion

Acute liver regeneration and cancer both depend on cellular growth and proliferation mechanisms. It is unclear if regeneration during chronic injury is as dependent on these mechanisms, since cell

turnover is less dramatic than it is during acute tissue damage. It is also unknown if cancer is more or less dependent on these growth mechanisms. In the normal liver, tissue and cell growth can occur even when cytokinesis is impaired. This occurs when hepatocytes polyploidize after weaning and it occurs to an extreme extent in mutant models with mitosis and cytokinesis defects[187]. This ability to tolerate cytokinesis inhibition begs the question about the requirements for cytokinesis in the context of chronic liver damage, where there is an ongoing demand for cell division.

In this study, we used in vitro and in vivo models to determine if there is a therapeutic window for cytokinesis inhibition in several real-world contexts where liver cancer arises. As previously reported for other genes, we find that acute regeneration does not require completely intact cell division or cytokinesis, likely because only small increases in cellular mass are needed. As expected, it appeared that liver cancers such as hepatoblastoma and HCC were highly dependent on cytokinesis. Although polyploid genomes are observed in cancer, a continuous increase in ploidy did not permit cells to transform or clonally expansion in the models used. The therapeutic index could also be increased due to the ability to deliver siRNAs in a liver specific fashion, since the liver is potentially more able to tolerate incomplete cytokinesis than other tissues. This might represent an advantage for small RNA therapies that only efficiently target the liver over small molecules that result in toxicity in multiple tissues.

A more complex challenge presents itself when one imagines cytokinesis inhibition for HCCs that arise in the setting of chronic liver damage. Given the possibility that regeneration over longer time courses might require normal cytokinesis, it is possible that *Anln* suppression would not be tolerated even if it were effective against HCC formation. We were surprised to find continued survival and a lack of worsening hepatitis in *Anln* suppressed and CCl_4 exposed mice.

Because knockdown of *Anln* was not 100%, it is possible that partial cytokinesis inhibition permitted chronic regeneration but was enough to prevent HCC development. This suggests an adequate therapeutic window for cancer prevention. It was possible that the chronic shRNA expression in *TG-shAnln* transgenic mice might be toxic due to shRNA overexpression rather than any on target effects. However, the tests with GalNAc-siRNAs indicated that suppressing *Anln* will likely be well tolerated in terms of liver damage. It is unclear if GalNAc-based approaches will be effective as a preventative therapy, given the inability of GalNAc to target HCC cells, but our study provides a pre-clinical proof of concept to motivate further examination of cytokinesis inhibition in patients at high risk for HCC development. Within the 1-3 years after "curative" interventions such as resection, ablative techniques, or radiation therapy, there is a high risk for recurrence or de novo HCC[209]. One could imagine using *ANLN* suppression as an adjuvant treatment after such therapeutic interventions. We believe that cytokinesis inhibition could prevent transformation in these pre-malignant hepatocytes that are within a damaged liver "field".

Acknowledgements

This chapter was published as Zhang et al. 2017 [210].

CHAPTER 6

CONCLUDING REMARKS

Summary

This thesis is focused on questions related to liver cancer biology, and the three projects presented here explored this field from different angles.

In the first story, we took advantage of the genome editing tools, and developed efficient TALEN pairs to mutate *β-catenin* and *Apc* genes. Upon successful delivery of these TALENs into mouse livers, we could generate liver tumors with expected *β-catenin* activation mutations, and the homozygous *Apc* loss was more difficult to achieve due to liver polyploidy. This work illustrated an application of utilizing genome editing tools to generate liver cancer models in adult mouse, which significantly shortened the study time and recapitulated the mosaic nature of cancer mutagenesis.

Following the first work, we initiated the second project centered on liver polyploidy. While liver polyploidy has been described for a long time, its functional role is still largely unknown. To investigate the role of polyploidy in liver cancer, we developed several methods and models to efficiently alter liver ploidy in vivo while avoiding introducing permanent genetic changes. After diethylnitrosamine induced mutagenesis, polyploid livers exhibited much less

tumor burden compared to diploid livers, which was in part due to the lower likelihood of tumor suppressor loss in polyploid cells. This work reveals an important function and evolutionary role of polyploidy in mammalian livers.

The polyploidy nature of liver and its tolerance for cytokinesis failure also led us to seek for new therapeutic strategies of treating liver cancer. In the third story, we hypothesized that cytokinesis inhibition could be a potential strategy to suppress liver tumorigenesis without damaging normal liver. By using multiple liver cancer and liver regeneration models, we found that cytokinesis inhibition via *Anln* knockdown could significantly reduce tumorigenesis without impairing liver regeneration capacity. This work suggests that cytokinesis inhibition via *Anln* knockdown is potentially a safe and efficacious strategy for inhibiting liver cancer.

In summary, our work explored new ways for liver cancer modeling, investigated the roles of polyploidy in liver cancer, and sought for new therapeutic strategies for treating liver cancer. These studies, from different aspects, increased our knowledge about liver biology and cancer biology, and provided us with new perspectives in hepatocytes regeneration and liver tumorigenesis.

Future directions

In the second story, we investigated the role of polyploidy in the liver and demonstrated that polyploid hepatocytes were protected against tumorigenesis. However, there are still a few key questions that remain to be answered in this field. The first question is about how polyploid hepatocytes divide in vivo. Duncan *et al.* have shown that the polyploid hepatocytes can divide in vitro and generate diploid daughter cells, a phenomenon termed as “ploidy conveyor” [81]. However, whether this phenomenon also happens in vivo is still questionable and needs more

careful characterization. Another important question is about the tumor origin. Based on our ploidy study, the liver tumors are more likely to arise from diploid cells, but we lack a direct evidence to support this hypothesis. Both questions are critical for understanding the cancer initiation in liver and the dynamic changes of hepatocytes during homeostasis and regeneration.

One way to answer these questions is to develop a lineage tracing tool to specifically label polyploid cells and trace their fates. This polyploidy tracing can be accomplished by introducing a split-cre system, where only the polyploid cells that contain more than two alleles have the possibility of expressing both half-cre together and light up the reporter. With this system, we can examine the ploidy profile of labeled polyploids in order to detect the "ploidy conveyor" phenomenon. Other than that, we can induce tumorigenesis in these mice, and count the percentage of labeled tumors, so as to determine the tumor origin. We hope this lineage tracing approach can allow us to further understand the unique features of polyploid hepatocytes and help us to design better therapies for liver cancer.

Appendix

Supplemental Materials

Figure S1: *β-catenin* TALEN induced mutations in H2.35 cells.

H2.35 cells were transfected with GoldyTALEN vector, left, right, or both *β-catenin* TALENs. Genomic DNA was extracted after 72 hours of transfection, PCR amplified for the TALEN target region. The amplicons were then subjected to XmnI restriction enzyme digestion, and the uncut bands were purified and subjected to TA cloning. Then clones were randomly picked and sequenced. TALEN binding sites are highlighted in yellow.

A Single clone genotyping of *Apc* TALEN treated H2.35 cells

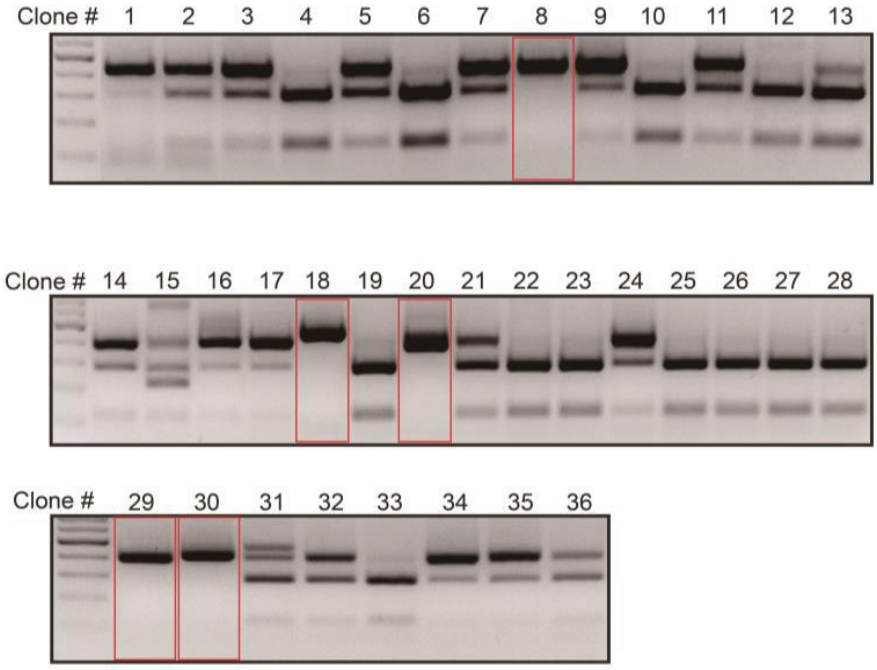

B *Apc* TALEN induced mutantions

```
aactttgctAGCTATGTCCAGCTCCCaagacagctgtatatcCATGCGGCAGTCTGGatgtcttcct (wt)
aactttgctAGCTATGTC----------------------------------TGGatgtcttcct (Δ36)
aactttgctAGCTATGTCCAGCTCCCaagac------------------------GGatgtcttcct (Δ24)
aactttgctAGCTATGTCCAGCTCCCaagaca----tataacCATGCGGCAGTCTGGatgtcttcct (Δ4)
aactttgctAGCTATGTCCAGCTCCCaagacac-----------TGCGGCAGTCTGGatgtcttcct (Δ11)
aactttgctAGCTATGTCCAGCTCCCaagaca------tatcCATGCGGCAGTCTGGatgtcttcct (Δ6)
aactttgctAGCTATGTCCAGCTCCCaagacag---tatatcCATGCGGCAGTCTGGatgtcttcct (Δ3)
aactttgctAGCTATGTCCAGCTCCCa----------------TGCGGCAGTCTGGatgtcttcct (Δ17)
aactttgctAGCTATGTCCAGCTCCCaaga----------------GCAGTCTGGatgtcttcct (Δ18)
aactttgctAGCTATGTCCAGCTCCCaagacagaa--atatcCATGCGGCAGTCTGGatgtcttcct (Δ2)
aactttgctAGCTATGTCCAGCTCCCaagacagct|gtatatcCATGCGGCAGTCTGGatgtcttcct (ins50)
aactttgctAGCTATGTCCAGCTCCCaagacagct|gtatatcCATGCGGCAGTCTGGatgtcttcct (ins6)
aactttgctAGCTATGTCCAGCTCCCaagacagctgt|atatcCATGCGGCAGTCTGGatgtcttcct (ins11)
```

Figure S2: *Apc* TALEN induced mutations in H2.35 cells.

(A) Genotyping results of the H2.35 cell single clones. The H2.35 cells were transfected with both arms of *Apc* TALEN and then plated as single cell clones. Clones were subjected to restriction enzyme digestion genotyping. Shown is the genotyping result for all the 36 clones. 5 clones are *Apc* homozygous mutant clones (highlighted by red rectangles) that only have uncut bands, and 18 are heterozygous clones that have both uncut and cut bands. (B) H2.35 cells were transfected with GoldyTALEN vector, left, right, or both *Apc* TALENs. Genomic DNA was extracted after 72 hours of transfection, PCR amplified for the TALEN target region. The amplicons were then subjected to PvuII restriction enzyme digestion, and the uncut bands were purified and subjected to TA cloning. Then clones were randomly picked and sequenced. TALEN binding sites are highlighted in yellow.

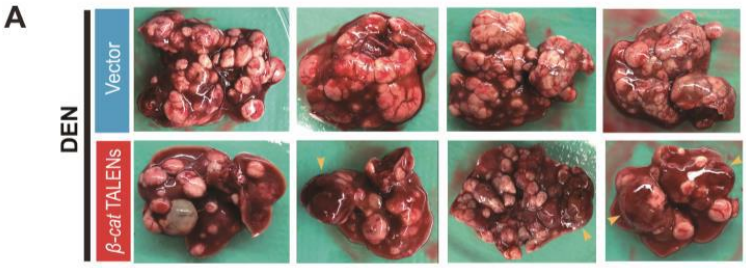

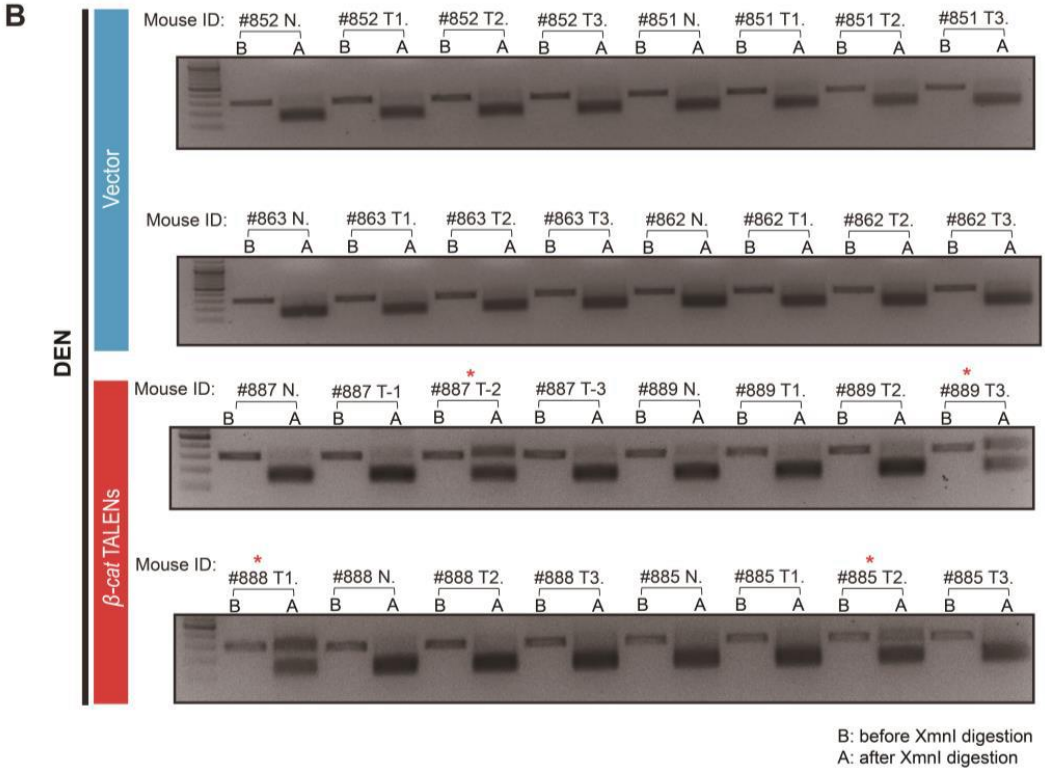

C

```
tcagccactGGCAGCAGCAGTCTTacttggattctggaatccattcTGGTGCCACCACCACagctccttc (wt)
tcagccactGGCAGCAGCAGTCTTacttggatt---------attcTGGTGCCACCACCACagctccttc (#887 tumor1, Δ9)
tcagccactGGCAGCAGCAGTCTTacttggattcta------attcTGGTGCCACCACCACagctccttc (#888 tumor1, Δ6)
tcagccactGGCAGCAGCAGTCTTacttggattctgg------------TGCCACCACCACagctccttc (#889 tumor3, Δ12)
```

Figure S3: *β-catenin* TALENs plus DEN were able to induce extensive liver tumorigenesis in C3H mice.

(A) C3H mice were treated with GoldyTALEN vector (20ug) plus DEN or *β-catenin* TALEN (10ug of each) plus DEN according to the schema in Figure 3C. n = 4. The yellow arrows point to distinct tumors with a red, fleshy appearance. (B) Genotyping of liver samples from the C3H mice. Adjacent normal tissue (labeled as "N") and tumor (labeled as "T") were taken from each liver. The red asterisks indicate TALEN induced *β-catenin* mutations. (C) Sequencing results of the *β-catenin* mutated tumors. Highlighted in yellow are the TALEN binding sites.

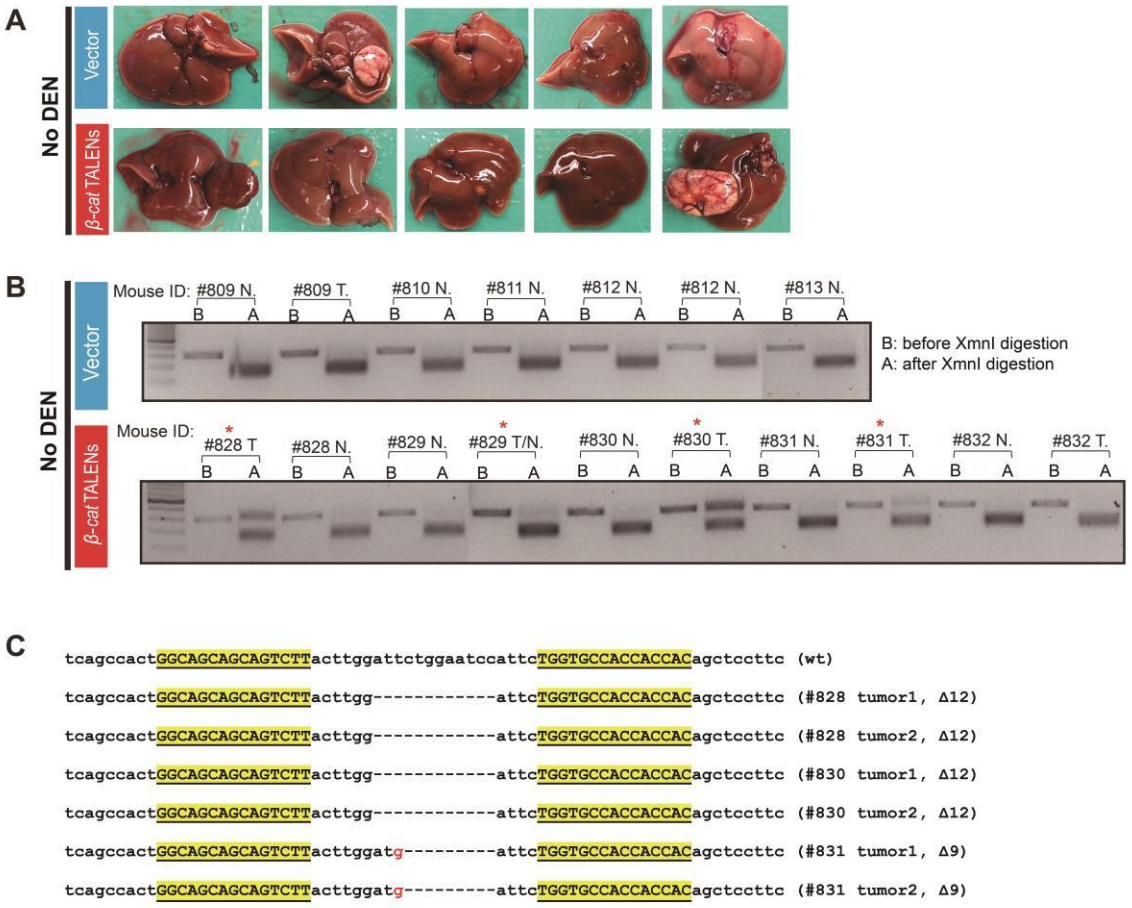

Figure S4: *β-catenin* TALENs alone are able to induce liver tumors.

(A) C3H mice were treated with GoldyTALEN vector (20ug) only or *β-catenin* TALEN (10ug of each) only, without DEN (n = 5). The yellow arrows point to distinct tumors with a red, fleshy appearance. (B) Genotyping of liver and tumor samples. (C) Sequencing results of the *β-catenin* mutated tumors. Highlighted sequences are TALEN binding sites.

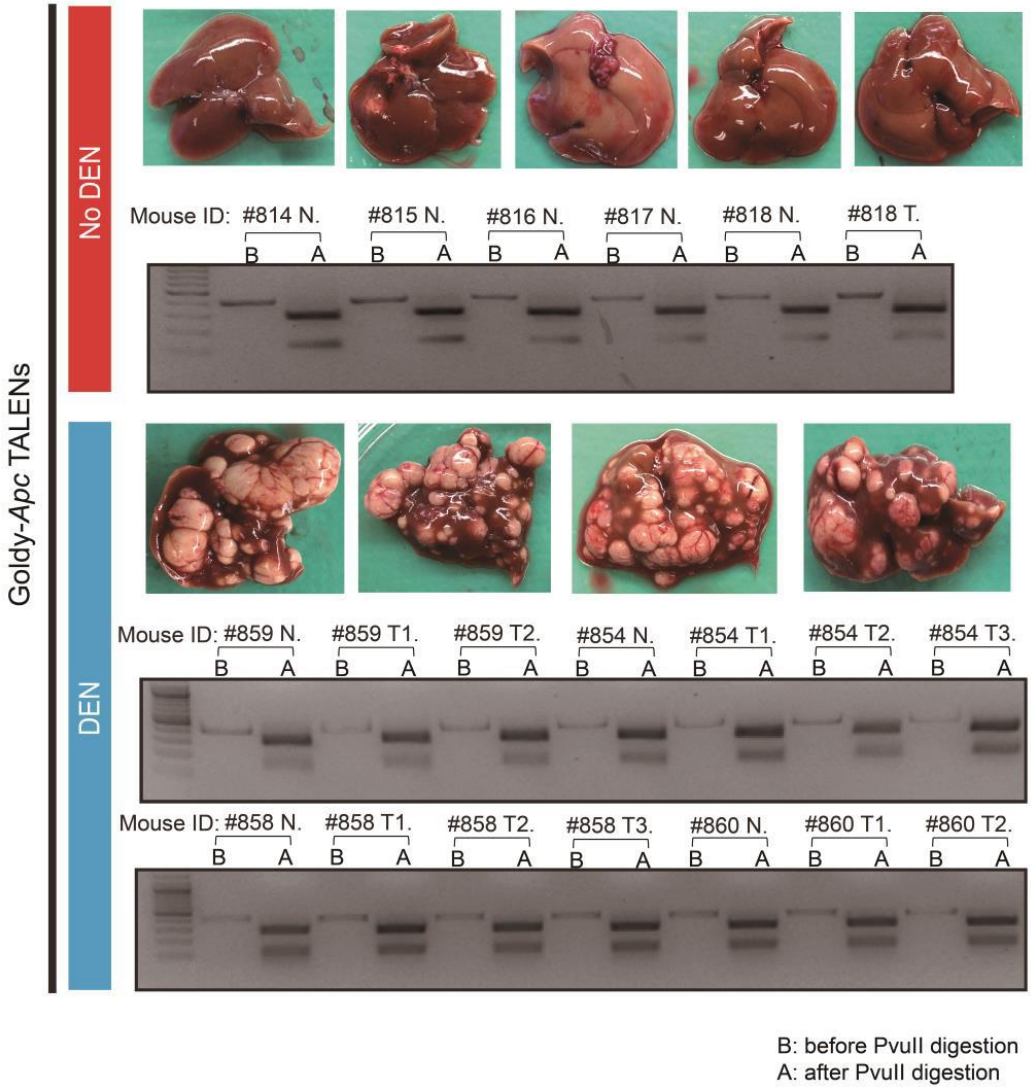

Figure S5: *Apc* TALENs lack the ability to induce *Apc* mutated tumors, with or without DEN.

C3H mice were treated with *Apc* TALENs (10ug of each arm) in the presence or absence of DEN (DEN group: n = 4; NO DEN group: n = 5). The liver images from *Apc* TALEN treated mice and their corresponding genotyping results are shown in the panels. “N” indicates normal tissue. “T” indicates tumor.

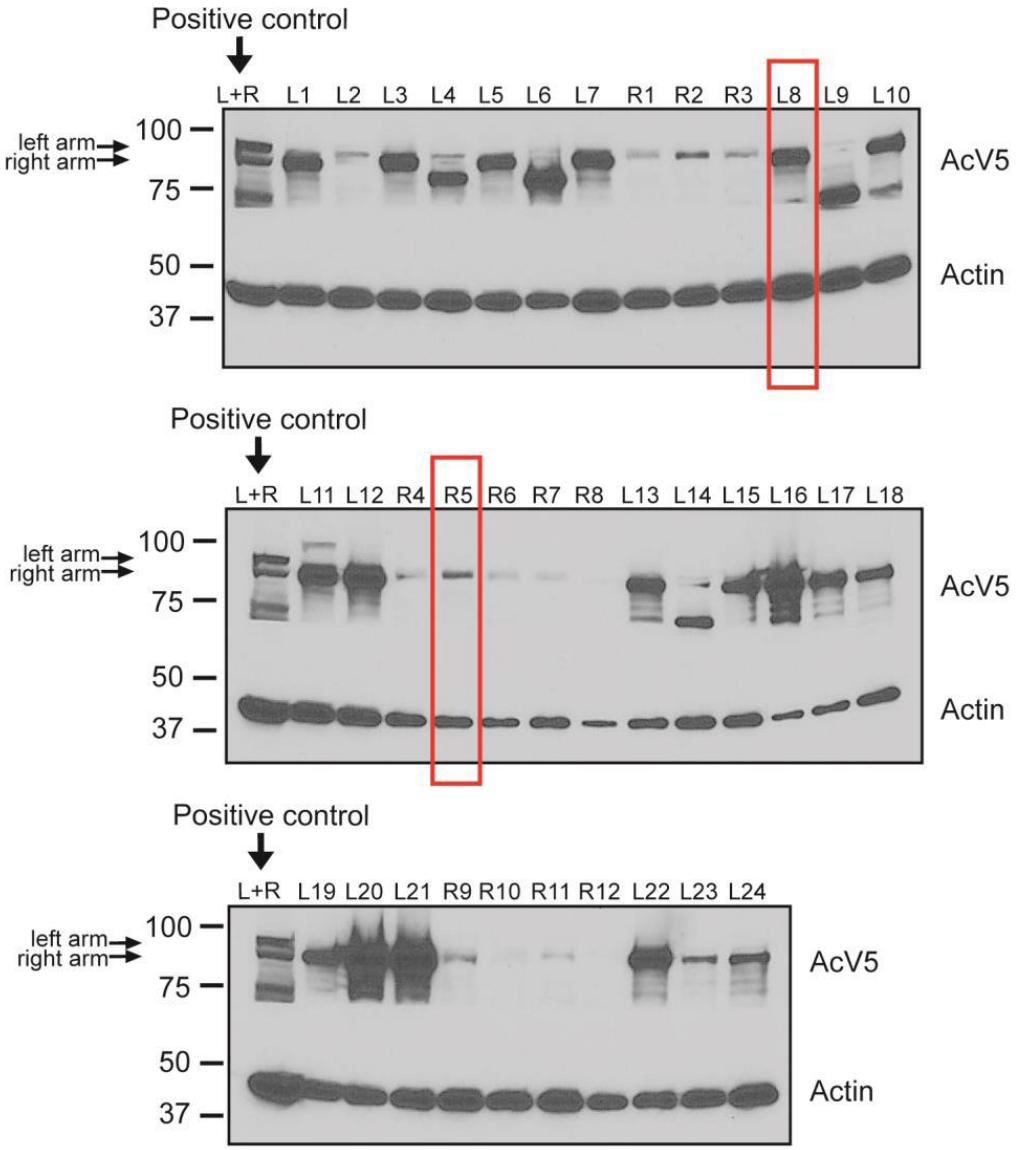
Positive control
L+R L1 L2 L3 L4 L5 L6 L7 R1 R2 R3 L8 L9 L10
left arm
right arm
100
75
50
37
AcV5
Actin
Positive control
L+R L11 L12 R4 R5 R6 R7 R8 L13 L14 L15 L16 L17 L18
left arm
right arm
100
75
50
37
AcV5
Actin
Positive control
L+R L19 L20 L21 R9 R10 R11 R12 L22 L23 L24
left arm
right arm
100
75
50
37
AcV5
Actin

Figure S6: Expression screening of adenoviral plaques for Ad-*Apc*-TAL

Adenoviral plaques made from 911 cells were harvested to test the TALEN protein expression. The first lane of each gel is the positive control expressing TALENs from the GoldyTALEN plasmids: upper band is left arm and lower band is right arm. L8 and R5, shown in the red boxes, were picked for further experimentation.

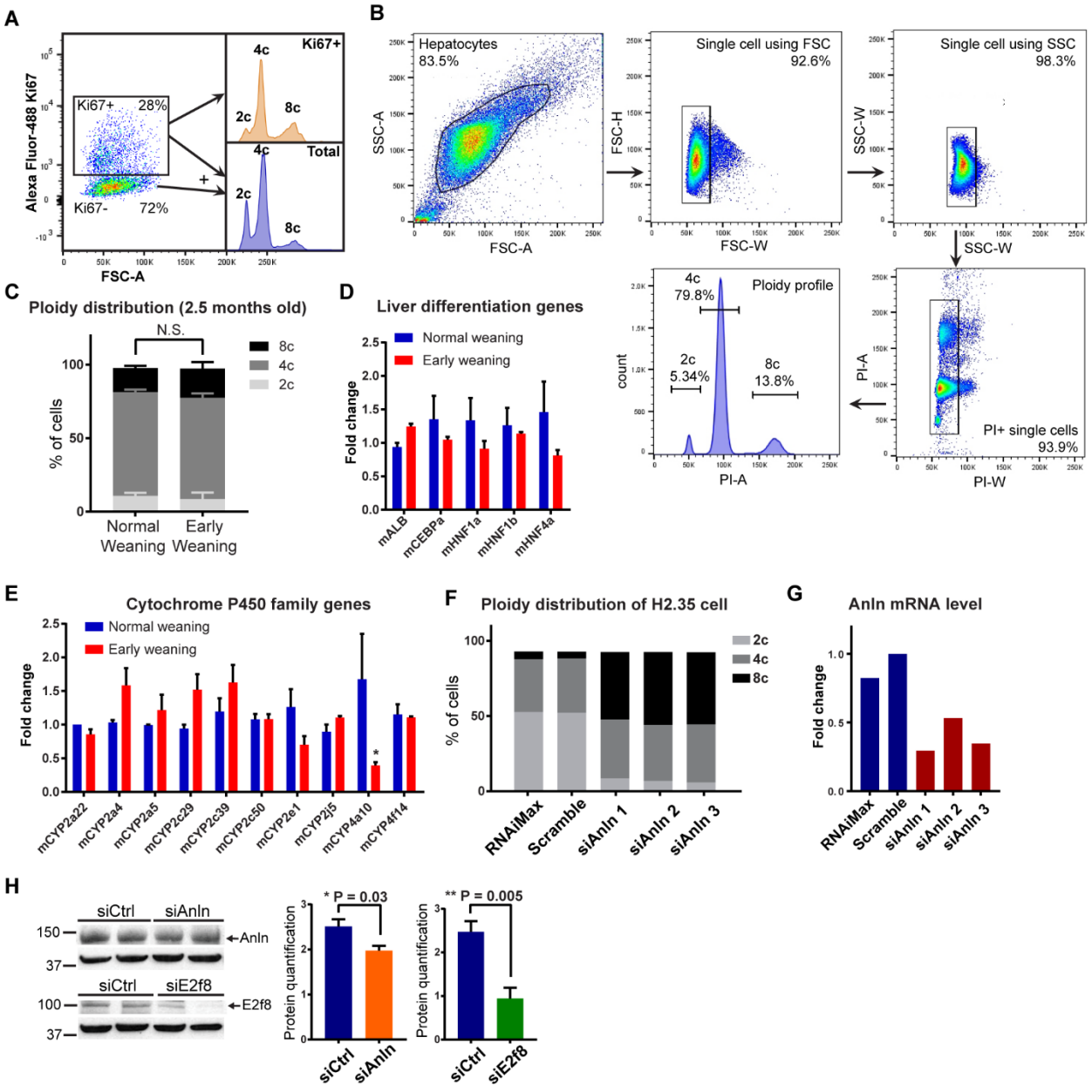
A
Alexa Fluor-488 Ki67
FSC-A
Ki67+ 28%
Ki67- 72%
Ki67+
4c
2c
8c
Total
B
Hepatocytes
83.5%
SSC-A
FSC-A
Single cell using FSC
92.6%
FSC-H
FSC-W
Single cell using SSC
98.3%
SSC-W
SSC-W
PI-A
PI-W
PI+ single cells
93.9%
Ploidy profile
4c
79.8%
2c
5.34%
8c
13.8%
count
PI-A
C
Ploidy distribution (2.5 months old)
N.S.
8c
4c
2c
% of cells
Normal Weaning
Early Weaning
D
Liver differentiation genes
Normal weaning
Early weaning
Fold change
mALB
mCEBPa
mHNF1a
mHNF1b
mHNF4a
E
Cytochrome P450 family genes
Normal weaning
Early weaning
Fold change
mCYP2a22
mCYP2a4
mCYP2a5
mCYP2c29
mCYP2c39
mCYP2c50
mCYP2e1
mCYP2j5
mCYP4a10
mCYP4f14
F
Ploidy distribution of H2.35 cell
2c
4c
8c
% of cells
RNAiMax
Scramble
siAnln 1
siAnln 2
siAnln 3
G
Anln mRNA level
Fold change
RNAiMax
Scramble
siAnln 1
siAnln 2
siAnln 3
H
siCtrl
siAnln
150
37
Anln
siCtrl
siE2f8
100
37
E2f8
* P = 0.03
Protein quantification
siCtrl
siAnln
** P = 0.005
Protein quantification
siCtrl
siE2f8

Figure S7: *Anln* and *E2f8* siRNA knockdown altered ploidy *in vitro* and *in vivo*.

(A) Primary hepatocytes from a P29 WT B6 mouse were stained with Ki67 and PI to detect the ploidy distribution of the proliferating Ki67+ population (orange histogram) and the total population (blue histogram). The Ki67+ population contains a clear group of 8c cells, demonstrating that 4c tetraploid polyploid hepatocytes are also proliferating. (B) Complete gating strategy for determining ploidy distribution of hepatocytes. (C) The ploidy distribution of differentially weaned livers at the age of 2.5 months old (n = 5), as analyzed by flow cytometry with PI staining. (D) qPCR for liver differentiation genes in differentially weaned livers (n = 2 mice per group). (E) qPCR for Cytochrome P450 family genes in normally and early weaned livers (n = 2 mice per group). (F) The ploidy distribution of H2.35 immortalized hepatocytes transfected with *Anln* siRNA, as analyzed by flow cytometry with PI staining. (G) *Anln* mRNA levels in H2.35 cells transfected with *Anln* siRNA, as detected by qPCR. (H) The *in vivo* knockdown efficiency of *Anln* and *E2f8* siRNAs on protein levels as assessed by western blotting. Liver tissues were collected four days after the last in vivo siRNA injection. The band intensities were quantified on the right. All data in this figure are represented as mean ± SEM.

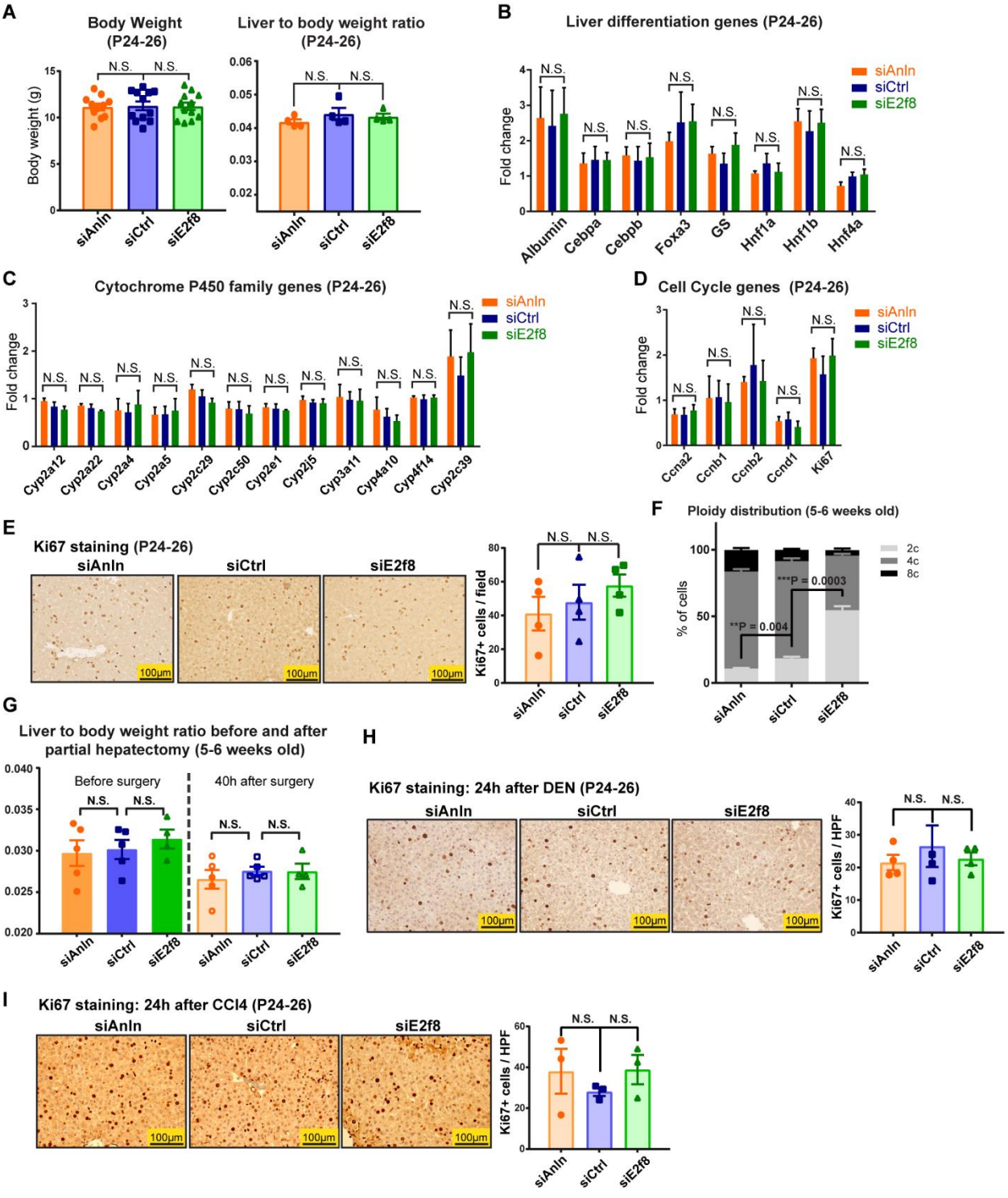
A
Body Weight (P24-26)
Body weight (g)
N.S.
siAnln
siCtrl
siE2f8
Liver to body weight ratio (P24-26)
B
Liver differentiation genes (P24-26)
Fold change
Albumin
Cebpa
Cebpb
Foxa3
GS
Hnf1a
Hnf1b
Hnf4a
C
Cytochrome P450 family genes (P24-26)
Cyp2a12
Cyp2a22
Cyp2a4
Cyp2a5
Cyp2c29
Cyp2c50
Cyp2e1
Cyp2j5
Cyp3a11
Cyp4a10
Cyp4f14
Cyp2c39
D
Cell Cycle genes (P24-26)
Ccna2
Ccnb1
Ccnb2
Ccnd1
Ki67
E
Ki67 staining (P24-26)
100μm
Ki67+ cells / field
F
Ploidy distribution (5-6 weeks old)
% of cells
2c
4c
8c
**P = 0.004
***P = 0.0003
G
Liver to body weight ratio before and after partial hepatectomy (5-6 weeks old)
Before surgery
40h after surgery
H
Ki67 staining: 24h after DEN (P24-26)
Ki67+ cells / HPF
I
Ki67 staining: 24h after CCl4 (P24-26)

Figure S8: siRNA treatment and altered ploidy did not impact overall liver development and regeneration.

(A) Body and liver to body weight ratios of siRNA treated mice. (B) qPCR for liver differentiation genes in siRNA treated livers (n = 4 mice per group). (C) qPCR for Cytochrome P450 family genes in siRNA treated livers (n = 4 mice per group). (D) qPCR for cell cycle genes in siRNA treated livers (n = 4 mice per group). (E) Ki67 staining in siRNA treated livers (left panel), quantification on the right. (F) The ploidy distribution of siAnln, siCtrl or siE2f8 treated mice livers at 5-6 weeks of age (n = 3), as analyzed by flow cytometry with PI staining. (G) Liver to body weight ratios before and 40 hours after partial hepatectomy. siRNA treated mice underwent 70% partial hepatectomy at six weeks of age and remnant livers were harvested and analyzed 40 hours after surgery. (H) Ki67 staining of siRNA treated livers given DEN (left panel). Four days after the last siRNA injection, these mice received one dose of DEN (75μg/g of mouse) and were euthanized 24 hours later. Ki67+ cells were quantified in the right panel. (I) Ki67 staining of siRNA treated livers given CCl4 (left panel). Four days after the last siRNA injection, these mice received one dose of CCl4 (100μL total, 10% CCl4 by volume) and livers were harvested 24 hours later. Ki67+ cells were quantified in the right panel. All data in this figure are represented as mean ± SEM.

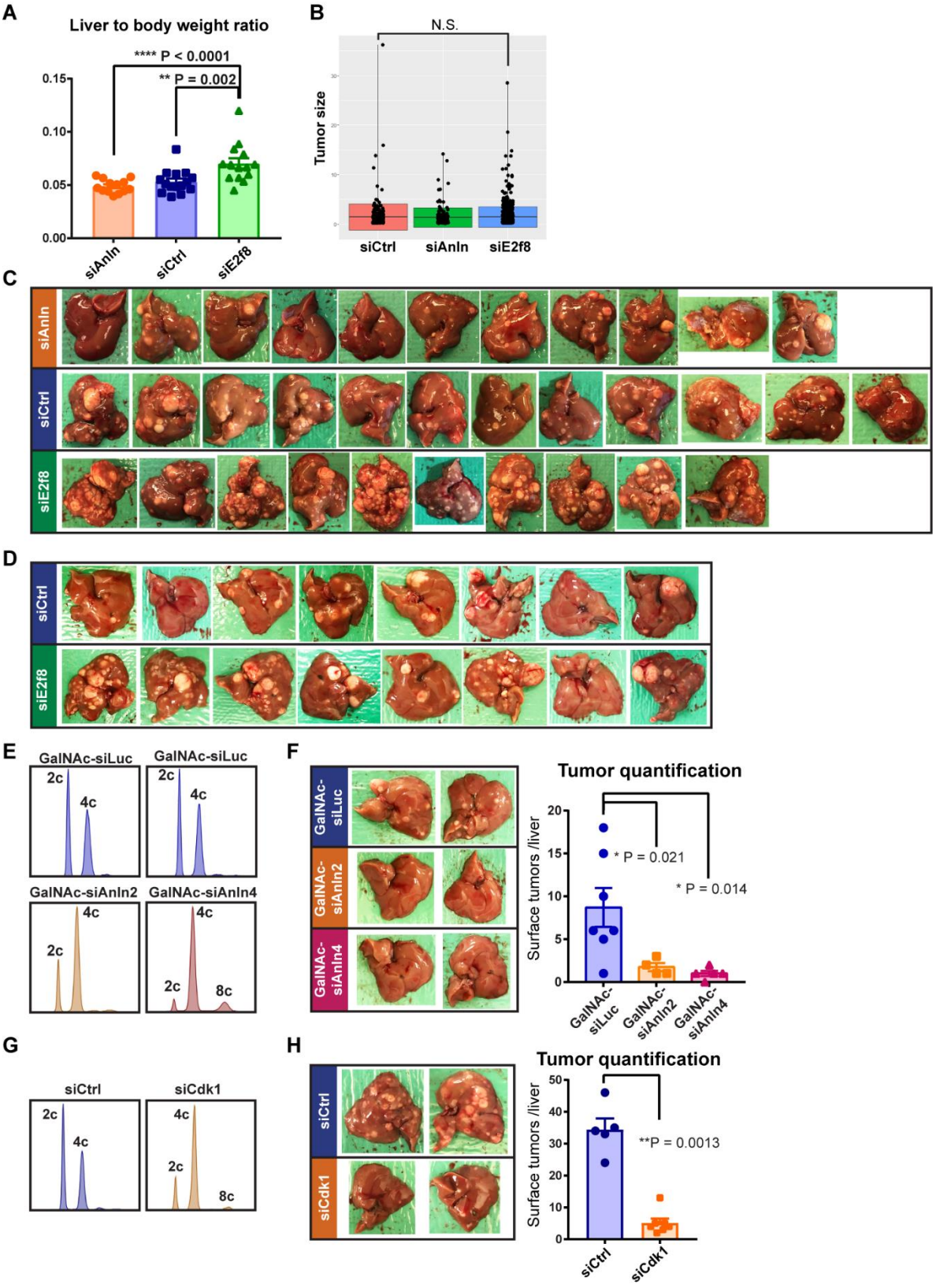
A
Liver to body weight ratio
**** P < 0.0001
** P = 0.002
0.15
0.10
0.05
0.00
siAnln
siCtrl
siE2f8
B
N.S.
Tumor size
siCtrl
siAnln
siE2f8
C
siAnln
siCtrl
siE2f8
D
siCtrl
siE2f8
E
GalNAc-siLuc
GalNAc-siLuc
2c
4c
GalNAc-siAnln2
GalNAc-siAnln4
8c
F
GalNAc-siLuc
GalNAc-siAnln2
GalNAc-siAnln4
Tumor quantification
Surface tumors /liver
* P = 0.021
* P = 0.014
G
siCtrl
siCdk1
H
siCtrl
siCdk1
Tumor quantification
Surface tumors /liver
**P = 0.0013

Figure S9: The polyploid state protected against DEN-induced HCC development.

(A) Liver to body weight ratios of different ploidy groups 6 months after DEN induction. The liver mass includes tumor burden and normal liver tissue. (B) Quantified individual tumor sizes from three ploidy groups. Tumor sizes were measured using ImageJ. (C) All livers from the DEN experiment (n = 11 for siAnln group, n = 12 for siCtrl group, n = 10 for siE2f8 group) are shown. (D) All livers treated with DEN 14 days after siRNA delivery. 14 days after four doses of siRNAs, one dose of DEN (100μg/g) was given. 7.5 months later, tumor burden was assessed (n = 8 in each group). (E) Ploidy distribution of *GalNAc-siLuc*, *GalNAc-siAnln#2* and *GalNAc-siAnln#4* treated livers at P26, analyzed by flow cytometry with PI staining. (F) Representative gross tumor burden from the *GalNAc-siRNA* DEN experiment: C3H mice were subcutaneously treated with three doses of 4.0mg/kg of *GalNAc-siLuc*, *GalNAc-siAnln#2* or *GalNAc-siAnln#4* starting at P8-10, given 4 days apart. DEN (75ug/g) was given at P26. Five months after DEN, tumors on the liver surface were quantified (right). (G) Ploidy distribution of siCtrl and siCdk1 treated livers at P26, analyzed by flow cytometry with PI staining. (H) Representative gross tumor burden from the siCdk1 DEN experiment: *Cdk1* and scramble siRNAs (siCtrl) were injected into WT C3H mice starting at P10. Four total injections (two intraperitoneal and two retro-orbital) were performed twice per week. At P26, mice were injected with DEN (75μg/g). Tumors on the liver surface were quantified at 6 months (right). All data in this figure are represented as mean ± SEM.

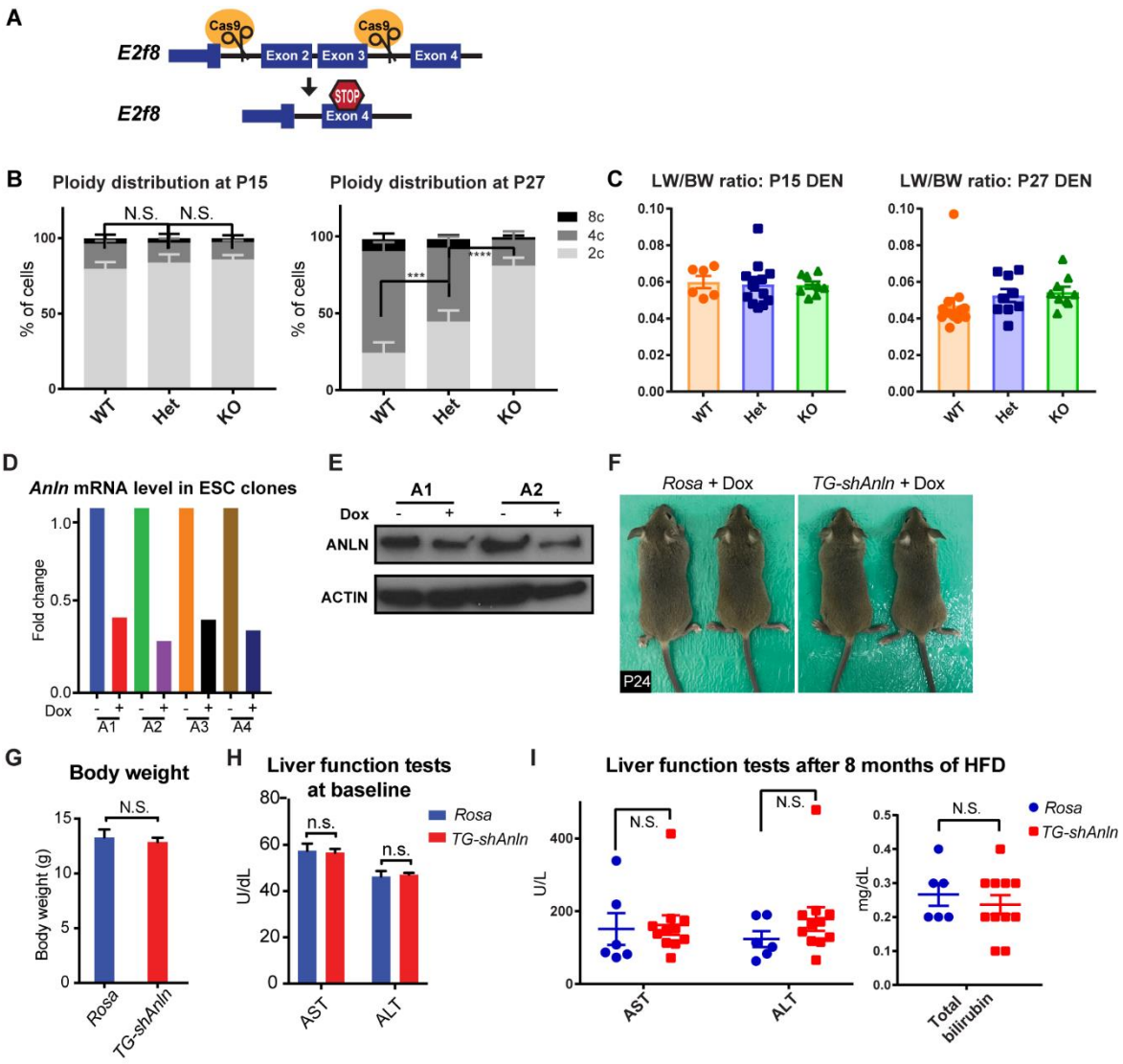
A
Cas9
Cas9
E2f8
Exon 2
Exon 3
Exon 4
STOP
E2f8
Exon 4
B
Ploidy distribution at P15
N.S.
N.S.
% of cells
WT
Het
KO
Ploidy distribution at P27
***
****
8c
4c
2c
C
LW/BW ratio: P15 DEN
LW/BW ratio: P27 DEN
D
Anln mRNA level in ESC clones
Fold change
Dox
A1
A2
A3
A4
E
A1
A2
Dox
ANLN
ACTIN
F
Rosa + Dox
TG-shAnln + Dox
P24
G
Body weight
Body weight (g)
N.S.
Rosa
TG-shAnln
H
Liver function tests at baseline
U/dL
n.s.
n.s.
AST
ALT
I
Liver function tests after 8 months of HFD
U/L
N.S.
N.S.
AST
ALT
mg/dL
N.S.
Total bilirubin

Figure S10: Design and characterization of the *E2f8* KO and *TG-shAnln* mouse models.

(A) CRISPR/Cas9 was used to generate whole-body *E2f8* knockout (KO) mice. Two guide RNAs were designed to target introns 1 and 3 in order to delete exon 2 and 3. Successful deletion was predicted create a premature stop codon in exon 4. (B) Ploidy distribution of *E2f8* WT, Het and KO livers at P15 (n = 3) or P27 (n = 6 for WT, n = 7 for Het, n = 4 for KO), analyzed by flow cytometry with PI staining. (C) The liver to body weight ratios of DEN treated *E2f8* WT, Het, and KO mice at six months of age. The mice were given DEN at P15 or at P27, and euthanized 4.5-5 months later. (D) Inducible *TG-shAnln* embryonic stem cells showing *Anln* expression levels after dox induction for 72 hours. (E) Western blot of Anln protein levels in embryonic stem cell clones after dox induction. (F) *Rosa* or *TG-shAnln* transgenic mice exposed to dox water from P0-P20 develop normally. (G) Body weight of the *Rosa* and *TG-shAnln* mice (n = 3) after dox water treatment from P0-P20. (H) AST/ALT serum liver function tests at base line in *Rosa* and *TG-shAnln* mice (n = 3) after dox treatment. (I) The AST/ALT and total bilirubin levels of *Rosa* and *TG-shAnln* mice after 8 months of HFD feeding. All data in this figure are represented as mean ± SEM.

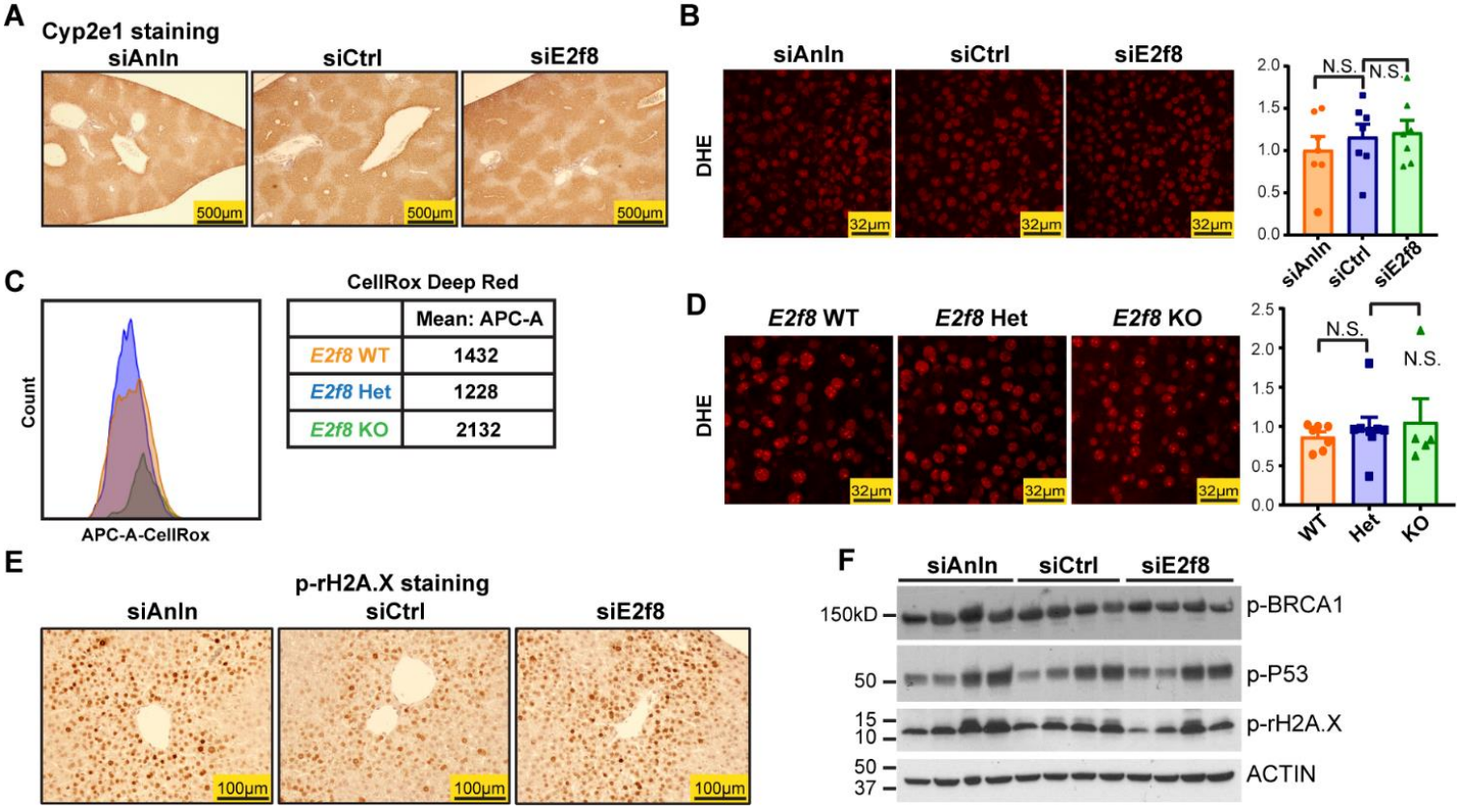
A
Cyp2e1 staining
siAnln
siCtrl
siE2f8
500μm
B
siAnln
siCtrl
siE2f8
DHE
32μm
N.S.
N.S.
siAnln
siCtrl
siE2f8
C
Count
APC-A-CellRox
CellRox Deep Red
Mean: APC-A
E2f8 WT 1432
E2f8 Het 1228
E2f8 KO 2132
D
E2f8 WT
E2f8 Het
E2f8 KO
DHE
32μm
N.S.
N.S.
WT
Het
KO
E
p-rH2A.X staining
siAnln
siCtrl
siE2f8
100μm
F
siAnln
siCtrl
siE2f8
150kD
p-BRCA1
50
p-P53
15
10
p-rH2A.X
50
37
ACTIN

Figure S11. After DEN, livers with altered ploidy did not exhibit differential xenobiotic metabolism, oxidative stress, or DNA damage response.

(A) CYP2E1 staining in siRNA treated livers with altered ploidy. (B) Dihydroethidium (DHE) staining of siAnln, siCtrl or siE2f8 treated livers at P26. Staining intensities are quantified on the right, 20 cells from 5 fields in each mouse were measured and averaged. (C) CellRox Deep Red staining for ROS in *E2f8* WT, Het, and KO livers, as analyzed by flow cytometry. The table on the right shows the mean values for the APC-A channel, which detects CellRox. (D) DHE staining of *E2f8* WT, Het and KO livers at P30. Staining intensities are quantified on the right, 20 cells from 5 fields in each mouse were measured and averaged. (E) Four days after the last siRNA injection, one dose of DEN (75μg/g) was given. 24 hours later, livers were stained for p-γH2A.X. (F) The DNA damage response proteins, p-Brca1, p-p53, and p-γH2A.X, as assessed by western blots. All data in this figure are represented as mean ± SEM.

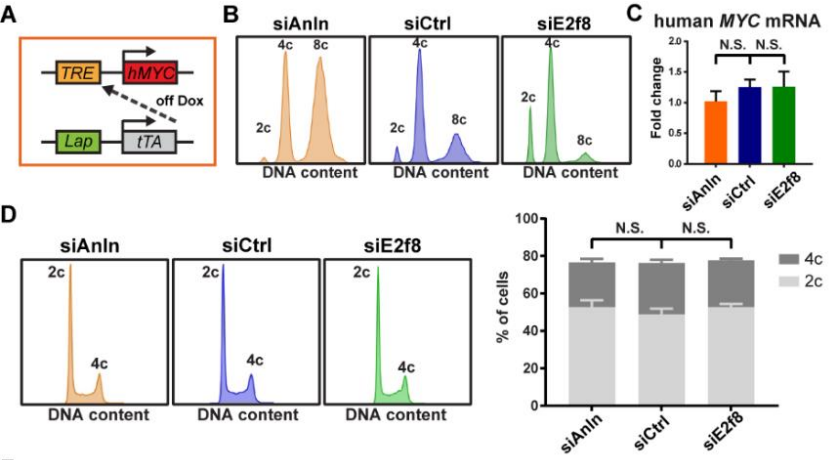
A
TRE
hMYC
off Dox
Lap
tTA
B
siAnln
siCtrl
siE2f8
4c
8c
2c
DNA content
C
human MYC mRNA
N.S.
Fold change
siAnln
siCtrl
siE2f8
D
siAnln
siCtrl
siE2f8
2c
4c
DNA content
% of cells
4c
2c
F
Cas9
Apc exon8 gRNA
Cas9 + Apc exon8 gRNA
B
A
siA
siE
52%
E
siCtrl
siE2f8
200μm
GFP+ cells / HPFmber
N.S.
G
siAnln
siCtrl
siE2f8
H
LW/BW ratio
P = 0.13
P = 0.075

Figure S12. Polyploids were protected from TSG loss but not oncogene activation.

(A) The *LAP-tTA; TRE-MYC* liver cancer model. Withdrawing doxycycline drives human *MYC* expression under the control of a liver specific promoter (*LAP*). (B) Representative cellular ploidy of *LAP-tTA; TRE-MYC* livers at P30, analyzed by flow cytometry with PI staining. (C) Relative human *MYC* mRNA expression in *LAP-tTA; TRE-MYC* livers with different ploidies as measured by qPCR. Expression was analyzed at P30 in non-tumor tissues. (D) Representative cellular ploidy of the MYC tumors from different ploidy groups, analyzed by flow cytometry with PI staining. 6 tumors were analyzed from each group and the ploidy is summarized on the right. (E) GFP expression (left panel) in siCtrl and siE2f8 treated livers 5 days after Adenovirus-GFP (1.4×10^8 pfu/mouse) injection. GFP+ cells were quantified in the right panel. (F) The surveyor assay was used to test the efficiency of the *Apc* exon 8 sgRNA in the H2.35 cell line. B: before surveyor enzyme digestion; A: after surveyor enzyme digestion. Cutting efficiency (52%) was quantified by comparing the intensity of the cut bands. (G) Representative cellular ploidy of FVB livers treated with siAnln, siCtrl or siE2f8, analyzed by flow cytometry with PI staining. (H) Gross tumor burden from the Ad-*Cas9-gPten* plus AAV-*KPL* experiment: four doses of *Anln, E2f8* and scramble siRNAs (siCtrl) were injected into WT FVB strain mice starting at P10. One week later, the mice were injected with Ad-*Cas9-sgPten* (10^9 pfu/mouse) and AAV-*KPL* (10^{12} pfu/mouse). Tumor burden 2 months after virus injection is shown. Liver to body weight ratio (right). All data in this figure are represented as mean ± SEM.

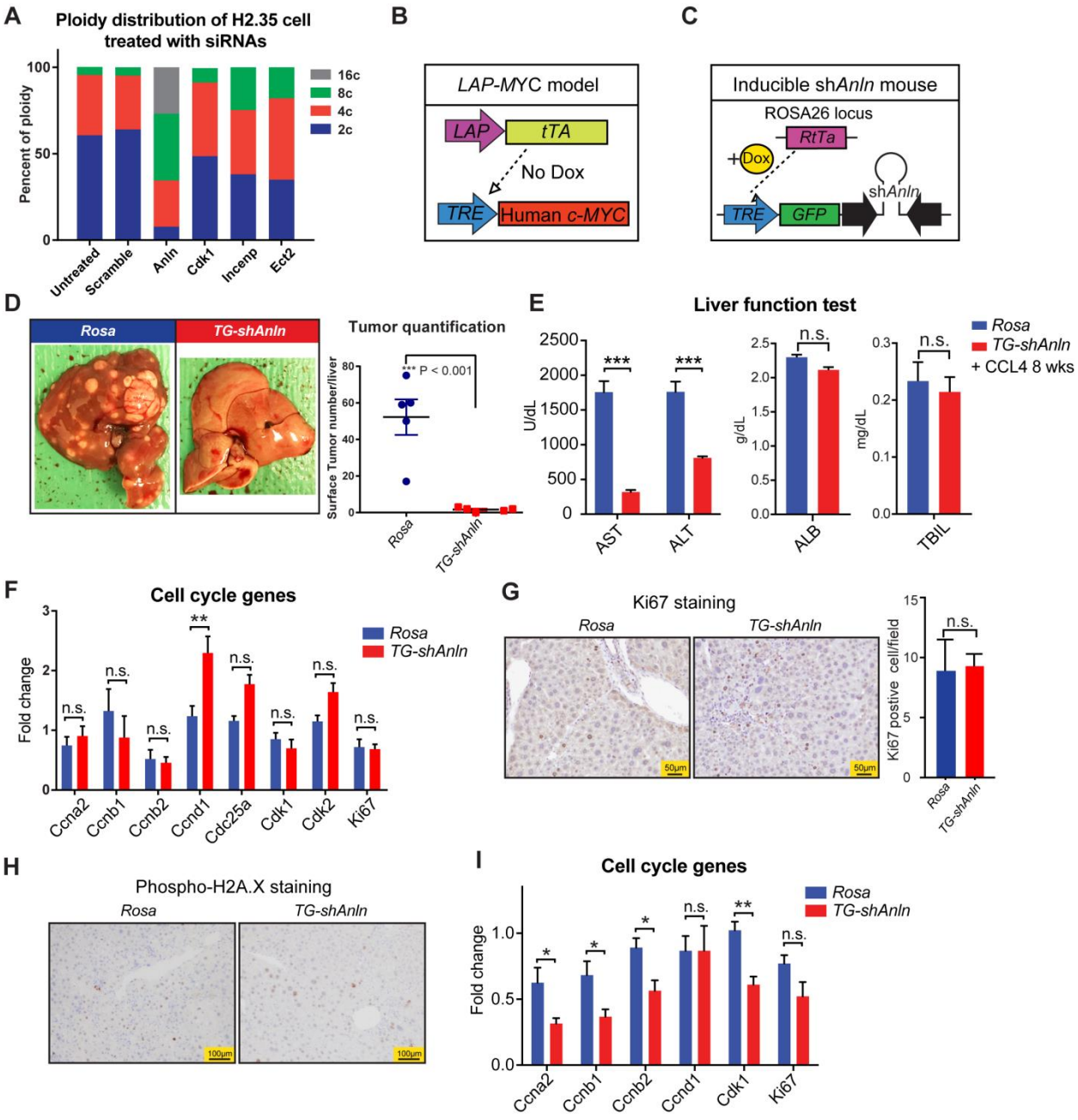
A
Ploidy distribution of H2.35 cell treated with siRNAs
Pencent of ploidy
16c
8c
4c
2c
Untreated
Scramble
Anln
Cdk1
Incenp
Ect2
B
LAP-MYC model
LAP
tTA
No Dox
TRE
Human c-MYC
C
Inducible shAnln mouse
ROSA26 locus
RtTa
Dox
shAnln
TRE
GFP
D
Rosa
TG-shAnln
Tumor quantification
Surface Tumor number/liver
*** P < 0.001
E
Liver function test
Rosa
TG-shAnln
+ CCL4 8 wks
U/dL
g/dL
mg/dL
AST
ALT
ALB
TBIL
n.s.
F
Cell cycle genes
Fold change
Ccna2
Ccnb1
Ccnb2
Ccnd1
Cdc25a
Cdk1
Cdk2
Ki67
G
Ki67 staining
Ki67 postive cell/field
H
Phospho-H2A.X staining
I
Cell cycle genes

Figure S13: *Anln* suppression in transgenic mice did not impair liver function.

(A) Ploidy distribution in H2.35 cells treated with Scramble, *Anln, Cdk1, Incenp, Ect2* siRNAs. (B) A schematic of *LAP-tTA; TRE-MYC* mouse model. (C) An inducible double-transgenic mouse model carrying sh*Anln* cassette under the control of a tetracycline responsive promoter element (TRE). These mice carry a *Rosa-rtTA* knockin construct, allowing induction of *Anln* suppression with Doxycycline (Dox) water. (D) Representative gross tumor burden from *Rosa* and *TG-shAnln* mice. Mice were given one dose of DEN (25ug/g) at P15. Dox water started at P30, cycled every other week. Dox water was taken off at P126. Mice were sacrificed at P180. (E) Liver function tests of *Rosa* and *TG-Anln* mice after 8 weeks of CCl_4 injury (n = 6 and 7). (F) qPCR for cell cycle genes in *Rosa* and *TG-Anln* livers. *Rosa* and *TG-Anln* mice were treated with DEN and CCl_4 injury as described in Figure 5. (G) Ki67 staining of the above livers. Ki67+ cell quantification was shown on the right. (H) Phospho-H2A.X staining on *Rosa* and *TG-shAnln* livers treated with DEN and CCl_4. Mice were sacrificed at 2 weeks after the last dose of CCl_4 injury, so the phospho-H2A.X staining was not strong. (I) qPCR for cell cycle genes in *Rosa* and *TG-Anln* livers (n = 5). *Rosa* and *TG-Anln* mice were put on dox water from P0 to P20. Then their livers were harvested for qPCR test.

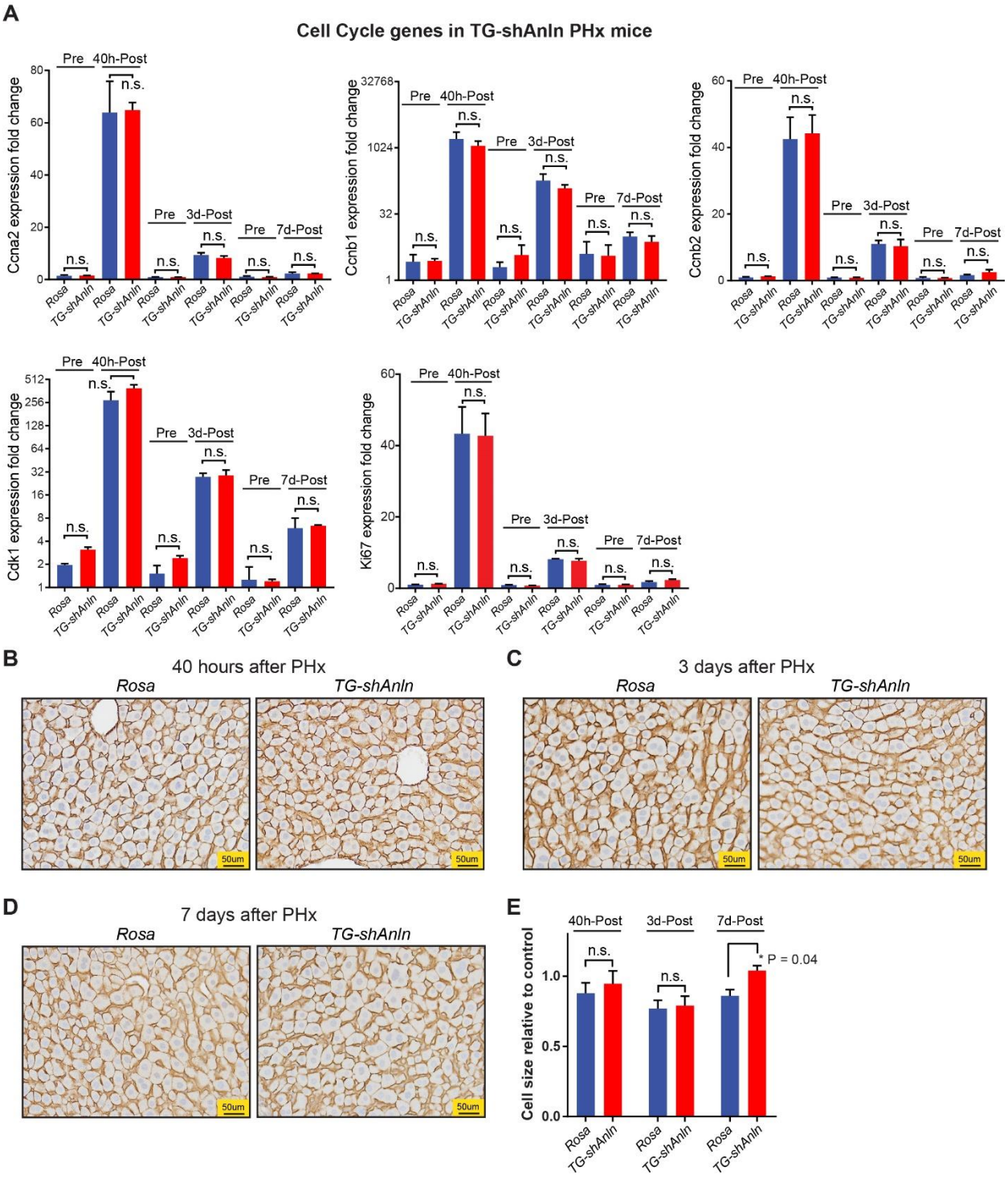
A
Cell Cycle genes in TG-shAnln PHx mice
Ccna2 expression fold change
Ccnb1 expression fold change
Ccnb2 expression fold change
Cdk1 expression fold change
Ki67 expression fold change
Pre
40h-Post
3d-Post
7d-Post
n.s.
Rosa
TG-shAnln
B
40 hours after PHx
C
3 days after PHx
D
7 days after PHx
50um
E
Cell size relative to control
* P = 0.04

Figure S14: *Anln* suppression in transgenic mice did not impair liver regeneration after partial hepatectomy.

(A) Cell cycle genes expression in *Rosa* and *TG-shAnln* mice receiving partial hepatectomy. Six week old *Rosa* and *TG-Anln* mice were given dox for 7 days before surgery, then underwent 70% partial hepatectomy and remnant livers were harvested and analyzed at 40 hours, 3 days and 7 days after surgery (n = 3 mice per group for the 40-hour and 3-day time points, n = 4 mice for 7 day time point). Cell cycle genes expression was measured by Qpcr on these liver. (B) β-catenin staining of the above livers at 40 hours, (C) 3 days and (D) 7 days after hepatectomy. (E) Cell size quantification of the *Rosa* and *TG-shAnln* livers after hepatectomy. The cell size quantification was based on the β-catenin staining. Photoshop was used to draw the outline of the hepatocyte and measure the area in pixel. 4 images were taken from each mouse (n = 3 mice per group for the 40-hour and 3-day time points, n = 4 mice for 7 day time point). 10 random hepatocytes were measured in each image. All the cell area data were normalized to one of the *Rosa* mice in 40h group.

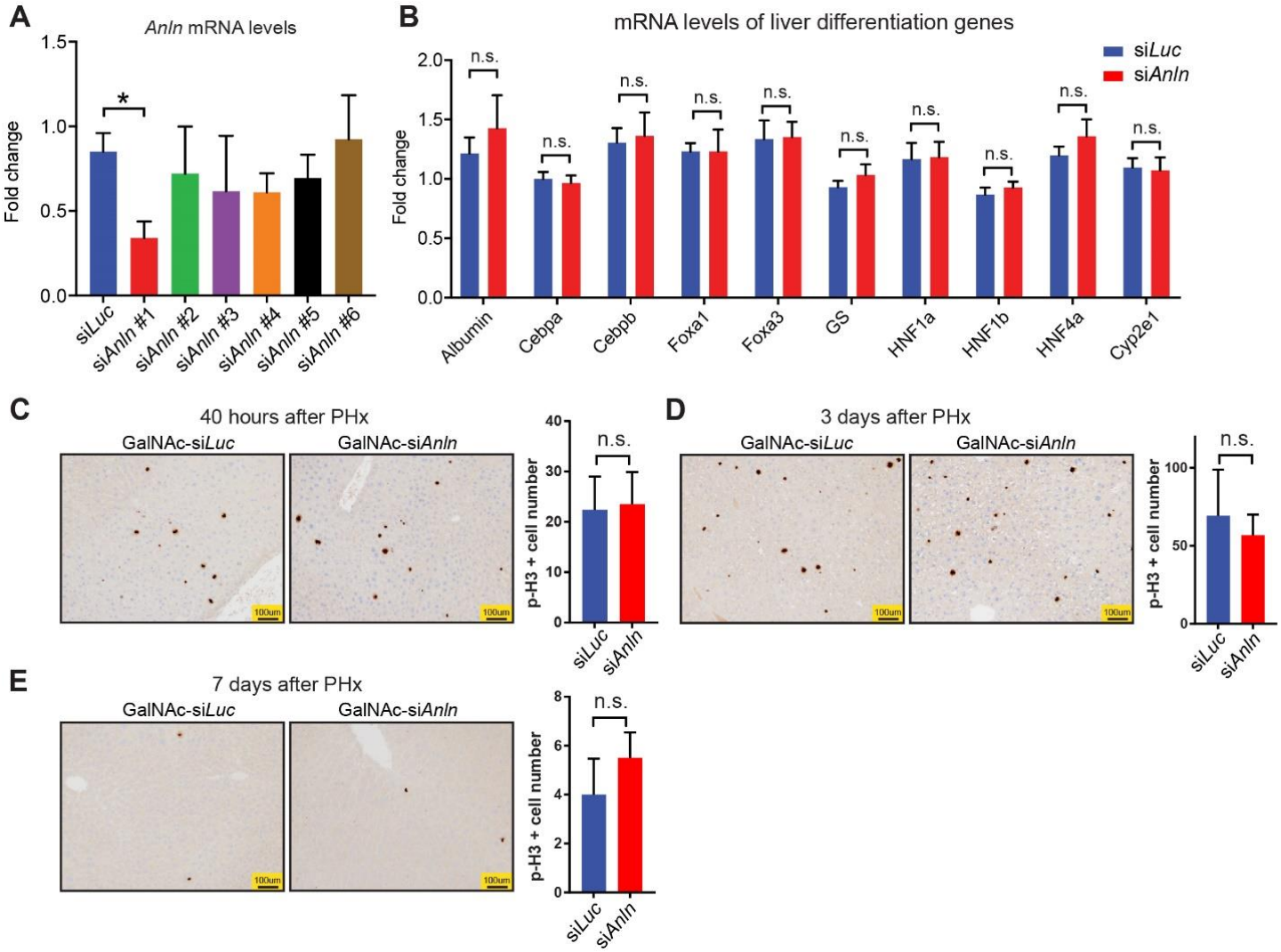
A
Anln mRNA levels
Fold change
1.5
1.0
0.5
0.0
*
siLuc
siAnln #1
siAnln #2
siAnln #3
siAnln #4
siAnln #5
siAnln #6
B
mRNA levels of liver differentiation genes
siLuc
siAnln
Fold change
2.0
1.5
1.0
0.5
0.0
n.s.
Albumin
Cebpa
Cebpb
Foxa1
Foxa3
GS
HNF1a
HNF1b
HNF4a
Cyp2e1
C
40 hours after PHx
GalNAc-siLuc
GalNAc-siAnln
100um
p-H3 + cell number
40
30
20
10
0
n.s.
siLuc
siAnln
D
3 days after PHx
GalNAc-siLuc
GalNAc-siAnln
100um
p-H3 + cell number
100
50
0
n.s.
siLuc
siAnln
E
7 days after PHx
GalNAc-siLuc
GalNAc-siAnln
100um
p-H3 + cell number
8
6
4
2
0
n.s.
siLuc
siAnln

Figure S15: ***GalNAc mediated siAnln delivery did not affect normal liver physiology or impair liver regeneration after partial hepatectomy*****.**

(A) *Anln* mRNA levels of the wild type livers treated with different GalNAc conjugated si*Anln*. Wild type mice were subcutaneously treated with 6 different GalNAc-si*Anln* or GalNAc-si*Luc* at 1mg/kg. Livers were harvested at 3 days after treatment (n = 3). (B) qPCR for liver specific differentiation genes and transcription factors in livers treated with GalNAc-si*Anln* or GalNAc-si*Luc* at 1mg/kg (n = 7 per group). (C-E) Phospho-H3 staining of the regenerated livers after partial hepatectomy. Six week old CD1 mice were given GalNAc-si*Luc* or GalNAc-si*Anln* (4mg/kg) 1 week before surgery, then underwent 70% partial hepatectomy and remnant livers were harvested and analyzed at 40 hours, 3 days and 7 days after surgery (n = 4 for 40-hour time point, n = 3 for 3-day and 7-day time points). Quantification is shown on the right.

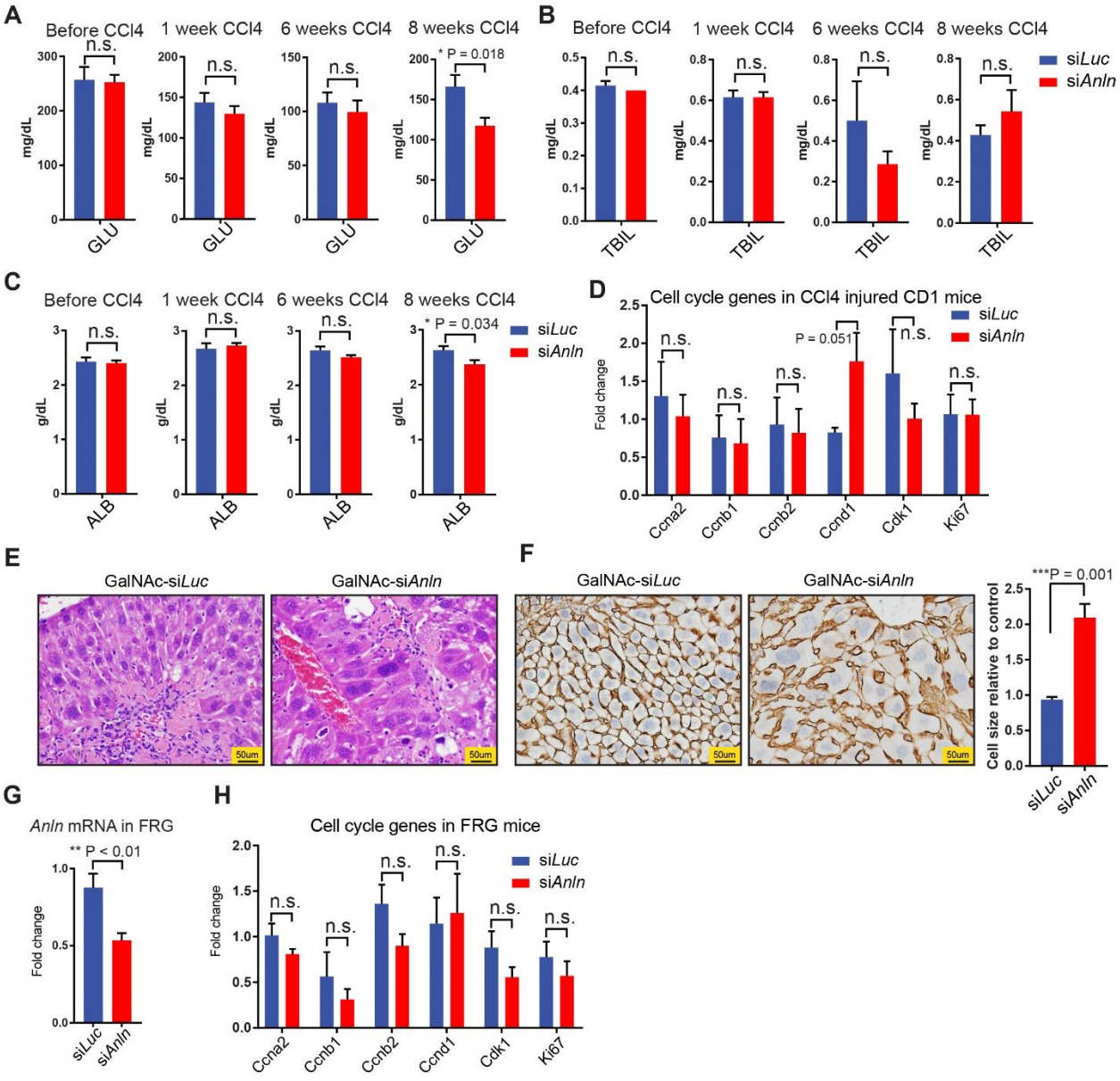
A
Before CCl4
1 week CCl4
6 weeks CCl4
8 weeks CCl4
n.s.
* P = 0.018
mg/dL
GLU
B
TBIL
siLuc
siAnln
C
g/dL
ALB
* P = 0.034
D
Cell cycle genes in CCl4 injured CD1 mice
Fold change
P = 0.051
Ccna2
Ccnb1
Ccnb2
Ccnd1
Cdk1
Ki67
E
GalNAc-siLuc
GalNAc-siAnln
50um
F
***P = 0.001
Cell size relative to control
G
Anln mRNA in FRG
** P < 0.01
H
Cell cycle genes in FRG mice

Figure S16: ***GalNAc mediated siAnln delivery did not impair liver regeneration in chronic CCl_4 injury or FRG liver repopulation assay*****.**

(A-C) Liver function tests of CD1 mice before, after one week, after 6 weeks and after 8 weeks of CCl_4 injury. The mice were treated with GalNAc-si*Luc* (4mg/kg) or GalNAc-si*Anln* (4mg/kg) (n = 7). The treatment started at 1 week before injury and was given weekly. The CCl_4 injury was given twice every week. (D) qPCR for cell cycle genes of the above livers. (E) H&E histology of the above livers. (F) β-catenin staining of the above livers. Cell size quantification of the GalNAc-si*Luc* and GalNAc-si*Anln* treated livers after CCl_4 injury is shown on the right. The cell size quantification was based on β-catenin staining. Photoshop was used to draw the outline of the hepatocyte and measure the area in pixel. 4 images were taken from each mouse (n = 7 for each group). 25 random hepatocytes were measured in each image. All the cell area data were normalized to one of the GalNAc-si*Luc* treated mice.

REFERENCES

1. Rieseberg, L.H. and J.H. Willis, *Plant speciation.* Science, 2007. **317**(5840): p. 910-4.
2. Meyers, L.A. and D.A. Levin, *On the abundance of polyploids in flowering plants.* Evolution, 2006. **60**(6): p. 1198-206.
3. Rosalind A. Leggatt, G.K.I., *Occurrence of polyploidy in the fishes.* Reviews in Fish Biology and Fisheries, 2003. **13**(3): p. 9.
4. Tymowska, J. and H.R. Kobel, *Karyotype analysis of Xenopus muelleri (Peters) and Xenopus laevis (Daudin), Pipidae.* Cytogenetics, 1972. **11**(4): p. 270-8.
5. Winkelmann, M., P. Pfitzer, and W. Schneider, *Significance of polyploidy in megakaryocytes and other cells in health and tumor disease.* Klin Wochenschr, 1987. **65**(23): p. 1115-31.
6. Liu, Z., et al., *Regulation of cardiomyocyte polyploidy and multinucleation by CyclinG1.* Circ Res, 2010. **106**(9): p. 1498-506.
7. Ishikawa, H., R. Bischoff, and H. Holtzer, *Mitosis and intermediate-sized filaments in developing skeletal muscle.* J Cell Biol, 1968. **38**(3): p. 538-55.
8. Frade, J.M., *Somatic tetraploidy in vertebrate neurons: Implications in physiology and pathology.* Commun Integr Biol, 2010. **3**(2): p. 201-3.
9. Celton-Morizur, S. and C. Desdouets, *Polyploidization of liver cells.* Adv Exp Med Biol, 2010. **676**: p. 123-35.
10. Sroga, J.M., X. Ma, and S.K. Das, *Developmental regulation of decidual cell polyploidy at the site of implantation.* Front Biosci (Schol Ed), 2012. **4**: p. 1475-86.

11. Fei, F., et al., *The number of polyploid giant cancer cells and epithelial-mesenchymal transition-related proteins are associated with invasion and metastasis in human breast cancer.* J Exp Clin Cancer Res, 2015. **34**: p. 158.

12. Mosieniak, G., et al., *Polyploidy Formation in Doxorubicin-Treated Cancer Cells Can Favor Escape from Senescence.* Neoplasia, 2015. **17**(12): p. 882-893.

13. Nguyen, H.G. and K. Ravid, *Polyploidy: mechanisms and cancer promotion in hematopoietic and other cells.* Adv Exp Med Biol, 2010. **676**: p. 105-22.

14. Storchova, Z. and D. Pellman, *From polyploidy to aneuploidy, genome instability and cancer.* Nat Rev Mol Cell Biol, 2004. **5**(1): p. 45-54.

15. Gentric, G. and C. Desdouets, *Polyploidization in liver tissue.* Am J Pathol, 2014. **184**(2): p. 322-31.

16. Fox, D.T. and R.J. Duronio, *Endoreplication and polyploidy: insights into development and disease.* Development, 2013. **140**(1): p. 3-12.

17. Yaffe, D. and M. Feldman, *The Formation of Hybrid Multinucleated Muscle Fibers from Myoblasts of Different Genetic Origin.* Dev Biol, 1965. **11**: p. 300-17.

18. White, J., J. Kartenbeck, and A. Helenius, *Membrane fusion activity of influenza virus.* EMBO J, 1982. **1**(2): p. 217-22.

19. Wang, X., et al., *Cell fusion is the principal source of bone-marrow-derived hepatocytes.* Nature, 2003. **422**(6934): p. 897-901.

20. Faggioli, F., et al., *Cell fusion is a physiological process in mouse liver.* Hepatology, 2008. **48**(5): p. 1655-64.

21. Royzman, I., et al., *The E2F cell cycle regulator is required for Drosophila nurse cell DNA replication and apoptosis.* Mech Dev, 2002. **119**(2): p. 225-37.

22. Ullah, Z., et al., *Differentiation of trophoblast stem cells into giant cells is triggered by p57/Kip2 inhibition of CDK1 activity*. Genes Dev, 2008. **22**(21): p. 3024-36.

23. Goncalves, C.R., et al., *Developmental changes in the ploidy of mouse implanting trophoblast cells in vitro.* Histochem Cell Biol, 2003. **119**(3): p. 189-98.

24. Davoli, T., E.L. Denchi, and T. de Lange, *Persistent telomere damage induces bypass of mitosis and tetraploidy.* Cell, 2010. **141**(1): p. 81-93.

25. Russell, P., et al., *Cyclin G1 regulates the outcome of taxane-induced mitotic checkpoint arrest.* Oncogene, 2012. **31**(19): p. 2450-60.

26. Tsuda, Y., et al., *Mitotic slippage and the subsequent cell fates after inhibition of Aurora B during tubulin-binding agent-induced mitotic arrest.* Sci Rep, 2017. **7**(1): p. 16762.

27. Dalton, W.B. and V.W. Yang, *Role of prolonged mitotic checkpoint activation in the formation and treatment of cancer.* Future Oncol, 2009. **5**(9): p. 1363-70.

28. Lordier, L., et al., *Megakaryocyte endomitosis is a failure of late cytokinesis related to defects in the contractile ring and Rho/Rock signaling.* Blood, 2008. **112**(8): p. 3164-74.

29. Trakala, M., et al., *Functional reprogramming of polyploidization in megakaryocytes.* Dev Cell, 2015. **32**(2): p. 155-67.

30. Cao, J., et al., *Tension Creates an Endoreplication Wavefront that Leads Regeneration of Epicardial Tissue.* Dev Cell, 2017. **42**(6): p. 600-615 e4.

31. Lima, J.P., *[Anatomy and physiology of the liver secretory apparatus]*. Arq Gastroenterol, 1980. **17**(3): p. 149-60.

32. Michalopoulos, G.K., *Principles of liver regeneration and growth homeostasis.* Compr Physiol, 2013. **3**(1): p. 485-513.

33. Duncan, A.W., *Aneuploidy, polyploidy and ploidy reversal in the liver.* Semin Cell Dev Biol, 2013. **24**(4): p. 347-56.

34. Duncan, A.W., et al., *Frequent aneuploidy among normal human hepatocytes.* Gastroenterology, 2012. **142**(1): p. 25-8.

35. Guidotti, J.E., et al., *Liver cell polyploidization: a pivotal role for binuclear hepatocytes.* J Biol Chem, 2003. **278**(21): p. 19095-101.

36. Celton-Morizur, S., et al., *The insulin/Akt pathway controls a specific cell division program that leads to generation of binucleated tetraploid liver cells in rodents.* J Clin Invest, 2009. **119**(7): p. 1880-7.

37. Miyaoka, Y., et al., *Hypertrophy and unconventional cell division of hepatocytes underlie liver regeneration.* Curr Biol, 2012. **22**(13): p. 1166-75.

38. Faktor, V.M. and I.V. Uryvaeva, *[Progressive polyploidy in mouse liver following repeated hepatectomy]*. Tsitologiia, 1975. **17**(8): p. 909-16.

39. Yamada, T., et al., *Increased polyploidy, delayed mitosis and reduced protein phosphatase-1 activity associated with excess copper in the Long Evans Cinnamon rat.* Res Commun Mol Pathol Pharmacol, 1998. **99**(3): p. 283-304.

40. Gentric, G., et al., *Oxidative stress promotes pathologic polyploidization in nonalcoholic fatty liver disease.* J Clin Invest, 2015. **125**(3): p. 981-92.

41. Wang, B., et al., *Self-renewing diploid Axin2(+) cells fuel homeostatic renewal of the liver.* Nature, 2015. **524**(7564): p. 180-5.

42. Kietzmann, T., *Metabolic zonation of the liver: The oxygen gradient revisited.* Redox Biol, 2017. **11**: p. 622-630.

43. Tanami, S., et al., *Dynamic zonation of liver polyploidy.* Cell Tissue Res, 2017. **368**(2): p. 405-410.

44. Cross, J.C., *Genetic insights into trophoblast differentiation and placental morphogenesis.* Semin Cell Dev Biol, 2000. **11**(2): p. 105-13.

45. Huch, M., et al., *In vitro expansion of single Lgr5+ liver stem cells induced by Wnt-driven regeneration.* Nature, 2013. **494**(7436): p. 247-50.

46. Raven, A., et al., *Cholangiocytes act as facultative liver stem cells during impaired hepatocyte regeneration.* Nature, 2017. **547**(7663): p. 350-354.

47. Tarlow, B.D., M.J. Finegold, and M. Grompe, *Clonal tracing of Sox9+ liver progenitors in mouse oval cell injury.* Hepatology, 2014. **60**(1): p. 278-89.

48. Schaub, J.R., et al., *Evidence against a stem cell origin of new hepatocytes in a common mouse model of chronic liver injury.* Cell Rep, 2014. **8**(4): p. 933-9.

49. Lin, S., et al., *Distributed hepatocytes expressing telomerase repopulate the liver in homeostasis and injury.* Nature, 2018.

50. Furuyama, K., et al., *Continuous cell supply from a Sox9-expressing progenitor zone in adult liver, exocrine pancreas and intestine.* Nat Genet, 2011. **43**(1): p. 34-41.

51. Carpentier, R., et al., *Embryonic ductal plate cells give rise to cholangiocytes, periportal hepatocytes, and adult liver progenitor cells.* Gastroenterology, 2011. **141**(4): p. 1432-8, 1438 e1-4.

52. Pandit, S.K., et al., *E2F8 is essential for polyploidization in mammalian cells.* Nat Cell Biol, 2012. **14**(11): p. 1181-91.

53. Conner, E.A., et al., *E2F1 blocks and c-Myc accelerates hepatic ploidy in transgenic mouse models.* Biochem Biophys Res Commun, 2003. **302**(1): p. 114-20.

54. Chen, H.Z., et al., *Canonical and atypical E2Fs regulate the mammalian endocycle.* Nat Cell Biol, 2012. **14**(11): p. 1192-202.

55. Nevzorova, Y.A., et al., *Aberrant cell cycle progression and endoreplication in regenerating livers of mice that lack a single E-type cyclin.* Gastroenterology, 2009. **137**(2): p. 691-703, 703 e1-6.

56. Kurinna, S., et al., *p53 regulates a mitotic transcription program and determines ploidy in normal mouse liver.* Hepatology, 2013. **57**(5): p. 2004-13.

57. Sheahan, S., et al., *Additive effect of p53, p21 and Rb deletion in triple knockout primary hepatocytes.* Oncogene, 2004. **23**(8): p. 1489-97.

58. Mayhew, C.N., et al., *Liver-specific pRB loss results in ectopic cell cycle entry and aberrant ploidy.* Cancer Res, 2005. **65**(11): p. 4568-77.

59. Diril, M.K., et al., *Cyclin-dependent kinase 1 (Cdk1) is essential for cell division and suppression of DNA re-replication but not for liver regeneration.* Proc Natl Acad Sci U S A, 2012. **109**(10): p. 3826-31.

60. Minamishima, Y.A., K. Nakayama, and K. Nakayama, *Recovery of liver mass without proliferation of hepatocytes after partial hepatectomy in Skp2-deficient mice.* Cancer Res, 2002. **62**(4): p. 995-9.

61. Kim, S.H., et al., *Hepatocyte homeostasis for chromosome ploidization and liver function is regulated by Ssu72 protein phosphatase.* Hepatology, 2016. **63**(1): p. 247-59.

62. Li, D., et al., *Hepatic loss of survivin impairs postnatal liver development and promotes expansion of hepatic progenitor cells in mice.* Hepatology, 2013. **58**(6): p. 2109-21.

63. Hsu, S.H., et al., *MicroRNA-122 regulates polyploidization in the murine liver.* Hepatology, 2016. **64**(2): p. 599-615.

64. Zack, T.I., et al., *Pan-cancer patterns of somatic copy number alteration.* Nat Genet, 2013. **45**(10): p. 1134-40.

65. Kaneko, Y. and A.G. Knudson, *Mechanism and relevance of ploidy in neuroblastoma.* Genes Chromosomes Cancer, 2000. **29**(2): p. 89-95.

66. Gusnanto, A., et al., *Correcting for cancer genome size and tumour cell content enables better estimation of copy number alterations from next-generation sequence data.* Bioinformatics, 2012. **28**(1): p. 40-7.

67. Carter, S.L., et al., *Absolute quantification of somatic DNA alterations in human cancer.* Nat Biotechnol, 2012. **30**(5): p. 413-21.

68. Shackney, S.E., et al., *Model for the genetic evolution of human solid tumors.* Cancer Res, 1989. **49**(12): p. 3344-54.

69. Reid, B.J., et al., *Barrett's esophagus: ordering the events that lead to cancer.* Eur J Cancer Prev, 1996. **5 Suppl 2**: p. 57-65.

70. Levine, D.S., et al., *Formation of the tetraploid intermediate is associated with the development of cells with more than four centrioles in the elastase-simian virus 40 tumor antigen transgenic mouse model of pancreatic cancer.* Proc Natl Acad Sci U S A, 1991. **88**(15): p. 6427-31.

71. Margolis, R.L., O.D. Lohez, and P.R. Andreassen, *G1 tetraploidy checkpoint and the suppression of tumorigenesis.* J Cell Biochem, 2003. **88**(4): p. 673-83.

72. Fujiwara, T., et al., *Cytokinesis failure generating tetraploids promotes tumorigenesis in p53-null cells.* Nature, 2005. **437**(7061): p. 1043-7.

73. Davoli, T. and T. de Lange, *Telomere-driven tetraploidization occurs in human cells undergoing crisis and promotes transformation of mouse cells.* Cancer Cell, 2012. **21**(6): p. 765-76.

74. Andreassen, P.R., et al., *Tetraploid state induces p53-dependent arrest of nontransformed mammalian cells in G1.* Mol Biol Cell, 2001. **12**(5): p. 1315-28.

75. Kuffer, C., A.Y. Kuznetsova, and Z. Storchova, *Abnormal mitosis triggers p53-dependent cell cycle arrest in human tetraploid cells.* Chromosoma, 2013. **122**(4): p. 305-18.

76. Ganem, N.J., et al., *Cytokinesis failure triggers hippo tumor suppressor pathway activation.* Cell, 2014. **158**(4): p. 833-848.

77. Zhang, S., et al., *TALEN-mediated somatic mutagenesis in murine models of cancer.* Cancer Res, 2014. **74**(18): p. 5311-21.

78. Bouchonville, K., et al., *Aneuploid chromosomes are highly unstable during DNA transformation of Candida albicans.* Eukaryot Cell, 2009. **8**(10): p. 1554-66.

79. Selmecki, A.M., et al., *Polyploidy can drive rapid adaptation in yeast.* Nature, 2015. **519**(7543): p. 349-52.

80. Chao, D.Y., et al., *Polyploids exhibit higher potassium uptake and salinity tolerance in Arabidopsis.* Science, 2013. **341**(6146): p. 658-9.

81. Duncan, A.W., et al., *The ploidy conveyor of mature hepatocytes as a source of genetic variation.* Nature, 2010. **467**(7316): p. 707-10.

82. Knouse, K.A., et al., *Single cell sequencing reveals low levels of aneuploidy across mammalian tissues.* Proc Natl Acad Sci U S A, 2014. **111**(37): p. 13409-14.

83. Duncan, A.W., et al., *Aneuploidy as a mechanism for stress-induced liver adaptation.* J Clin Invest, 2012. **122**(9): p. 3307-15.

84. Holland, A.J. and D.W. Cleveland, *Losing balance: the origin and impact of aneuploidy in cancer.* EMBO Rep, 2012. **13**(6): p. 501-14.

85. Premsrirut, P.K., et al., *A rapid and scalable system for studying gene function in mice using conditional RNA interference.* Cell, 2011. **145**(1): p. 145-58.

86. Doyle, E.L., et al., *TAL Effector-Nucleotide Targeter (TALE-NT) 2.0: tools for TAL effector design and target prediction.* Nucleic Acids Res, 2012. **40**(Web Server issue): p. W117-22.

87. Cermak, T., et al., *Efficient design and assembly of custom TALEN and other TAL effector-based constructs for DNA targeting.* Nucleic Acids Res, 2011. **39**(12): p. e82.

88. Love, K.T., et al., *Lipid-like materials for low-dose, in vivo gene silencing.* Proc Natl Acad Sci U S A, 2010. **107**(5): p. 1864-9.

89. Beer, S., et al., *Hepatotoxin-induced changes in the adult murine liver promote MYC-induced tumorigenesis.* PLoS One, 2008. **3**(6): p. e2493.

90. Mitchell, C. and H. Willenbring, *A reproducible and well-tolerated method for 2/3 partial hepatectomy in mice.* Nat Protoc, 2008. **3**(7): p. 1167-70.

91. Zhu, H., et al., *Lin28a transgenic mice manifest size and puberty phenotypes identified in human genetic association studies.* Nat Genet, 2010. **42**(7): p. 626-30.

92. Sun, X., et al., *Arid1a Has Context-Dependent Oncogenic and Tumor Suppressor Functions in Liver Cancer.* Cancer Cell, 2017. **32**(5): p. 574-589 e6.

93. Bard-Chapeau, E.A., et al., *Transposon mutagenesis identifies genes driving hepatocellular carcinoma in a chronic hepatitis B mouse model.* Nat Genet, 2014. **46**(1): p. 24-32.

94. Keng, V.W., et al., *A conditional transposon-based insertional mutagenesis screen for genes associated with mouse hepatocellular carcinoma.* Nat Biotechnol, 2009. **27**(3): p. 264-74.

95. Shen, J., et al., *Oncogenic mutations and dysregulated pathways in obesity-associated hepatocellular carcinoma.* Oncogene, 2016. **35**(49): p. 6271-6280.

96. Vogelstein, B., et al., *Cancer genome landscapes.* Science, 2013. **339**(6127): p. 1546-58.

97. Totoki, Y., et al., *High-resolution characterization of a hepatocellular carcinoma genome.* Nat Genet, 2011. **43**(5): p. 464-9.

98. Guichard, C., et al., *Integrated analysis of somatic mutations and focal copy-number changes identifies key genes and pathways in hepatocellular carcinoma.* Nat Genet, 2012. **44**(6): p. 694-8.

99. Kan, Z., et al., *Whole-genome sequencing identifies recurrent mutations in hepatocellular carcinoma.* Genome Res, 2013. **23**(9): p. 1422-33.

100. Fujimoto, A., et al., *Whole-genome sequencing of liver cancers identifies etiological influences on mutation patterns and recurrent mutations in chromatin regulators.* Nat Genet, 2012. **44**(7): p. 760-4.

101. El-Serag, H.B., *Hepatocellular carcinoma.* N Engl J Med, 2011. **365**(12): p. 1118-27.

102. Lambeth, L.S. and C.A. Smith, *Short hairpin RNA-mediated gene silencing.* Methods Mol Biol, 2013. **942**: p. 205-32.

103. Miller, J.C., et al., *A TALE nuclease architecture for efficient genome editing.* Nat Biotechnol, 2011. **29**(2): p. 143-8.

104. Boch, J., *TALEs of genome targeting.* Nat Biotechnol, 2011. **29**(2): p. 135-6.

105. Cong, L., et al., *Multiplex genome engineering using CRISPR/Cas systems.* Science, 2013. **339**(6121): p. 819-23.

106. Mali, P., et al., *RNA-guided human genome engineering via Cas9.* Science, 2013. **339**(6121): p. 823-6.

107. Burgess, D.J., *Technology: a CRISPR genome-editing tool.* Nat Rev Genet, 2013. **14**(2): p. 80.

108. Zu, Y., et al., *TALEN-mediated precise genome modification by homologous recombination in zebrafish.* Nat Methods, 2013. **10**(4): p. 329-31.

109. Bedell, V.M., et al., *In vivo genome editing using a high-efficiency TALEN system.* Nature, 2012. **491**(7422): p. 114-8.

110. Xiao, A., et al., *Chromosomal deletions and inversions mediated by TALENs and CRISPR/Cas in zebrafish.* Nucleic Acids Res, 2013. **41**(14): p. e141.

111. Lei, Y., et al., *Efficient targeted gene disruption in Xenopus embryos using engineered transcription activator-like effector nucleases (TALENs).* Proc Natl Acad Sci U S A, 2012. **109**(43): p. 17484-9.

112. Suzuki, K.T., et al., *High efficiency TALENs enable F0 functional analysis by targeted gene disruption in Xenopus laevis embryos.* Biol Open, 2013. **2**(5): p. 448-52.

113. Ferguson, C., et al., *Toll-like receptor 4 (Tlr4) knockout rats produced by transcriptional activator-like effector nuclease (TALEN)-mediated gene inactivation.* Alcohol, 2013.

114. Sung, Y.H., et al., *Knockout mice created by TALEN-mediated gene targeting.* Nat Biotechnol, 2013. **31**(1): p. 23-4.

115. Wang, H., et al., *TALEN-mediated editing of the mouse Y chromosome.* Nat Biotechnol, 2013. **31**(6): p. 530-2.

116. Kato, T., et al., *Production of Sry knockout mouse using TALEN via oocyte injection.* Sci Rep, 2013. **3**: p. 3136.

117. Wefers, B., et al., *Generation of targeted mouse mutants by embryo microinjection of TALEN mRNA.* Nat Protoc, 2013. **8**(12): p. 2355-79.

118. Liu, F., Y. Song, and D. Liu, *Hydrodynamics-based transfection in animals by systemic administration of plasmid DNA.* Gene Ther, 1999. **6**(7): p. 1258-66.

119. Yam, J.W., C.M. Wong, and I.O. Ng, *Molecular and functional genetics of hepatocellular carcinoma.* Front Biosci (Schol Ed), 2010. **2**: p. 117-34.

120. Anna, C.H., et al., *Beta-catenin mutations and protein accumulation in all hepatoblastomas examined from B6C3F1 mice treated with anthraquinone or oxazepam.* Cancer Res, 2000. **60**(11): p. 2864-8.

121. Inaba, K., et al., *Hepatocellular adenoma associated with familial adenomatous polyposis coli.* World J Hepatol, 2012. **4**(11): p. 322-6.

122. Krawczuk-Rybak, M., et al., *Hepatoblastoma as a result of APC gene mutation.* J Pediatr Gastroenterol Nutr, 2012. **55**(3): p. 334-6.

123. Csepregi, A., et al., *APC promoter methylation and protein expression in hepatocellular carcinoma.* J Cancer Res Clin Oncol, 2008. **134**(5): p. 579-89.

124. Kim, M.J. and N. Ahituv, *The hydrodynamic tail vein assay as a tool for the study of liver promoters and enhancers.* Methods Mol Biol, 2013. **1015**: p. 279-89.

125. Bilger, A., et al., *A potent modifier of liver cancer risk on distal mouse chromosome 1: linkage analysis and characterization of congenic lines.* Genetics, 2004. **167**(2): p. 859-66.

126. Loeppen, S., et al., *Overexpression of glutamine synthetase is associated with beta-catenin-mutations in mouse liver tumors during promotion of hepatocarcinogenesis by phenobarbital.* Cancer Res, 2002. **62**(20): p. 5685-8.

127. Kudryavtsev, B.N., et al., *Human hepatocyte polyploidization kinetics in the course of life cycle.* Virchows Arch B Cell Pathol Incl Mol Pathol, 1993. **64**(6): p. 387-93.

128. Gentric, G., S. Celton-Morizur, and C. Desdouets, *Polyploidy and liver proliferation.* Clin Res Hepatol Gastroenterol, 2012. **36**(1): p. 29-34.

129. Moser, A.R., et al., *ApcMin, a mutation in the murine Apc gene, predisposes to mammary carcinomas and focal alveolar hyperplasias.* Proc Natl Acad Sci U S A, 1993. **90**(19): p. 8977-81.

130. Azuma, H., et al., *Robust expansion of human hepatocytes in Fah-/-/Rag2-/-/Il2rg-/- mice.* Nat Biotechnol, 2007. **25**(8): p. 903-10.

131. Colnot, S., et al., *Liver-targeted disruption of Apc in mice activates beta-catenin signaling and leads to hepatocellular carcinomas.* Proc Natl Acad Sci U S A, 2004. **101**(49): p. 17216-21.

132. Wuestefeld, T., et al., *A Direct in vivo RNAi screen identifies MKK4 as a key regulator of liver regeneration.* Cell, 2013. **153**(2): p. 389-401.

133. Grimm, D., et al., *Fatality in mice due to oversaturation of cellular microRNA/short hairpin RNA pathways.* Nature, 2006. **441**(7092): p. 537-41.

134. Beer, S., et al., *Low-level shRNA cytotoxicity can contribute to MYC-induced hepatocellular carcinoma in adult mice.* Mol Ther, 2010. **18**(1): p. 161-70.

135. Sawyer, G.J., et al., *Hydrodynamic gene delivery to the liver: theoretical and practical issues for clinical application.* Curr Gene Ther, 2009. **9**(2): p. 128-35.

136. Kozarsky, K., *Gene delivery to the liver.* Curr Protoc Hum Genet, 2001. **Chapter 13**: p. Unit 13 10.

137. Zhang, X., et al., *In vivo gene delivery via portal vein and bile duct to individual lobes of the rat liver using a polylysine-based nonviral DNA vector in combination with chloroquine.* Hum Gene Ther, 2001. **12**(18): p. 2179-90.

138. Liu, F. and L. Huang, *Noninvasive gene delivery to the liver by mechanical massage.* Hepatology, 2002. **35**(6): p. 1314-9.

139. Yin, H., et al., *Genome editing with Cas9 in adult mice corrects a disease mutation and phenotype.* Nat Biotechnol, 2014.

140. Comai, L., *The advantages and disadvantages of being polyploid.* Nat Rev Genet, 2005. **6**(11): p. 836-46.

141. Schwartz-Arad, D., G. Zajicek, and E. Bartfeld, *The streaming liver IV: DNA content of the hepatocyte increases with its age.* Liver, 1989. **9**(2): p. 93-9.

142. Margall-Ducos, G., et al., *Liver tetraploidization is controlled by a new process of incomplete cytokinesis.* J Cell Sci, 2007. **120**(Pt 20): p. 3633-9.

143. Tamura, J., et al., *Cell kinetics of regenerating liver after 70% hepatectomy in rats--2-color flow cytometric analysis.* HPB Surg, 1992. **5**(2): p. 103-14; discussion 114-5.

144. Chao, D.Y., et al., *Polyploids Exhibit Higher Potassium Uptake and Salinity Tolerance in Arabidopsis.* Science, 2013. **341**(6146): p. 658-659.

145. Jamal-Hanjani, M., et al., *Tracking the Evolution of Non-Small-Cell Lung Cancer.* N Engl J Med, 2017. **376**(22): p. 2109-2121.

146. Otto, S.P., *The evolutionary consequences of polyploidy.* Cell, 2007. **131**(3): p. 452-62.

147. Weaver, B.A., et al., *Aneuploidy acts both oncogenically and as a tumor suppressor.* Cancer Cell, 2007. **11**(1): p. 25-36.

148. Sheltzer, J.M., et al., *Single-chromosome Gains Commonly Function as Tumor Suppressors.* Cancer Cell, 2017. **31**(2): p. 240-255.

149. Ben-David, U., et al., *Aneuploidy induces profound changes in gene expression, proliferation and tumorigenicity of human pluripotent stem cells.* Nat Commun, 2014. **5**: p. 4825.

150. Shoshani, O., et al., *Polyploidization of murine mesenchymal cells is associated with suppression of the long noncoding RNA H19 and reduced tumorigenicity.* Cancer Res, 2012. **72**(24): p. 6403-13.

151. Chen, H.Z., et al., *Canonical and atypical E2Fs regulate the mammalian endocycle.* Nature Cell Biology, 2012. **14**(11): p. 1192-+.

152. Kent, L.N., et al., *E2f8 mediates tumor suppression in postnatal liver development.* J Clin Invest, 2016. **126**(8): p. 2955-69.

153. Shihao Zhang, Q.C., Qingxu Liu, Yuxi Li,1 Xiufeng Sun,1 Lixin Hong,1 Suyuan Ji,1 Chengyan Liu,1, et al., *Hippo Signaling Suppresses Cell Ploidy and Tumorigenesis through Skp2.* Cancer Cell, 2017. **31**(5): p. 669–684.

154. Celton-Morizur, S., et al., *The insulin/Akt pathway controls a specific cell division program that leads to generation of binucleated tetraploid liver cells in rodents.* Journal of Clinical Investigation, 2009. **119**(7): p. 1880-1887.

155. Kittler, R., et al., *Genome-scale RNAi profiling of cell division in human tissue culture cells.* Nat Cell Biol, 2007. **9**(12): p. 1401-12.

156. Zhou, K.J., et al., *Modular degradable dendrimers enable small RNAs to extend survival in an aggressive liver cancer model.* Proceedings of the National Academy of Sciences of the United States of America, 2016. **113**(3): p. 520-525.

157. Premsrirut, P.K., et al., *A Rapid and Scalable System for Studying Gene Function in Mice Using Conditional RNA Interference.* Cell, 2011. **145**(1): p. 145-158.

158. Heindryckx, F., I. Colle, and H. Van Vlierberghe, *Experimental mouse models for hepatocellular carcinoma research.* Int J Exp Pathol, 2009. **90**(4): p. 367-86.

159. Wang, Z., et al., *Oxidative Stress and Liver Cancer: Etiology and Therapeutic Targets.* Oxid Med Cell Longev, 2016. **2016**: p. 7891574.

160. Nijhawan, D., et al., *Cancer vulnerabilities unveiled by genomic loss.* Cell, 2012. **150**(4): p. 842-54.

161. Davoli, T., et al., *Cumulative haploinsufficiency and triplosensitivity drive aneuploidy patterns and shape the cancer genome.* Cell, 2013. **155**(4): p. 948-62.

162. Shachaf, C.M., et al., *MYC inactivation uncovers pluripotent differentiation and tumour dormancy in hepatocellular cancer.* Nature, 2004. **431**(7012): p. 1112-7.

163. Xue, W., et al., *CRISPR-mediated direct mutation of cancer genes in the mouse liver.* Nature, 2014. **514**(7522): p. 380-4.

164. Schaffer, B.E., et al., *Loss of p130 accelerates tumor development in a mouse model for human small-cell lung carcinoma.* Cancer Res, 2010. **70**(10): p. 3877-83.

165. Platt, R.J., et al., *CRISPR-Cas9 knockin mice for genome editing and cancer modeling.* Cell, 2014. **159**(2): p. 440-55.

166. Buchmann, A., et al., *Mutations at Codon 61 of the Ha-Ras Proto-Oncogene in Precancerous Liver-Lesions of the B6c3f1 Mouse.* Molecular Carcinogenesis, 1989. **2**(3): p. 121-125.

167. Yamada, Y., et al., *Beta-catenin (Ctnnb1) gene mutations in diethylnitrosamine (DEN)-induced liver tumors in male F344 rats.* Jpn J Cancer Res, 1999. **90**(8): p. 824-8.

168. Nagasue, N., et al., *Lack of intratumoral heterogeneity in DNA ploidy pattern of hepatocellular carcinoma.* Gastroenterology, 1993. **105**(5): p. 1449-54.

169. Anti, M., et al., *DNA ploidy pattern in human chronic liver diseases and hepatic nodular lesions. Flow cytometric analysis on echo-guided needle liver biopsy.* Cancer, 1994. **73**(2): p. 281-8.

170. Fujimoto, J., et al., *Flow cytometric DNA analysis of hepatocellular carcinoma.* Cancer, 1991. **67**(4): p. 939-44.

171. Caselitz, M., et al., *Increasing sensitivity of morphological diagnosis in hepatocellular carcinoma (HCC) by combination of cytological and fine-needle histological examination after ultrasound guided fine needle biopsy.* Z Gastroenterol, 2003. **41**(6): p. 559-64.

172. Toyoda, H., et al., *Changes to hepatocyte ploidy and binuclearity profiles during human chronic viral hepatitis.* Gut, 2005. **54**(2): p. 297-302.

173. Silk, A.D., et al., *Chromosome missegregation rate predicts whether aneuploidy will promote or suppress tumors.* Proc Natl Acad Sci U S A, 2013. **110**(44): p. E4134-41.

174. Lee, J.S., et al., *Application of comparative functional genomics to identify best-fit mouse models to study human cancer.* Nat Genet, 2004. **36**(12): p. 1306-11.

175. Westcott, P.M., et al., *The mutational landscapes of genetic and chemical models of Kras-driven lung cancer.* Nature, 2015. **517**(7535): p. 489-92.

176. Liu, Y. and F. Wu, *Global burden of aflatoxin-induced hepatocellular carcinoma: a risk assessment.* Environ Health Perspect, 2010. **118**(6): p. 818-24.

177. Zhang, S., et al., *The Polyploid State Plays a Tumor-Suppressive Role in the Liver.* Dev Cell, 2018. **44**(4): p. 447-459 e5.

178. Barr, F.A. and U. Gruneberg, *Cytokinesis: placing and making the final cut.* Cell, 2007. **131**(5): p. 847-60.

179. Pampalona, J., et al., *Progressive telomere dysfunction causes cytokinesis failure and leads to the accumulation of polyploid cells.* PLoS Genet, 2012. **8**(4): p. e1002679.

180. Lv, L., et al., *Tetraploid cells from cytokinesis failure induce aneuploidy and spontaneous transformation of mouse ovarian surface epithelial cells.* Cell Cycle, 2012. **11**(15): p. 2864-75.

181. Hognas, G., et al., *Cytokinesis failure due to derailed integrin traffic induces aneuploidy and oncogenic transformation in vitro and in vivo.* Oncogene, 2012. **31**(31): p. 3597-3606.

182. Duncan, A.W., et al., *Frequent Aneuploidy Among Normal Human Hepatocytes.* Gastroenterology, 2012. **142**(1): p. 25-28.

183. Duncan, A.W., et al., *The ploidy conveyor of mature hepatocytes as a source of genetic variation.* Nature, 2010. **467**(7316): p. 707-U93.

184. Gentric, G., C. Desdouets, and S. Celton-Morizur, *Hepatocytes polyploidization and cell cycle control in liver physiopathology.* Int J Hepatol, 2012. **2012**: p. 282430.

185. Margall-Ducos, G., et al., *Liver tetraploidization is controlled by a new process of incomplete cytokinesis.* Journal of Cell Science, 2007. **120**(20): p. 3633-3639.

186. Simson, I.W., *Polyploid, aneuploid and multinucleate cells in the human liver.* J Pathol Bacteriol, 1963. **85**: p. 35-9.

187. Diril, M.K., et al., *Cyclin-dependent kinase 1 (Cdk1) is essential for cell division and suppression of DNA re-replication but not for liver regeneration.* Proceedings of the National Academy of Sciences of the United States of America, 2012. **109**(10): p. 3826-3831.

188. Hickson, G.R. and P.H. O'Farrell, *Anillin: a pivotal organizer of the cytokinetic machinery.* Biochem Soc Trans, 2008. **36**(Pt 3): p. 439-41.

189. Piekny, A.J. and A.S. Maddox, *The myriad roles of Anillin during cytokinesis.* Semin Cell Dev Biol, 2010. **21**(9): p. 881-91.

190. Piekny, A.J. and M. Glotzer, *Anillin is a scaffold protein that links RhoA, actin, and myosin during cytokinesis.* Current Biology, 2008. **18**(1): p. 30-36.

191. D'Avino, P.P., et al., *Isolation of protein complexes involved in mitosis and cytokinesis from Drosophila cultured cells.* Methods Mol Biol, 2009. **545**: p. 99-112.

192. Oegema, K., et al., *Functional analysis of a human homologue of the Drosophila actin binding protein anillin suggests a role in cytokinesis.* J Cell Biol, 2000. **150**(3): p. 539-52.

193. Field, C.M. and B.M. Alberts, *Anillin, a contractile ring protein that cycles from the nucleus to the cell cortex.* J Cell Biol, 1995. **131**(1): p. 165-78.

194. Giansanti, M.G., S. Bonaccorsi, and M. Gatti, *The role of anillin in meiotic cytokinesis of Drosophila males.* Journal of Cell Science, 1999. **112**(14): p. 2323-2334.

195. Oegema, K., et al., *Functional analysis of a human homologue of the Drosophila actin binding protein anillin suggests a role in cytokinesis.* Journal of Cell Biology, 2000. **150**(3): p. 539-551.

196. Zhou, W., et al., *Knockdown of ANLN by lentivirus inhibits cell growth and migration in human breast cancer.* Mol Cell Biochem, 2015. **398**(1-2): p. 11-9.

197. Suzuki, C., et al., *ANLN plays a critical role in human lung carcinogenesis through the activation of RHOA and by involvement in the phosphoinositide 3-kinase/AKT pathway.* Cancer Res, 2005. **65**(24): p. 11314-25.

198. Magnusson, K., et al., *ANLN is a prognostic biomarker independent of Ki-67 and essential for cell cycle progression in primary breast cancer.* Bmc Cancer, 2016. **16**.

199. Hall, P.A., et al., *The septin-binding protein anillin is overexpressed in diverse human tumors.* Clin Cancer Res, 2005. **11**(19 Pt 1): p. 6780-6.

200. Wang, G., et al., *Overexpression of Anillin (ANLN) is correlated with colorectal cancer progression and poor prognosis.* Cancer Biomark, 2016. **16**(3): p. 459-65.

201. Zhou, K., et al., *Modular degradable dendrimers enable small RNAs to extend survival in an aggressive liver cancer model.* Proceedings of the National Academy of Sciences of the United States of America, 2016. **113**(3): p. 520-525.

202. Zuber, J., et al., *Toolkit for evaluating genes required for proliferation and survival using tetracycline-regulated RNAi.* Nat Biotechnol, 2011. **29**(1): p. 79-83.

203. Azuma, H., et al., *Robust expansion of human hepatocytes in Fah(-/-)/Rag2(-/-)/Il2rg(-/-) mice.* Nature Biotechnology, 2007. **25**(8): p. 903-910.

204. Budhu, A., et al., *Prediction of venous metastases, recurrence, and prognosis in hepatocellular carcinoma based on a unique immune response signature of the liver microenvironment.* Cancer Cell, 2006. **10**(2): p. 99-111.

205. Shafritz, D.A., *A human hepatocyte factory.* Nat Biotechnol, 2007. **25**(8): p. 871-2.

206. Grompe, M. and S. Strom, *Mice with human livers.* Gastroenterology, 2013. **145**(6): p. 1209-14.

207. H., Z.S.Z.K.L.X.L.L.N.L.Z.Y.T.B.S.D.a.Z., *The polyploid state plays a tumor suppressive role in the liver.* Biorxiv, 2017.

208. Mu, X., et al., *Hepatocellular carcinoma originates from hepatocytes and not from the progenitor/biliary compartment.* J Clin Invest, 2015. **125**(10): p. 3891-903.

209. Saraswat, V.A., G. Pandey, and S. Shetty, *Treatment algorithms for managing hepatocellular carcinoma.* J Clin Exp Hepatol, 2014. **4**(Suppl 3): p. S80-9.

210. Zhang, S., et al., *Knockdown of Anillin Actin Binding Protein Blocks Cytokinesis in Hepatocytes and Reduces Liver Tumor Development in Mice Without Affecting Regeneration.* Gastroenterology, 2017.